Stony Brook University

Functional Characterization of Electrospun Dextran/ Poly lactide-co-glycolide Scaffold *in vitro* and *in vivo* and its Potential as a Wound Dressing in Diabetic Chronic Wound Treatment

A Dissertation Presented

by

Hui Pan

to

The Graduate School

in Partial Fulfillment of the

Requirements

For the Degree of

Doctor of Philosophy

in

Biomedical Engineering

Stony Brook University

May 2008

Stony Brook University

The Graduate School

Hui Pan

We, the disseration committee for the above candidate for the Doctor of Philosophy degree, hereby recommend acceptance of this dissertation.

Dr. Weiliam Chen- Disseration Advisor

Associate Professor, Department of Biomedical Engineering

Dr. Michael Hadjiargyrou-Chairperson of Defense

Associate Professor, Department of Biomedical Engineering

Dr. Anil Dhundale

Research Assistant Professor, Department of Biomedical Engineering

Dr. Howard Fleit

Associate Professor, Department of Pathology, Stony Brook University

This dissertation is accepted by the Graduate School

Lawrence Martin

Dean of the Graduate School

Abstract of the Disseration

Functional Characterization of Electrospun Dextran/ Poly lactide-co-glycolide Scaffold *in vitro* and *in vivo* and its Potential as a Wound Dressing in Diabetic Chronic Wound Treatment

by

Hui Pan
Doctor of Philosophy

in

Biomedical Engineering
Stony Brook University
2008

Diabetic chronic wounds have been unmet medical problems. In this study, an electrospun Dextran/PLGA (poly lactide-co-glycolide) scaffold was fabricated. Its biocompatibility and biodegradability were investigated comprehensively using dermal fibroblasts and macrophages, separately and coordinately. Finally, the potentials of this scaffold as a wound dressing will be explored with a mice diabetic chronic wounds healing model. This study showed that this scaffold had excellent biocompatibility and degradability. The Dextran/PLGA scaffold could efficiently facilitate diabetic chronic wound healing.

Table of Contents

List of symbols

PLGA: poly lactide-co-glycolide
PCR: polymer chain reaction
ECM: Extracellular matrix

List of Figures

Chapter 6

List of Tables

Acknowledgement

This study was supported by the NIH (DK068401, WC). I would appreciate all the support and help from my advisor Dr. Weiliam Chen. I would also thank Dr. Michael Hadjiargyrou, Dr. Anil Dhundale and Dr. Howard Fleit for their insights. I would thank Dr. Hongliang Jiang for the synthesis of the materials for this study, Dr. Julia Zakhaleva for helping the animal surgery, Mr.Zhijia Yuan for helping taking the pictures of wound beds, Dr. Jim Quinn for helping the SEM and Dr. Wenjuan Su for helping the antibody arrays. I appreciate all the training and support from the Department of Biomedical engineering of Stony Brook University.

Chapter 1 Hypothesis and Specific aims

Significant efforts have been made to produce new and more effective treatments for intractable diabetic chronic wounds. However, till now, all attempts have been less than satisfactory (1). Recently, much attention has been focused on designing implantable compliant biodegradable polymer scaffolds that target accelerating chronic wound repairs. In this study, a highly porous electrospun Dextran/PLGA scaffold, aiming to functionally mimic the dermal tissue was prepared for treating diabetic chronic wounds.

Our working **hypothesis** is that: the constitution and structure of the electrospun Dextran/PLGA scaffold is biocompatible and biodegradable, and could favorably support the growths and functions of dermal cells. We further **hypothesize** that the scaffold could be used as a potential wound dressing in facilitating diabetic chronic wound healing.

In accordance, four specific aims were proposed for this project.

Specific aim 1: *In vitro* interaction of dermal fibroblasts with electrospun Dextran/PLGA scaffold;

Specific aim 2: Evaluation of the biocompatibility and immunocompatibility of electrospun Dextran/PLGA scaffold using an *in vitro* fibroblast/macrophage co-culture model;

Specific aim 3: Evaluation of the biodegradability of electrospun Dextran/PLGA scaffold using an *in vitro* fibroblast/macrophage co-culture model;

Specific aim 4: Electrospun Dextran/PLGA scaffold as a potential wound dressing in treating diabetic chronic wounds *in vivo.*

Chapter 2 Introduction

2.1 Diabetic chronic wound

Diabetes affects approximately 170 million people in the United Stated (2). Diabetic chronic ulcers are the most frequent medical complications of these patients and often lead to lower-limb amputations (3). This not only compromises the quality of patients' life, but is also a significant financial burden on the health care system (average about $27,987 for the first 2 years for each patient) (3).

Wound healing is a complex and highly orchestrated process that encompasses inflammation, cell proliferation (fibroplasia, granulation and re-epithelialization) and tissue remodeling (4). Normal wound healing involves the interaction of many cell types, including inflammatory cells, fibroblasts, keratinocytes and endothelial cells as well as the participation of cytokines and enzymes (5). Immediately after injury, platelets aggregate at the wound bed and multiple cytokines are released, this in turn, induces vasodilation and enhances vascular permeability, allowing infiltration of inflammatory cells such as neutrophils and macrophages. Formation of fibrin clot fills the wound bed and forms a provisional matrix for cell infiltration to initiate the healing process. Neutrophils and macrophages secrete chemokines to attract epidermal and dermal cells to the wound site initiating re-epithelialization and granulation tissue formation (5). In addition, fibroblasts and

other dermal cells deposit extracellular matrix (ECM) in the wound bed to replace the provisional matrix; contraction of fibroblasts results in the decrease of wound sizes. Accumulation of collagen leads to eventual scar formation covering the newly formed skin (5).

Over 100 known pathophysiological factors (Table 1: Summary of causes of diabetic wounds) (5, 6) contribute to the wound healing deficiencies in diabetic individuals (2). Improper molecular, cellular and systemic responses, including insufficient blood supply, faulty cell infiltration/proliferation, reduction in growth factors, imbalanced ECM turnover and impaired neo-angiogenesis are contributory to the failure of healing. A large number of cytokines have been reported as abnormal in diabetic wounds, these include insulin-like growth factor (IGF), transforming growth factor-β (TGF-β), platelet-derived growth factor (PDGF), vascular endothelial growth factor (VEGF) and so on (5, 7). These cytokines profoundly influence cell recruitment, proliferation and functions in the process of wound healing (5, 7). Nitric oxide is produced by many cell types in the skin and plays various roles in many physiological processes including wound healing, inflammatory responses, angiogenesis and so on. However, in diabetic patients, the levels of plasma NO are elevated resulting in severely compromising both the ECM and cellular DNA (5, 7). Therefore, the ECM turnover is disrupted in diabetic ulcers, this influences the ECM metabolism, angiogenesis, cell migration, cytokine profile, and wound contraction (5, 7). In addition, the cellular profile and functions are altered in diabetic wounds (5). Impaired functions and abnormal numbers of inflammatory cells such as B cells, T cells,

neutrophils and macrophages have been reported. Dermal fibroblasts exhibit damaged proliferation, collagen synthesis, response to cytokines, migration, apoptosis, and so on (5, 7). Angiogenesis, crucial in wound healing, is reduced significantly in diabetic wounds, and it could hypothetically be restored by applying VEGF or bFGF (5, 7).

Tremendous efforts have been made to both enhance the understanding and correct the pathophysiological factors contributing to chronic wounds (Table 2: Summary of current treatments of diabetic wounds) (3). The major treatment modalities, both experimental and in clinical use, for modulating the abnormalities of diabetic wounds include growth factors, matrix replacement, revising enzymes, stem cells therapy, gene therapy, and bioengineered skin (8). However, an efficacious solution which is easy to process, effective and economical has yet to be identified.

Advances in biomaterial development have led to the emergence of newer treatments for diabetic chronic wounds. Currently available wound dressings include films, foams, hydrogels, hydrocolloids, and hydrofibers (5, 8). Most wound dressings showed certain efficacy in clinical trials (8), and they function through different mechanisms such as promoting macrophage activation, promoting keratinocyte migration, reducing the concentration of proteases, absorption of wound exude and so on (8). However, the efficacies of many experimental dressings are still suboptimal without incorporating potent bioactive agents (8) (9-14).

2.2 Electrospun Dextran/PLGA scaffold

Electrospinning is a facile technique capable of fabricating polymers into large flexible sheets of nanofibrous structures. Electrospun scaffolds generally have

large surface area-to-volume ratios and large interconnected pores, which allow free permeation of water, gas, and bioactive agents. Biocompatible and biodegradable electrospun scaffolds have been applied in many biomedical fields including deliveries of bioactive agents and as soft tissue substitutes, particularly as provisional dermal replacements (15, 16).

Our lab had previously demonstrated the feasibility of blending a natural biocompatible hydrophilic polysaccharide, dextran, with a commonly used model biocompatible hydrophobic polymer, poly lactide-co-glycolide (PLGA), and co-processed them into highly porous fibrous structures by electrospinning (15) (Figure 1: Schemes of PLGA and Dextran). PLGA is a relatively hydrophobic and water insoluble synthetic polymer, easy to process with good mechanical properties. However, it is more immunogenic than most naturally derived polymers. Conversely, dextran is a water soluble natural polysaccharide with exceptional biocompatibility, but its mechanical property is poor and crosslinking is needed for achieving a certain degree of stability in aqueous solution. Electrospun scaffolds prepared from pure PLGA readily shrink (>80% of shrinkage) in an aqueous environment, whilst crosslinked electrospun dextran scaffolds readily swelled and disintegrated in an aqueous medium (15). Thus, their potential for biomedical applications is rather limited. Homogeneously combining dextran and PLGA to form fibers (thereby scaffold) by electrospinning could leverage the advantageous aspects of both materials and mutually offset their deficiencies. We had shown that blending PLGA with dextran and photo-crosslinking of the dextran in solid state enabled direct

stabilization of the scaffold formed without the need of using crosslinking reagents that were difficult to control and could also be toxic. This resulted in producing a hybrid Dextran/PLGA composite scaffold with good mechanical property, resistant to shrinkage and theoretically with enhanced biocompatibility. Material properties of this scaffold as well as its potential to deliver bioactive agents have been well investigated (Figure 2: SEM scanning of scaffold morphology) (15). In this investigation, prior to apply the scaffold *in vivo* for treating chronic wounds, biocompatibility and biodegradability of the scaffold, which are the most basic requirements, have to be studied.

2.3 Biocompatibility and immunocompatibility of the scaffold

Biocompatibility is the most fundamental requirement in designing implantable biomaterials and all the related safety issues have to be fully addressed. Ideally, implantable biomaterials should provide a metabolically and mechanically conducive environment for cell seeding, attachment, growth, ECM production and other cell functions.

Fibroblasts are critical cells involved in dermal wounds healing and fibroblasts from diabetic wounds exhibited impaired migration/proliferation, abnormal turnover and distribution of ECM, decreased contractibility and imbalanced produce of growth factors and cytokines (16). Accordingly, in specific aim 1 (chapter 3), a comprehensive set of experiments were performed to investigate whether dermal fibroblasts seeded on Dextran/PLGA nanofibrous scaffolds maintained their normal biological functions including morphology, attachment, distribution, proliferation,

ECM turnover, contraction, cytoskeleton organization as well as the production of key growth factors.

Further, upon *in vivo* implantation, all biomaterials invoke tissue responses, ranging from mild to intense, which is aiming at eliminating them as foreign bodies. Implanted biomaterials are typically encased by collagenous capsules, with fibroblasts and macrophages as the two dominate cell types inside interacting strongly with the encased implants (17, 18). Fibroblasts are crucial in many physiological responses such as inflammation, synthesis of ECM and tissue regeneration (16). Macrophages play vital roles in the first line of host defense against invaded microorganisms, foreign particles/materials, altered self-tissues, and so forth (19). They also regulate the recruitment, proliferation and differentiation of other cell types, including fibroblasts, endothelial cells, and keratinocytes (17). Moreover, these two cell types secrete a myriad of bioactive agents including ions, cytokines, chemokines, growth factors, ECM, enzymes and so forth (18, 20).

More importantly, macrophages play critical roles in wounds healing. Evidence from human and mice chronic wounds strongly supported that wound macrophages interfered with the repair process. Excess and extended existence of macrophages in chronic wound beds caused delayed resolution of inflammation which led to nonhealing wounds (21, 22). Moreover, the balance of cytokine productions such as MIF (23), MCP-1, MIP-2 (24) and TNF-alpha (25, 26) was significantly disturbed in diabetic wounds. In addition, abnormal production of nitric oxide has been reported in diabetic wounds although the results from different reports were

equivocal (27-29).

In accordance, in specific aim 2 (chapter 4), we developed an *in vitro* fibroblast/macrophage co-culture model to investigate the biocompatibility/immunocompatibility of scaffold under the influence of these two cell types, individually and cooperatively. Although macrophages and fibroblasts have different effects on implanted biomaterials (30), they coordinate with each other through autocrine and paracrine, and thus orchestrate the physiological responses to biomaterials (18). Therefore, understanding the complex synergistic interactions between macrophages/fibroblasts and scaffold is important. Previous studies using either macrophages (31, 32) or fibroblasts (16) for cell-material interactions did not adequately address the cooperative interaction between these two cell types with biomaterials. Accordingly, cell proliferation and their long-term viability in the presence of the Dextran/PLGA scaffold were monitored for up to eight weeks. Cell attachments as well as their morphological changes were evaluated. Anti-F4/80 (a macrophage specific marker) antibody (33) was used to distinguish macrophages from fibroblasts and their distributions inside the scaffold. Changes in numbers of each cell population over three weeks were quantified with flow cytometry. Additionally, the degree of scaffold induced macrophage activation was evaluated by an oxidative burst assay and by observing macrophage morphological changes. The magnitude and time span of inflammation evoked by scaffold were monitored by nitric oxide production. Moreover, antibody arrays were used to profile subtle changes of forty inflammatory cytokines/chemokines released from the cells following exposure to the scaffold. In

each assay, the combined effect of the two cell types was compared with the function of individual cell type. Scaffold biocompatibility and immunocompatibility were validated by a mouse subcutaneous implantation model.

2.4 Biodegradability of the scaffold

In the past three decades, much advance has been made in the fields of bioactive agent delivery and impaired organ repair (34), which typically entails implantation of biodegradable materials. Implanted biomaterials are recognized as foreign by the hosts, which generally involve materials' integration and/or elimination followed by reconstitution of tissues at the implant sites (34). Ideally, the degradation rates of implants should be engineered to only last the intended span of needed efficacy and synchronize with the pace of tissue reconstitution. In particular, the degradation profile of biomaterials serving as drug delivery vehicles should be precisely controlled for optimal efficacy. Thus, a thorough understanding of material degradation in the active biological environment is prudent to their utilization *in vivo*.

Most *in vitro* biomaterial degradation studies have hitherto been performed in phosphate buffered saline (PBS) (35, 36) or concentrated enzyme solutions (37, 38). Non-physiological and very harsh conditions, such as papain and NaOH at 150ºC (39) which evidently did not resemble the biological environment, were also utilized as media to study biomaterial degradation. In contrast, cell mediated material degradation bears a greater resemblance to the *in vivo* physiological environment, which was exemplified by a recent study demonstrating the importance of intimate biomaterial-cell contact in the degradation of polyethylene carbonate (PEC) (40).

Cells can secrete potent hydrolytic and oxidative agents such as ions and enzymes to mediate or accelerate bond cleavage of implanted polymeric materials (18). They also deposit ECM on biomaterials and its turnover invokes increased production of enzymes to further polymer degradation (41). Additionally, the continuous stress applied by attached cells to polymer surface has also been shown to hasten the degradation process (18). More importantly, different cell types function synergically to modulate the local environment through cell-cell communication (autocrine, paracrine, and endocrine) (42), which adds more complexity to biomaterial degradation.

Upon *in vivo* implantation, all biomaterials are encapsulated by collagenous capsules with fibroblasts and macrophages being the two dominant cell types residing in. They both are active secreting cells and produce a variety of hydrolases (18) which might efficiently degrade biomaterials. In addition, both types of cells produce superoxide anions (43) that could be transformed to more potent oxidants capable of initiating homolytic reaction on polymers (18). As professional phagocytotic cells and non-professional phagocytes, respectively, macrophages and fibroblasts are involved in breaking down of many natural macromolecules (44, 45) and could ingest their degraded fragments (18). Macrophages alone have been used to investigate the degradation of many biomaterials such as polyurethanes (46), however, the effects of fibroblasts on biomaterial degradation is under-explored, which could be due to the partial understanding on fibroblast hydrolases, especially those connecting to polymer degradation.

Therefore, in specific aim 3 (chapter 5), a fibroblast/macrophage co-culture model was established to emulate the *in vivo* environment in order to study the behavior and the mechanisms of scaffold degradation. Accordingly, the effects of cells on scaffold morphology, its dry weight lost and changes in medium pH were monitored. The expressions of putative receptors (Toll like receptor 4 (TLR4), macrophage receptor with collagenous structure (MARCO), CD204, CD44 and uPARAP/Endo180) for recognition/clearance of the degraded scaffold were measured by real-time PCR. The activities of some major hydrolytic enzymes (lysozyme, nonspecific esterases, α-glucosidase, β-glucosidase, collagenases, and hyaluronidases) in the process of scaffold degradation were discerned. The biodegradability of the Dextran/PLGA scaffold was further validated by correlating the results with *in vivo* implanted scaffolds in a mouse subdermal model.

2.5 Scaffold as potential wound healing

Diabetic foot ulcer is a significant health issue and it has generally been addressed with wound dressings. According to the guidelines for treating diabetic (47), the ideal wound dressing should have the following characteristics: absence of antigenecity, tissue compatible, absence of local or systemic toxicity, impermeable to exogenous microorganisms, water vapor transmission similar to normal skin, rapid and sustained adherence to wound surface, conformal to surface irregularities, elastic to permit motion of underlying tissue, resistant to linear and shear stresses, adequate tensile strength to resist fragmentation, inhibition of wound surface flora and bacteria, long shelf life, minimal storage requirements, biodegradable, low cost minimize

nursing care of wound, minimize patient discomfort, translucent properties to allow direct observation of healing, reduce heal-time, not increase rate of infection, patient acceptance (48). The electrospun Dextran/PLGA scaffold could serve as a wound dressing that adequately covers many of the stated requirements.

In our previous study, we reported the diameters of the Dextran/PLGA scaffold fibers were very close to that of collagen fibers and the mechanical properties of the scaffold emulated those of dermal tissue (16), rendering the Dextran/PLGA scaffold a particularly appealing candidate as a biodegradable wound dressing for focal applications. In addition, the big pore sizes of the scaffold enable higher gas/liquid permeation and protect wound bed from dehydration. Therefore, in specific aim 4 (Chapter 6), the Dextran/PLGA scaffold was used as a wound dressing and its potential to facilitate diabetic wound healing was explored.

Table 1. Factors involved in nonhealing wounds

Local factors
Infection
Tissue maceration
Foreign bodies
Smoking
Ischemia
Local cancer (ie, basal cell cancer, squamous cell cancer, malignant melanoma)
Venous insufficiency
Mechanical Trauma (ie, pressure sores)
Toxins
Radiation
Iatrogenic
Systemic factors
Chronic diseases (ie, diabetes mellitus, renal disease)
Nutritional deficiencies (ie, deficiency in proteins, vitamins, minerals)
Congenital healing disorders (ie, Epidermolisis Bullosa, Ehlers-Danlos syndrome, Marfan's syndrome)
Alcoholism
Glucocorticoid steroids
Chemotherapeutic drugs (ie, methotrexate, cyclophosphamide, doxorubicin)
Advanced age
Distant cancer
Uremia

(Adapted from Medina A, et. al. The Journal of burn care & rehabilitation. 2005 Jul-Aug;26(4):306-19.)

Table 2. Treatment of nonhealing ulcers

Conventional therapies (local wound care)
Surgery (débridement, skin graftings, flaps, others)
Negative-pressure dressings (vacuum-assisted closure device)
Special dressings (hydrogels, hydrocolloids, alginates, hydrofibres)
Antiproteases: Topical application or stimulation of endogenous production
Protease inhibitors
Modulation of neutrophils
Glucocorticoid steroids
Cytokine/growth factor treatment (ie, bFGF, rhPDGF-BB, GM-CSF, KGF-2)
Adjuvant therapies (compression therapy, hyperbaric oxygen therapy, ultrasonography, hydrotherapy, electrical stimulation, pentoxifylline, micronized flavonoid fraction)

(Adapted from Medina A, et. al. The Journal of burn care & rehabilitation. 2005 Jul-Aug;26(4):306-19.)

Figure 1 Scheme of Dextran (A) (49) and PLGA (B)

(Adapted from http://www.polydex.com/v2/images/img_dextran_m.gif.)

A

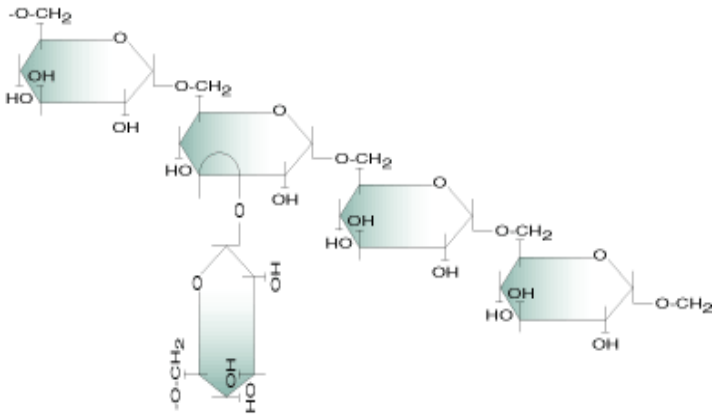

B

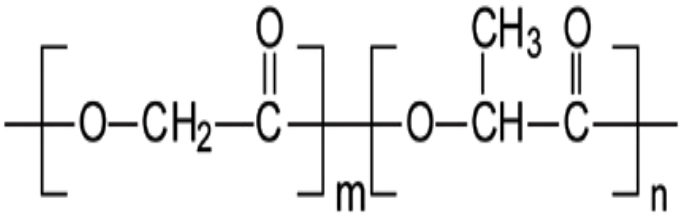

Figure 2 SEM scanning of Dextran/PLGA scaffold (15)

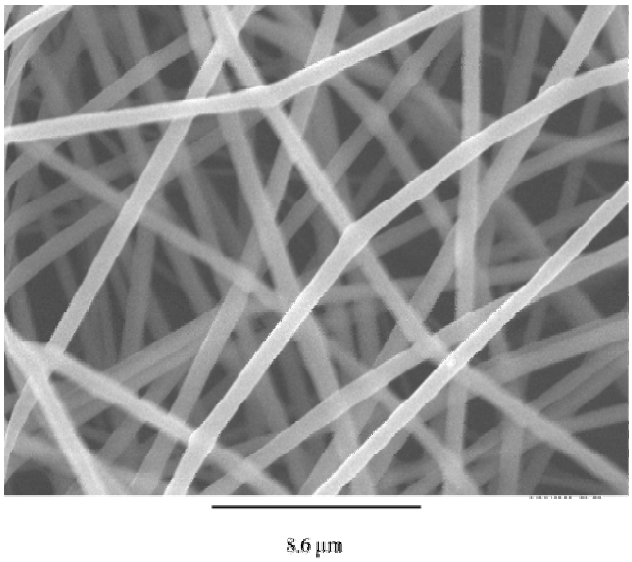

(Adopted from Jiang H et al. Biomacromolecules. 2004 Mar-Apr;5(2):326-33.)

Chapter 3 Specific Aim 1

Specific aim 1: *In vitro* interaction of dermal fibroblasts with electrospun Dextran/PLGA scaffold.

3.1. Materials and methods

Methacrylated dextran was synthesized and electrospun Dextran/PLGA scaffolds were prepared utilizing the same methods we had used previously (15).

3.1.1. Cell culture and seeding

M.DUNNI (clone III8C) mouse dermal fibroblasts CRL-2017 (ATCC, Manassas, VA, USA) were cultured in McCoy's 5A medium (ATCC, Manassas, VA, USA) supplemented with 10% Fetal Bovine Serum (Hyclone, Logan, UT, USA) and 1% Penicillin-Streptomycin solution (Gibco, Grand Island, NY, USA) at 37 °C under a humidified atmosphere of 5% CO2/95% air. Passages two to ten were used for the following experiments and cell culture media were changed every other day. The cell morphology, adhesion, distribution, viability, proliferation, migration and all relevant histological staining were examined with an inverted phase contrast light microscope (Axiovert 200M, Zeiss, Munich, Germany). All images were acquired with Axiovision 4 imaging software (Zeiss, Jena, Germany).

3.1.2. Cell morphology, attachment and distribution

Sub-confluent cells were washed by PBS twice, trypsinized and resuspended in media. Two hundred microliters of cell suspension (1×10^5 cells mL^{-1}) was deposited on each Dextran/PLGA scaffold ($\sim$0.6 cm^2 in size) in a 48-well plate and incubated for up to 5 days. Samples were withdrawn 3 h, 1 day, 3 days and 5 days after cell seeding. The cells were washed with PBS twice and then fixed with 70% ethanol for 10 min. The fixed samples were then stained with 0.1% crystal violet (in 200 mm boric acid, pH 8.0) for 5 min at ambient temperature. The dye solution was then aspirated and the cells were rinsed with PBS twice (50).

The samples at day 1 and day 3 were collected and embedded in Tissue-Tek® OTC (Sakura Finetek, Torrance, CA, USA) and snap-frozen in liquid nitrogen. Cross-sections (10 μm thick) were prepared on a cryostat (Jung/Frigocut 2800-N, Leica, Wetzlar, Germany) and stained with Mayer's Hematoxylin (Sigma-Aldrich, Saint Louis, MO, USA) to ascertain cell infiltration into the inner part of the scaffold and reside there three dimensionally.

3.1.3. Viability and proliferation assay

Cell viability and proliferation in the Dextran/PLGA scaffolds were quantified by MTS assay (CellTiter 96® aqueous non-radioactive cell proliferation assay kit, Promega, Madison, WI, USA). Approximately 1500 cells were seeded into each well of a 48-well plate with or without the Dextran/PLGA scaffold (0.6 cm^2) (area of the culture well: $\sim$0.8 cm^2). In order to isolate and measure the proliferation of cells inside the scaffold exclusively, the scaffolds were transferred from the original culture well to another well filled with 200 μL of fresh media at each time point

before measurement. Twenty microliters of MTS solution were added to the scaffold, the original culture well and the monolayer culture control, respectively. Upon addition of reagents, the cells were incubated at 37 °C for 1 h and the absorbance were determined at 490 nm. Cell viability and proliferation were evaluated on day 0, 1, 3, 6, and 10.

3.1.4. Cell migration

The ability of cell to migrate from an external substrate to and along the fibrous structures of Dextran/PLGA scaffolds was evaluated. Thermanox plastic cell culture coverslips (NUNC, Rochester, NY, USA) were placed in the bottom of the culture wells. Cells (1×10^6 cells mL^{-1}) were seeded onto the coverslip and incubated at 37 °C for 3 h to allow complete cell attachment. Mitomycin C (Roche, Indianapolis, IN, USA), a DNA synthesis inhibitor, was added to the culture (final concentration: 10 μg mL^{-1}) to prevent cell proliferation. After incubated at 37 °C for 2 h, the Mitomycin C containing media was removed and the cells were rinsed thrice with PBS. Coverslips were gently detached, with the cell-covered sides facing upward, and deposited on each Dextran/PLGA scaffold pre-positioned in empty culture wells. Approximately half of the scaffold's surface area was overlaid by the coverslip. In order to limit the mobility of the scaffolds in the culture dish, only sufficient media were added to cover them. After incubated at 37 °C for up to 3 days, the coverslips were decoupled from the scaffolds, and MTS assay was utilized to quantify the cells that migrated to the scaffolds. The scaffolds were then fixed in 70% ethanol and stained with a crystal violet solution as described above.

3.1.5. Extracellular matrix deposition

The Dextran/PLGA scaffolds were seeded with 1×10^5 cells. After 5 days, they were evaluated for collagen and elastin production. The scaffolds were rinsed with PBS twice and fixed in 70% ethanol for 10 min. Cell nuclei were first stained with Weigert's Hematoxylin for 1 min, followed by 10 min of rinsing in tap water. For collagen specific staining, the scaffolds were immersed in a 0.1% Sirius red F3BA (Sigma-Aldrich, Saint Louis, MO, USA) in a saturated picric acid solution (pH.2.0) for 1 h followed by washing with 0.01 n HCl (50). Verhoeff staining kit (Electron Microscopy Sciences, Fort Washington, PA, USA) was utilized to stain the scaffolds for visualization of elastin. Briefly, the fixed scaffold samples were immersed in Verhoeff solution for 7 min; the specimens were then washed in warm tap water for 1 min to remove the unbound dye (50).

To visualize total extracellular matrix production by cells residing inside the scaffold matrix, 3 days after cell seeding the samples were fixed with 4% paraformaldehyde, processed and imaged with Scanning electron microscopy (LEO/Zeiss 1550, Zeiss, Munich, Germany) following a method described elsewhere (51).

3.1.6. Collagen gel contraction assay

The contractility of dermal fibroblasts in the presence of scaffolds was evaluated using collagen gels on 48-well culture plates using a method described elsewhere (52). Briefly, three-dimensional collagen gels (2 mg mL^{-1}) were prepared following the manufacturer's protocol (BD Biosciences, San Diego, CA, USA) with

the final cell density of 1.0×10^6 cells mL^{-1}. Each scaffold was tailored to cover the culture well in its entirety and was embedded into the collagen solution prior to gelation. The collagen gels were detached from the culture wells and suspended in 200 μL fresh media. NIH Image J software (53) was used to quantify the areas of the collagen gels with and without scaffolds, 4 and 24 h after gelation.

3.1.7. Cytoskeleton organization

The mechanical effect of the fibrous scaffold on cell attachment was evaluated at sub-cellular level by observing its F-actin organization. Briefly, cell/scaffold samples were fixed in 4.0% formaldehyde for 10 min and rinsed three times with PBS before being treated with 0.5% Triton in PBS for 15 min. They were then stained with TRITC-labeled phalloidin (Molecular Probes, Eugene, OR, USA) and observed under a laser confocal fluorescence microscope (LSM 510, Zeiss, Munich, Germany)

3.1.8. Real-time PCR

The potential influence of the Dextran/PLGA scaffolds on cellular functions and behaviors were determined at the mRNA level. We targeted the detection of a series of marker gene expression by the cells cultured on scaffolds and compared with their counterparts grown on culture dishes by real-time PCR. The genes of interest were, growth factor genes: vascular endothelial growth factor (VEGF), platelet derived growth factor (PDGF), and basic fibroblast growth factor (bFGF); ECM turnover genes: tissue inhibitor of matrix metalloproteinase-1 (TIMP-1) and matrix metalloproteinase-1 (MMP-1); extracellular protein genes: collagen I (Col I) and

fibronectin (FN); focal adhesion genes: β-actin, paxillin, focal adhesion kinase (FAK), Integrin α1 and Integrin β1. These genes are closely related to the normal fibroblast functions. The housekeeping gene GAPDH was chosen to normalize the data obtained.

Cells were first cultured in Dextran/PLGA scaffold for one week, harvested by trypsinization and washed twice by PBS. Total RNA extraction was performed with commercially available RNeasy mini kit (Qiagen, Valencia, CA, USA). Real-time PCR was performed in a thermocycler (LightCycler, Roche, Mannheim, Germany) using the QuantiTect RT-PCR Kit (Qiagen, CA, USA). PCR primers were designed using Primer 3 software (54). They were picked from two adjacent exons to prevent amplification of genomic DNA. The primer sequences and products of selected genes for real-time PCR were summarized in Table 1. The target PCR products were about 100 bp. At least three replicates were performed on each sample and each experimental gene was tested by three PCR runs. In each run of PCR, housekeeping gene GAPDH was used as the reference. The software REST© (55) was used to analyze the relative gene expression ratios. Expression ratios above zero were considered as up-regulated, while those that were below zero were defined as down-regulated. If the gene expression is unaltered, the relative gene expression ratio should be 1 or −1. Any change in ratio between 0 and 2 or 0 and −2 is regarded as unchanged.

3.1.9. Statistics

All the experiments were performed with n=3 and the experimental results

were presented as mean±standard deviation. Whenever appropriate, two-tailed Student's t-test was used to discern the statistical difference between groups. The significant level was set as $p<0.05$.

3.2. Results

3.2.1. Cell morphology, attachment and distribution

The results of crystal violet staining for directly visualize the attachment and growth of dermal fibroblasts in Dextran/PLGA scaffolds were depicted in Fig.1 A-D (top view of the scaffold). Evidently, cells began to adhere to the Dextran/PLGA fibers 3 h after seeding (Fig. 1A) and the cell densities increased with incubation time. One day after seeding, cells were scattered throughout the fibrous meshes (Fig. 1B); by day 5, cells became highly confluent and were distributed evenly inside the scaffold (Fig. 1D). Figs. 1E-F depicted the cross-sections of the cryo-embedded specimens. On day 1, cells appeared to be interspersed among the scaffold fibers (Fig. 1E). By day 3, the cells were highly compacted and have organized into multi-layered structures residing not only on the surface but also inside the fibrous matrix (Fig. 1F). This pattern of cell distribution corroborated with the results presented above (see Figs. 1A-D).

3.2.2. Viability and proliferation of cells on scaffolds

Cell viability and proliferation inside the Dextran/PLGA scaffold were quantified by MTS assays. To estimate the cell numbers inside each scaffold, per se, it was removed from the original culture for MTS assay. As the area of the scaffold (~

0.6 cm^2) was smaller than that of the culture well (~0.8 cm^2) it resided in, the cell number on the area of the culture dish that was not previously covered by the scaffold (i.e., the margin of each well) also had to be analyzed. The total cell numbers in the wells where scaffolds were originally placed were compared with those of the control wells without scaffolds. These results were depicted in Fig. 2.

The same amounts of cells were seeded onto all culture wells, with or without Dextran/PLGA scaffolds, on day 0. One day after cell seeding (i.e., day 1), the combined cell number of the margin and the isolated scaffold was comparable to that of the monolayer control as suggested by the optical densities at 490 nm (1.91±0.15 vs. 1.82±0.11, $p=0.211$). At low cell density, the mesh structure of the scaffold hindered cell–cell contact leading to insufficient communication, which is crucial for cell proliferation (56-58). This accounted for the slower initial cell proliferation rate in the scaffold on day 1 (in scaffolds: 0.77±0.15 vs. monolayer: 1.82±0.11, $p<0.05$). On day 3, due to the lack of space for cells to further proliferate, the areas in the culture dish that was not previously covered by the scaffold as well as the monolayer control reached full confluence (optical densities, 1.61±0.14 and 2.49±0.11, respectively). When cells become confluent, contact inhibition resulted in the cease of mitosis (18), so the cell numbers on the culture wells plateau after day 3. However, the combined cell density of the margin and the isolated scaffold was significantly higher than that of the monolayer control (3.40±0.15 vs. 2.49±0.14, $p<0.05$). The 3D and high porosity structure of the Dextran/PLGA scaffold and thus, availability of void volume enabled the continual proliferation of cells and this accounted for the significantly

higher optical density observed. This finding was in good agreement with the scaffold histology results presented above (see Figs. 1E-F). The cells residing in the scaffold continued to proliferate reaching an optical density of 3.86±0.15 by day 10. The combined cell numbers in the scaffold and the margin of the same culture well were consistently higher than that of the monolayer culture. It was known that strong cell adhesion and spreading on biomaterial facilitates cell proliferation (59). As shown in Fig. 1, cells in the scaffolds were more stretched and spread, which could also contribute to the higher proliferation rate in scaffolds from day 3.

3.2.3. Cell migration from coverslips to scaffolds

Cell movement is a combined effect of cell division and cell migration (5). The migratory function of cells could be isolated by subjecting them to pre-treatment with Mitomycin C, an agent capable of inhibiting cell division but not cell mobility (60, 61). Each Dextran/PLGA scaffold was partially overlaid by a cell seeded coverslip with the cell-populated side facing up, which concealed approximately half of the area of the scaffold. The cell migration patterns on day 2 and day 3 were depicted in Fig. 3. A noticeable amount of cells could be seen on the non-concealed side of the scaffold on day 2 in Fig. 3A (i.e., the right side of the demarcation line outlined by the array of arrows). The number of cells migrated into the scaffold were evidently higher on day 3 (Fig. 3B) as indicated by the increase in cell density. In order to quantify the numbers of migrated cell, MTS assays were performed on the scaffolds recovered after 2 and 3 days of incubation, and the results were summarized in Fig. 3C. The cell number of the latter was approximately two times higher than that

of the former ($p<0.05$). This was a distinct contrast to many experimental polymer scaffolds (e.g., calcium alginate, crosslinked collagen matrix) that were capable of supporting cell attachment and proliferation, while greatly decreasing cell mobility (62, 63).

3.2.4. Deposition of extracellular matrix (ECM) in scaffolds

Fibroblasts-laden Dextran/PLGA scaffolds were stained for the presence of collagen and elastin using Sirius Red and Verhoeff's solutions, respectively (51). These two reagents do not have any affinity to the Dextran/PLGA scaffold. As shown in Figs. 4A-C, the Sirius Red stained cells could clearly be distinguished from the Dextran/PLGA fibers. The staining results showed that cells residing in the scaffold-produced collagen as they did on the 2D control (Fig. 4A). Evidently, the staining intensity increased from day 1 to day 3 (Figs. 4A and B, respectively) reaching the highest by day 5 (Fig. 4C), which suggested the synthesis and accumulation of a large amount of collagen. Likewise, the Verhoeff's solution stained Dextran/PLGA scaffolds showed the normal production of elastin by fibroblasts and a sample result for day 1 was depicted in Fig. 4D.

Fig. 5A showed a pristine Dextran/PLGA scaffold. The non-woven fibrous structure was formed by random deposition of fibers and thus, the formation of enormous amount of pores and interconnected channels. Fig. 5A depicted the SEM images of scaffold samples 3 days after cell seeding. Partial masking of the Dextran/PLGA scaffolds suggested the presence of a large amount of ECM. These results corroborated with the observations of extensive production of ECM proteins

filling the void spaces in the scaffolds (see Fig. 4). Apparently, ECM deposition by the cells was not affected by their entrapment in the Dextran/PLGA scaffold.

3.2.5. Collagen gel contraction assay

Three-dimensional collagen gels have been used as *in vitro* systems for modeling of cellular activities during wound healing (64). This model system was adapted to assess the capability of Dextran/PLGA scaffolds to induce collagen gel contraction in concert with cellular activities. These results were depicted in Fig. 6. Collagen gels with scaffold embedded contracted strongly after 4 h of incubation post-gelation; whereas, there was no obvious change in gel size in the scaffold-free control (Fig. 6A). The magnitudes of gel contraction were summarized in Fig. 6B. After 24 h of incubation, the presence of cell seeded scaffolds rendered the collagen gel to contract to approximately 39% of its original size. In contrast, the gel contracted to 69% ($p<0.05$) of its original size in the absence of cells. For comparison, cell-laden collagen gel (without embedded scaffold) contracted to 78% ($p<0.05$) and the pristine collagen gel did not show any apparent change in size.

3.2.6. Cytoskeleton organization of cells residing in scaffolds

Fig. 7 depicted the results of F-actin staining of cells residing in the 3D scaffolds and the 2D culture dishes. Due to the substantially less area for anchoring on the former, cells generally exhibited spindle-like and highly elongated morphology; this was a distinct contrast to the fully spread morphology of the latter. The monolayer cells (Figs. 7A and E) exhibited organized cytoskeleton appeared as long linear arrays throughout the entire cytoplasm and concentrated beneath the plasma membrane;

while the cells in the scaffold have shorter actin filaments and were dispersed randomly without any noticeable structural organization (Figs. 7 B and F).

3.2.7. Gene-expression analysis

The gene expression profiles of cells grown on the Dextran/PLGA scaffold were compared to those derived from cells on culture plate and identified key changes in transcripts associated with cell adhesion, signaling and ECM turnover. The expressions of fibroblast functional genes: VEGF, PDGF, bFGF, MMP-1, TIMP-1, collagen I, fibronectin, β-actin, integrin α1, integrin β1, paxillin and FAK were detected with real-time polymerase chain reaction.

The results of the real-time PCR reactions performed were summarized in Fig. 8. Relative gene expression ratios of cells in scaffold to monolayer control were between 0 and 2 or 0 and −2, indicating that the expressions of ECM proteins, cytokines, ECM turnover proteins, and the focal adhesion complex were not altered.

3.3. Discussion

The structures of tissue engineering scaffolds must be highly porous with the proper pore sizes and they must be interconnected in order to facilitate cell infiltration and cell–cell contact (46). The fibrous mesh structure is intended to better mimic the ECM. Besides, a scaffold composed of ultra-fine nanofibers provides the added benefit of improved mechanical properties and more extensive substrate for cell attachment (65). The cell morphology, attachment and distribution assay showed that dermal fibroblasts attached and moved to the interior of Dextran/PLGA scaffolds without the need of incorporating any cell-adhesion facilitating component. It was

distinctively different from the results of other studies describing various scaffolds in which cells failed to distribute uniformly in the matrices in conjunction with the majority of them attached only to the outer surfaces (66). Moreover, most biomaterials have to be modified by incorporating proteins or peptides like fibronectin and the RGD sequence, respectively, to induce cell attachment and infiltration (59). Evidently, the homogeneous distribution of the multilayered dermal fibroblasts inside the highly porous Dextran/PLGA scaffold resembles the structures of dermal tissue, which is a desirable feature for dermal tissue engineering scaffold design.

PLGA and dextran have well-established history of safety and biocompatibility. A minor modification of dextran was required to enable solid state photo-crosslinking, thereby stabilizing the Dextran/PLGA composite scaffold and rendered it insoluble in water (15). The results of MTS assay indicated that the photo-crosslinked Dextran/PLGA electrospun scaffolds were non-toxic to fibroblast cells, therefore suggested good biocompatibility despite chemical modification of dextran; the large pore size and the high surface area to volume ratio, and the strong binding of the cells to the scaffold indeed favored cell growth and proliferation.

Compromised cell migration and proliferation are two of the major contributory factors for impaired healing of chronic wounds (40, 67, 68). The migration assay results indicated that cells with impaired proliferation capacity were able to migrate along the Dextran/PLGA scaffold and it could be beneficial to healing of chronic dermal wound.

ECM is a collagen rich environment known to influence cell shape, their

survival and proliferation; it also controls the turnover of individual matrix components that facilitate cell migration (18). Fibroblasts are pivotal in the deposition, remodeling and organization of the ECM, especially during the wound healing process (40). A number of reports have indicated abnormal ECM protein distribution and deposition in diabetic individuals (69-73). One of the utilities of polymer scaffolds for tissue engineering is functional replacement of the native ECM to support the desired cellular functions and maintain phenotype-specific activities. The diameters of collagen fibers range from 10 to 300 nm (18); and the diameters of most electrospun Dextran/PLGA fibers are in the range of 100-150 nm, which are comparable to that of the collagen fibers. The results of ECM production assays suggested that the Dextran/PLGA scaffolds did not have any apparent adverse effect on both collagen and elastin production by dermal fibroblasts. It not only provides mechanical support for cells to maintain uniform distribution but also promote their secretion of ECM. The implication is that the Dextran/PLGA scaffold could be used as a provisional replacement of impaired ECM in chronic wounds to facilitate new tissue formation.

During the earliest stages of wound healing, activated dermal fibroblasts migrate from the wound edges to physically close the gaps between wound margins. The impaired contractibility of diabetic cells and the deficiency of cells in chronic wound beds contribute to the delayed healing (74, 75). The results of collagen contraction assay showed that Dextran/PLGA scaffold could significantly enhance collagen gel contraction even in the absence of dermal fibroblasts, which suggested

that the enhanced collagen gel contraction was due to the combined effect of fibroblasts and the Dextran/PLGA scaffold. The capacity of supporting dermal fibroblast contraction has important implication on any scaffold design aimed at enhancing healing and closure of chronic wounds.

Cell morphology is controlled by adhesive interactions between cells and the surface they are attached to (76). One of the key issues in tissue engineering is the adhesion of cells to polymer substrates and its regulation occurs at multiple levels including coordinated interactions with cytoskeleton (77). Many other functions of cells (e.g., attachment, migration and contraction) are also both originated and controlled by cytoskeleton, which also serves as an intracellular scaffold to provide supportive force and a physical basis for direct mechanical sensing (78). Unorganized cell cytoskeletons were previously observed in poly (ε-caprolactone) scaffolds (79). In our study, substitution of the native ECM by the Dextran/PLGA fibers could attribute to the unorganized actins of the dermal fibroblasts residing in the scaffold. It was previously reported that the structural integrity of collagen plays an important role in cell morphology and cytoskeleton expression. Fibroblasts that grew on denatured collagen showed poor capacity to maintain their phenotype and cytoskeleton organization (80). Although Dextran/PLGA nanofibers mimic the ECM and support new ECM synthesis from the cells bind to them, it is unlikely that the scaffold could replace the functions of native ECM entirely. Moreover, mechanical stimulation activates cytoskeleton reorganization (81). The existence of Dextran/PLGA nanofibers altered mechanical signals to the cells, which may also contribute to the unorganized

cytoskeleton.

Attachment of cell cytoskeleton to ECM is crucial in skin contraction and this is consistent with our observations of F-actin staining of cells in the collagen gel contraction assays. The cells in pure collagen gel displayed stellar shape as reported (82, 83); interestingly, cells in the scaffold/collagen gel exhibited neuron-like cell shape with small cell bodies and many long branched dendrites. Obviously, the actin fibers of cells residing in the scaffold-collagen gel were subjected to more stress than those in pure collagen gel (Fig. 7C-D). The phenomenon of collagen gel contraction has been widely accepted as a combined effect of the fibroblasts differentiation into myofibroblasts (84) and the condensation of collagen fibers along the fibroblasts migration paths (85). Yet, α-smooth muscle actin (the marker for myofibroblasts) immunostaining did not show the differentiation of fibroblasts into myofibroblasts (data not shown). Thus, the conspicuous change of the actin organization could be the alterations of the mechanical properties of the collagen gel in concert with the presence of Dextran/PLGA fibers. This led to altered cell attachment to scaffolds and thereby actin organization. Quantitative monitoring of the contractile forces between the cells and the scaffolds will require highly specialized instrumentations (38, 86-88) and is beyond the scope of this investigation.

Dermal fibroblasts play key roles in skin extracellular protein turnover, ECM interaction, cell–cell communication, etc.(18), which are closely related functions. Cell morphologies in the 3D scaffold (presumably in a more natural conformation) are vastly different from their counterparts on 2D culture plates (89); consequently, other

cell functions could be affected. Gene expressions can be affected by the functional reaction of cells with biomaterials (89, 90). It has recently been demonstrated that cells grown in different 3D scaffolds exhibited differential patterns of gene expression. Collagen II was found to be up-regulated in poly (ε-caprolactone) scaffolds and in poly (ethylene glycol)-based hydrogels. Elastin and fibromodulin expression were up-regulated, while MMP-1 and hyaluronidase expression were both decreased in Tecoflex™ (79, 91, 92). The information of gene expression pattern in response to the interaction with polymers could facilitate the future improvement of biomaterial designs.

Manifold cellular activities in the process of skin remodeling are orchestrated largely by interacting molecular signals, among which PDGF, VEGF, and bFGF are the primary cytokines (40). Collagen I and fibronectin are two of the primary ECM proteins in skin. The balance of MMPs and TIMPs is crucial in mediating ECM turnover and other cellular behaviors like migration and differentiation (57, 93). Altered TIMP-1, TIMP-2 and MMP-2 usually relate to aberrant ECM reorganization and chronic wound repair (94). Integrin α1, integrin β1, paxillin, and FAK form an actin-associated focal adhesion complex which connects cytoskeleton with the ECM proteins (95).

The real-time PCR results did not show statistically significant differences despite the modest changes (within the range from -2 to 2) on the gene expression level. This suggested that cells growing on them exhibited a trend of holding intact functionalities similar to cells growing on culture plates, and thus, the bio-inertness of

Dextran/PLGA scaffolds. However, we originally expected that the focal adhesion related genes would be regulated because the cell morphology, attachment, contraction and actin organization were obviously different from the monolayer control, which could be explained by two mechanisms. First, unlike binding to ECM via integrins, cells attach to the biomaterials directly through chemical bonds such as covalent bond, hydrophobic bond and hydrogen bond (59). Second, we showed above that the Dextran/PLGA scaffold supports normal cell ECM production and filled in the scaffolds' void space. It is known that proteins produced by the adherent cells adsorb to biomaterials and the cell adhesive proteins such as fibronectin and vibronectin on the biomaterial surface interact with the focal adhesion complex on the cell membrane thereby mediate the expressions of the related genes (59). The real-time PCR results indicated that the ECM produced by cells inside the scaffold was indeed functional. The altered cell morphology, attachment, contraction and actin organization in the presence of scaffold was attributable to the mechanical properties of the Dextran/PLGA fibers which are different from those of natural ECM.

3. 4. Conclusion

Coupling cells to polymeric scaffolds for producing tissue-mimicking structures of higher orders suitable for direct implantation into wounds has been a very challenging topic in the field of tissue engineering. Our results indicated that fibroblasts could be homogeneously seeded and maintained in long-term culture with high viability and thus, the scaffold was capable of supporting normal cell functions. Moreover, cells migrated into the highly porous 3D matrix of the scaffold and

organized into dense multi-layered structures that resembled dermal structure. It is known that the capabilities for proliferation, migration, contraction, protein production and ECM organization/turnover of cells derived from chronic wounds are impaired. The robust interaction between cells with the structure of these scaffolds suggested that they could be used for treating chronic or trauma wounds. Lastly, the Dextran/PLGA scaffold could also double as a carrier of cultured cells (stem cell, Xenogenic cell of animal origins) and/or bioactive agents like drugs, genes or proteins for sustained and localized delivery to the site of interest to accelerate wound closure.

Table 1 Real-time PCR primer sequences

Gene	Access number (Gene Bank)	Forward primer sequence	Reverse primer sequence
VEGF	NM-011697	5′CCA GAG CTG CCA TCT AAC AA 3′	5′ GCC AGA AGA TGC TCA CTT GAC 3′
PDGF	AY324648	5′ CCA TTC GCA GGA AGA GAA GT 3′	5′ AGG AAG TTG GCC GAT GTG 3′
bFGF	NM_008006	5′ CAA CCG GTA CCT TGC TAT GAA 3′	5′ TTC CGT GAC CGG TAA GTA TTG 3′
Collagen I	NM_007742	5′CAG AGG CGA AGG CAA CA 3′	5′ ATG TCC AAG GGA GCC ACA 3′
Fibronectin	MMFIBRON	5′ AAA TCA CAG CCA GCA GCT TT 3′	5′ TGT GGT TCA TCT CCC TCC TC 3′
TIMP-1	BC008107	5′ GCA TCT GGC ATC CTC TTG TT 3′	5′ CTT ATG ACC AGG TCC GAG TTG 3′
MMP-1	NM_032006	5′ GGA GAC CAT GGT GAC AAC AG 3′	5′ GGT CCA CGT CTC ATC AAG GT 3′
B-actin	V01217	5′ CTG TGC CCA TCT ATG AGG T 3′	5′ AGG AAG GAA GGC TGG AAG AG 3′
Integrin α1	BC014765	5′TTG GCT TCT CAC CGT TAT CC 3′	5′CCA GTT CTT GCT TTG GGT TG 3′
Integrin β1	NM_010578	5′CGG GGT ATT TGT GAA TGT GG 3′	5′GTG AGA TTG AAG TGG GAG CA 3′
Paxillin	BC025493	5′TTC TCC CCA CGC TGC TAC 3′	5′ TAC GCT TTG CCG TCC TTC 3′
FAK	AB030035	5′AGC AAG AAG AAC GGA TGA GG 3′	5′ CCT GGT AGT GAT TGG TCT GG 3′
GAPDH	BC083080	5 ACC AAC TGC TTA GCC C 3′	5′ CTT CCC GTT CAG CTC T 3′

Figure 1 Cell attachment, distribution and proliferation inside Dextran/PLGA scaffold: (A) 3 h, (B) 1 day, (C) 3 days and (D) 5 days after seeding. Samples were stained with crystal violet. Cross-sections of hematoxylin stained cells laden Dextran/PLGA scaffold: At 1 day (E), and 3 days (F), after seeding. A–D: 100×magnification; E–F: 400×magnification.

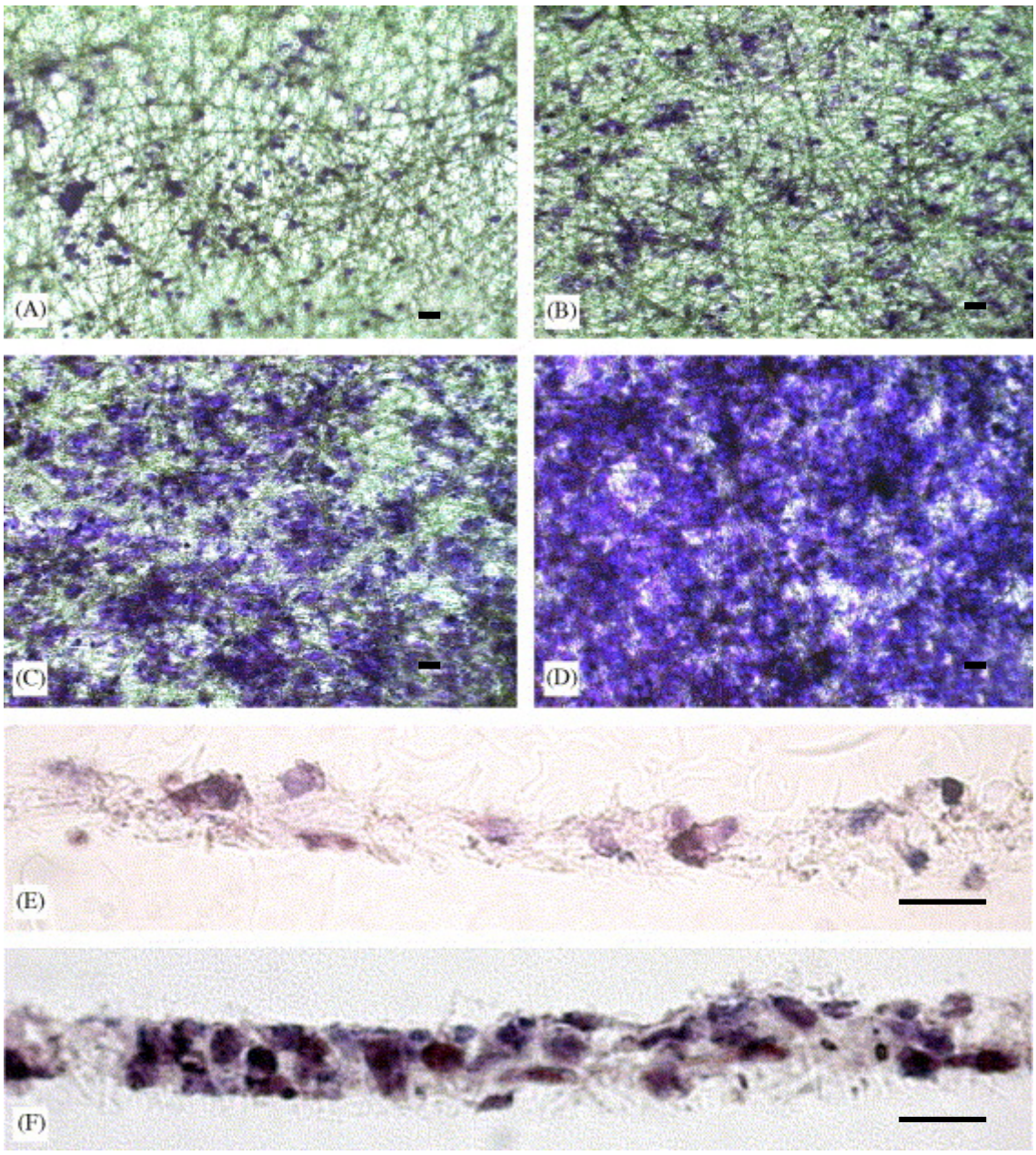

Figure 2 MTS assay of the cell proliferation inside Dextran/PLGA scaffold.

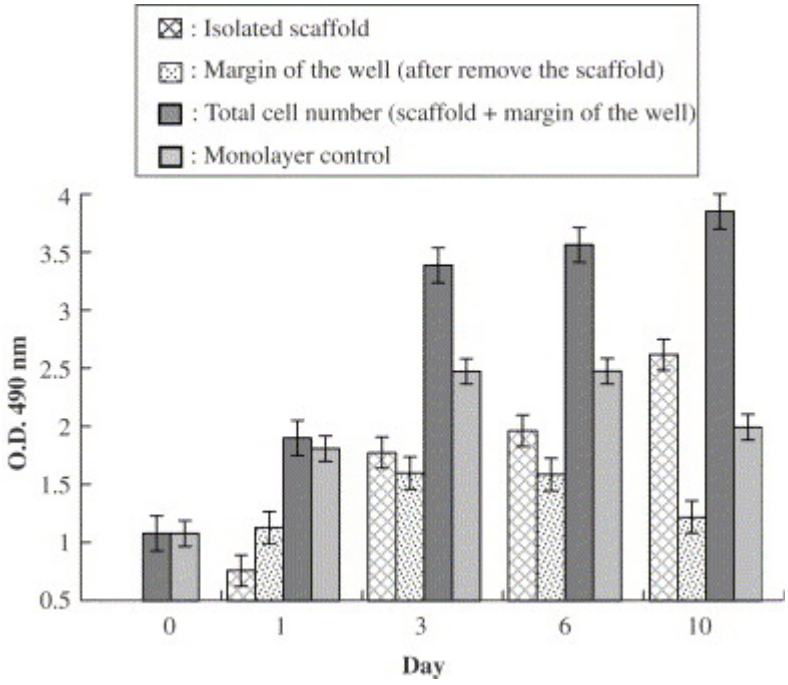

Figure 3 Migration of cells from the coverslips to the Dextran/PLGA scaffold: (A) the left side of the image that was originally covered by cell culture. After 2 days of incubation, the coverslip was removed, and cells on the scaffold were stained with crystal violet. (B) Migration of cells to scaffold 3 days after incubation. (Black arrows: original borderline of the coverslip.) (C) Quantification of cell migration in Dextran/PLGA scaffolds by MTS Assay.

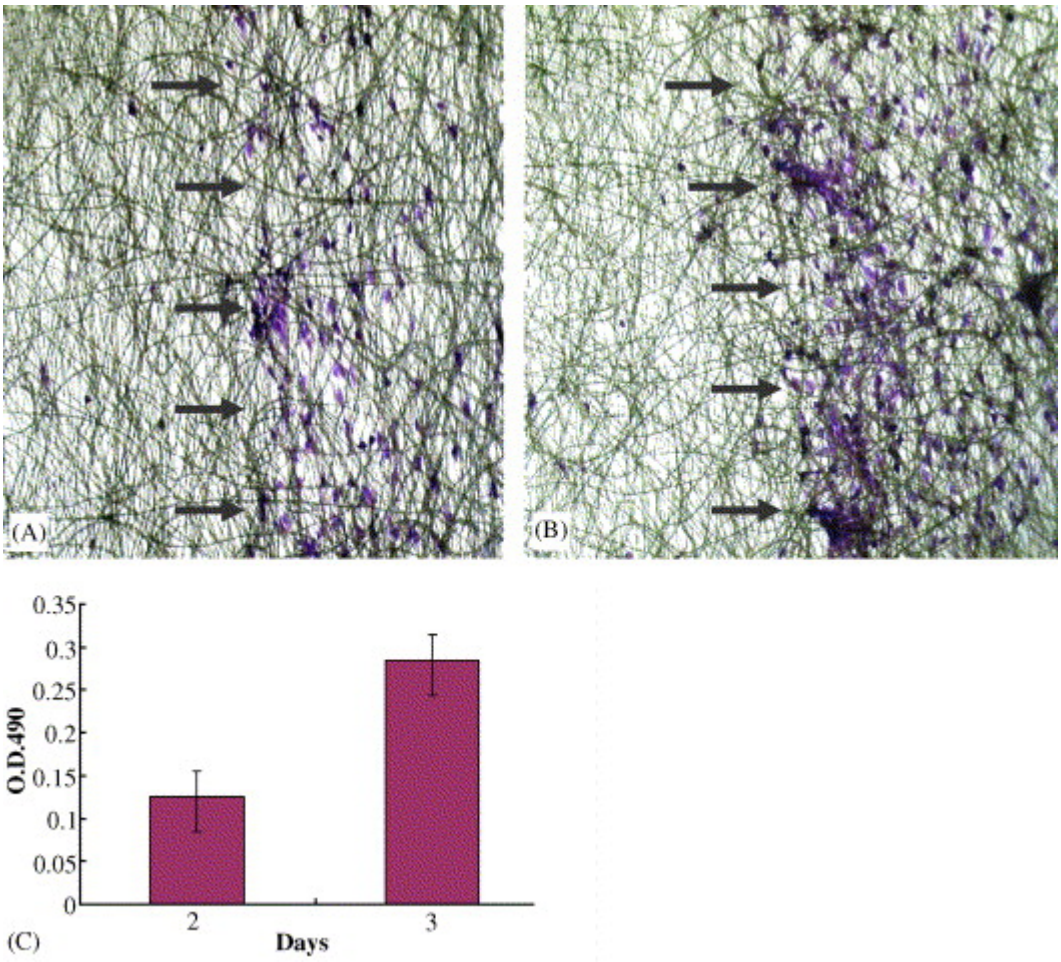

Figure 4 Fibroblasts deposition of ECM proteins in Dextran/PLGA scaffold: (A)–(C) Collagen production: (A) The extent of collagen production by cells in the scaffold (right) appeared to be the same as that of the cells of the monolayer control on day 1 (left). Increasing collagen production was apparent by day 3 (B), and day 5 (C). (D) Elastin production of the cells in the scaffold (right) was the same as the cells on the monolayer control on day 1 (left). 200×magnification.

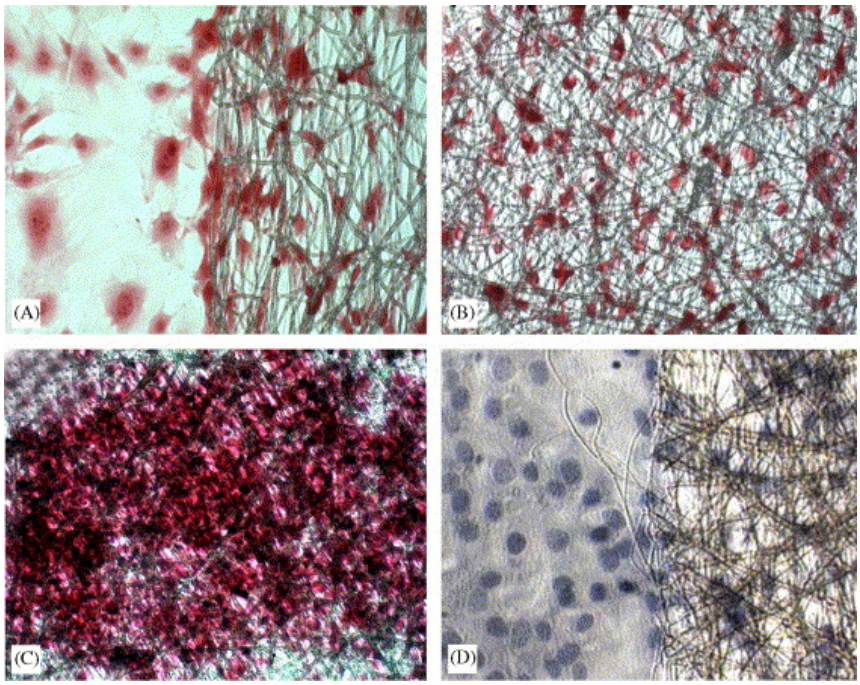

Figure 5 SEM scanning of ECM deposition by dermal fibroblast on a Dextran/PLGA scaffold 3 days after seeding: (A) Pristine scaffold (scale bar: 1 μm) and (B) scaffold filled with ECM (scale bar: 20 μm).

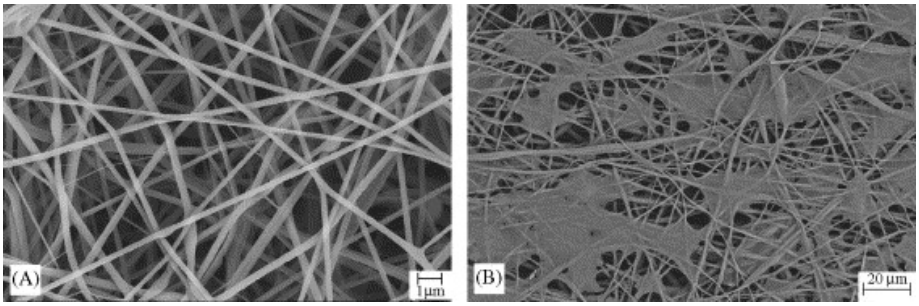

Figure 6 Collagen gel contraction assay: (A) Collagen gel contractions were monitored at 0, 4 and 24 h after gelation. (a) The Dextran/PLGA scaffold were embedded in collagen gels that were seeded with cells; (b) cell-laden collagen gels but without scaffold; (c) collagen gels with scaffold embedded but without cells; and (d) blank collagen gel control without cells and scaffold. (B) Area changes of the collagen gels at 4 and 24 h after gelation.

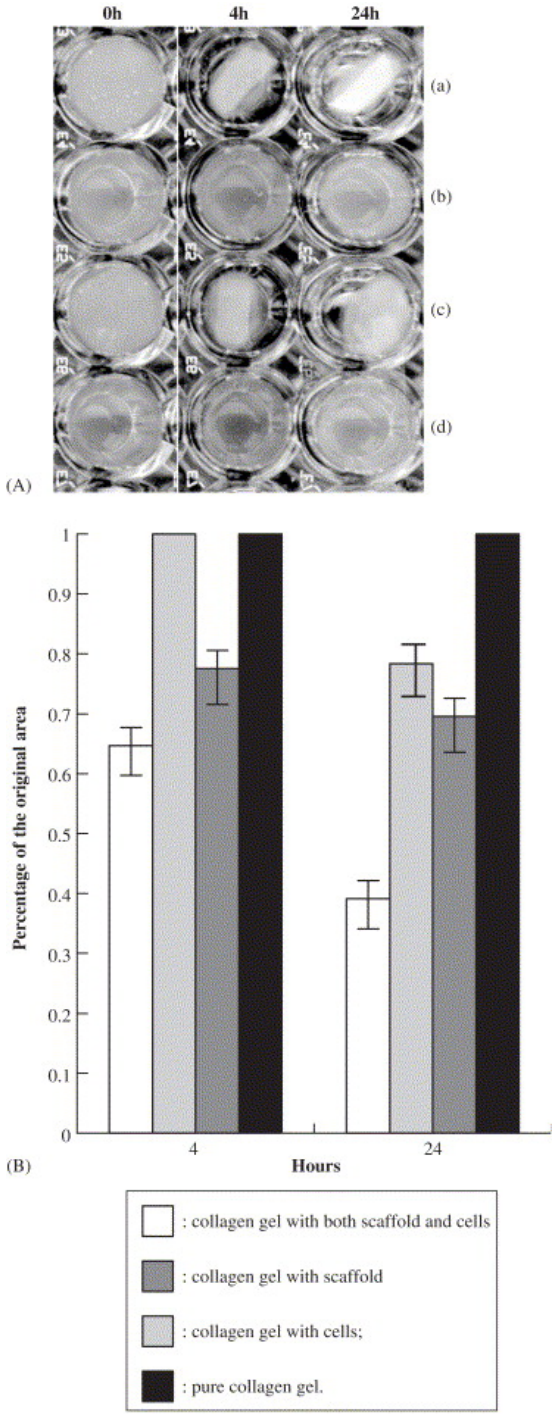

Figure 7 F-actin staining of the cells: (A)–(D) 20× magnification. (A) Cells on the plastic culture well; (B) cells in the Dextran/PLGA scaffold; (C) cells in the collagen gel; (D) cells in the scaffold that was embedded in the collagen gel; and (E) and (F) 100× magnification. (E) Cell on the plastic culture well and (F) cell inside the scaffold.

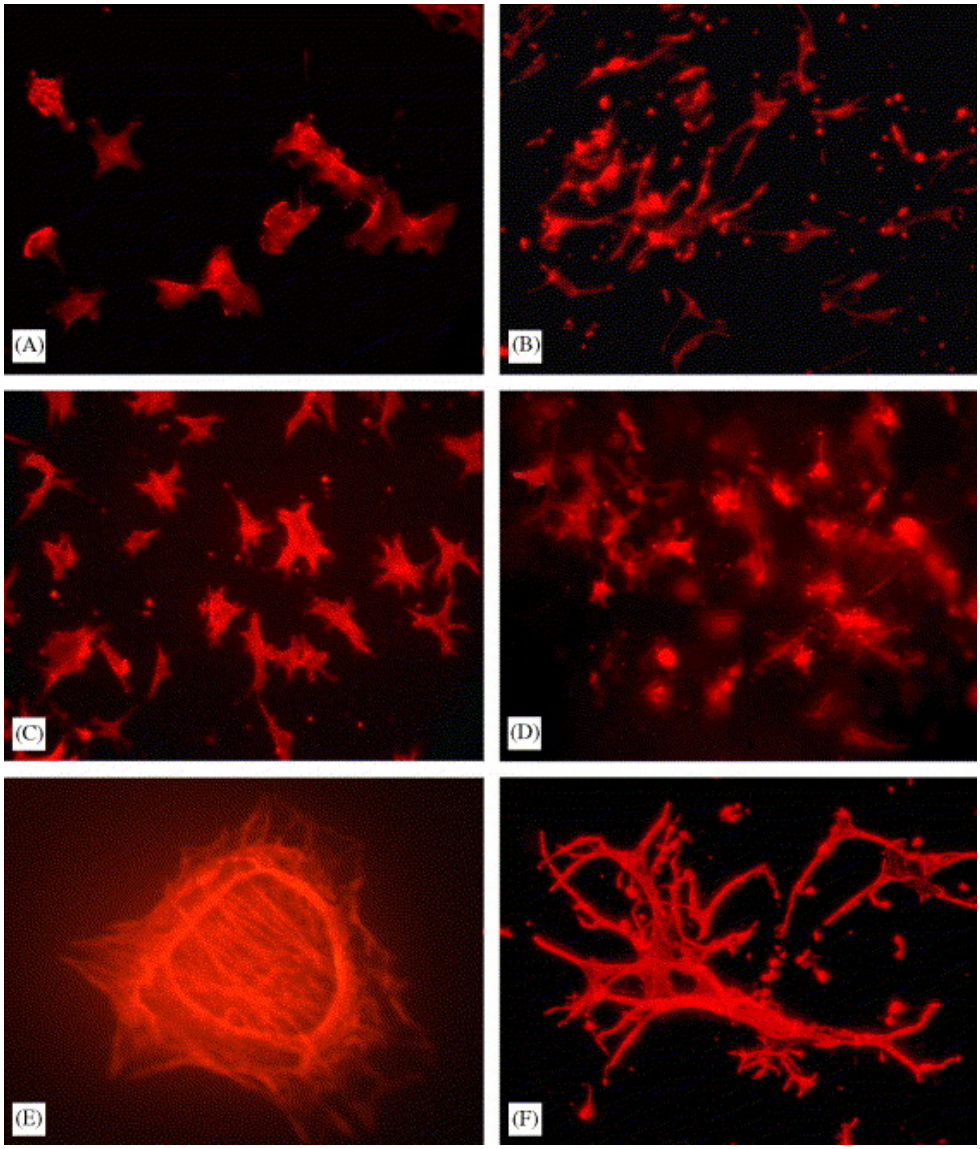

Figure 8 Relative quantitative real-time PCR analyses of gene expressions of cells in Dextran/PLGA scaffold.

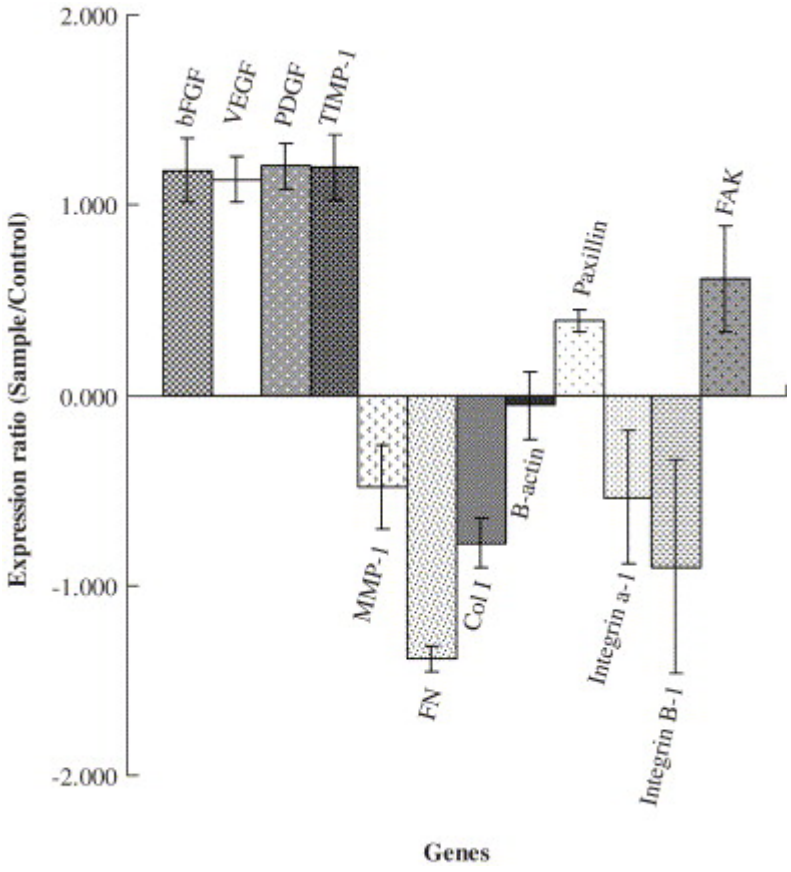

Chapter 4 Specific aim 2

Specific aim 2: Evaluation of the biocompatibility and immunocompatibility of electrospun Dextran/PLGA scaffold using an *in vitro* fibroblast/macrophage co-culture mode.

4.1. Materials and Methods

4.1.1. Fibroblast/macrophage co-culture model

M.DUNNI mouse dermal fibroblasts (CRL-2017) (ATCC, Manassas, VA, USA) were maintained in DMEM medium (Gibco Grand Island, NY, USA) supplemented with 10% fetal bovine serum (Hyclone, Logan, UT, USA) and 1% Penicillin-Streptomycin solution (Gibco Grand Island, NY, USA). RAW 264.7 macrophages (ATCC, Manassas, VA, USA) were cultured in DMEM containing inactivated fetal bovine serum (Hyclone, Logan, UT, USA) and 1% Penicillin/Streptomycin. Passages two to twenty were used for the experiments.

Scaffolds (~0.8 cm^2) were rinsed with PBS twice, cleaned with ethanol, and deposited in sterile 48-well plates. Fibroblasts and macrophages were mixed at a ratio of 1:1 (200 μL, 1×10^4 cells/mL each) and seeded onto the scaffolds. The controls included co-cultured cells (200 μL, 1×10^4 cells/mL each) without scaffolds, macrophages and fibroblasts, individually (200 μL, 1×10^4 cells/mL each), with and

without scaffolds. All samples (n=8) and controls (n=8) were incubated in DMEM containing inactivated fetal bovine serum at 37 °C under a humidified atmosphere of 5% CO_2 / 95% air and the media were changed every two days.

For quantitative assays, data were normalized with cell numbers (determined by cell counting) or with protein concentrations determined by a BCA™ assay kit (Pierce, Rockford, IL, USA). For all fluorescent signal quantitative assays, phenol red-free DMEM media were used 2 days before data collection, while pristine scaffolds in cell culture medium served as the blanks for fluorescent calibration. In all *in vitro* assays of testing macrophage activation and inflammatory responses, serum free DMEM media were used 2 days before data collection and macrophages (400 μL, 1×10^4 cells/mL) in the absence of scaffolds but cultured with lipopolysaccharide (LPS) (1 μg/mL in DMEM) for 20 hours were set as the positive controls. Images of cell morphology, distribution, proliferation, viability, and all histological stainings were observed with an inverted phase contrast microscope (Axiovert 200M, Zeiss, Munich, Germany) and images were acquired with Axiovision 4 imaging software (Zeiss, Jena, Germany).

4.1.2. Cell attachment and morphology

Cell-laden scaffold samples were withdrawn 7 days after cell seeding, rinsed with PBS twice, fixed with 10% formalin for 10 min, and stained with 0.1% crystal violet (in 200 mM boric acid, pH 8.0) for 3 min (16). Attachment of the two cell types to the scaffold (top view) and their corresponding morphologies were visualized (16).

4.1.3. Distribution of two cell types

The F4/80 antigen is one of the best markers for mature macrophages and can be used to distinguish macrophages from fibroblasts in the co-culture samples. Briefly, all samples collected at day 7 were rinsed with PBS twice and fixed with 10% formalin. Cell-laden scaffolds were embedded in Tissue-Tek® OTC (Sakura Finetek, Torrance, CA, USA) and snap-frozen in liquid nitrogen; cross-sections (10 μm) were cut on a cryostat (Jung/Frigocut 2800-N, Leica, Wetzlar, Germany), rinsed with PBS and blocked with 4% horse serum for 30 min. Samples were stained with rat anti-mouse F4/80 antibody (5 μg/mL) (eBioscience, San Diego, CA, USA) at room temperature, incubated with a secondary anti-rat antibody (1:500) (eBioscience, San Diego, CA, USA) for 30 min, and color-developed with ABC-AP kit (Vector, Burlingame, CA, USA). The distribution patterns of each cell type on the surface and in the interior of the scaffolds were assessed.

4.1.4. Dynamics of two cell populations

Flow cytometry was used to monitor the varying ratio of each cell population under the influence of scaffold over the culture span (day 7 and 21) in the co-culture samples. Briefly, fresh cells were collected at week 1 and 3 after seeding and were incubated with FITC-anti-mouse F4/80 antibody (0.5 μg for a million cells in 100 μL of PBS) (eBioscience, San Diego, CA, USA) for 30 min. After rinsed in PBS twice, cells were re-suspended in 1% formalin and analyzed with a FACScan flow-cytometer (BD BioSciences, San Jose, CA, USA). The dynamics of cell populations were expressed as the ratio of each cell type in the whole cell population.

4.1.5. Cell proliferation and long-term cell viability

The non-cytotoxicities of both the scaffold and its degradation byproducts were assessed by monitoring cell proliferation and their long-term viability in the presence of Dextran/PLGA scaffolds for 8 weeks. Numbers of living cells were quantified by MTS assay (CellTiter 96® aqueous non-radioactive cell proliferation assay kit, Promega, Madison, WI, USA)(16). 400 μL (1×10^4 cells/mL) of each cell type were used when macrophages and fibroblasts were cultured alone, with or without scaffold; whereas 200 μL (1×10^4 cells/mL) of each cell type were used when co-cultured. Samples were taken at day 1, 2 and 4, and week 1, 2, 3, 4, 5, 6, 7 and 8, respectively.

4.1.6. Live/dead staining

Live/Dead staining assay (Molecular Probes, Eugene, OR, USA) were performed to illustrate the viability of cells residing in scaffolds directly. One week after seeding, cell-laden scaffolds were rinsed with PBS twice and incubated in 200 μL of Live/Dead dye for 10 min. Living cells appeared as green and dead cells appeared as red.

4.1.7. Oxidative burst assay

The intracellular oxidative capacity (an indication of macrophage activation) of macrophages in the presence of scaffolds was assessed by modifying a method described previously (80, 96). Briefly, samples were treated with a 15 μM 2'7'-dichlorofluorescein (DCFH)-diacetate (Sigma, St. Louis, MO, USA) in DMEM on day 1 and 7, respectively, after cell seeding. After rinsed with PBS twice, cells were lysed in 0.1% Triton X-100 (Sigma, St. Louis, MO, USA) in PBS, and the

fluorescent activity in the sample was quantified every 90 seconds for 25 min at 504/530 nm by a fluorescence microplate reader (Cytofluor 4000; PerSpective Biosystems, Framingham, MA, USA). The results were expressed as percentage of fluorescence intensity relative to macrophages stimulated with LPS (positive control).

4.1.8. Nitric oxide production

Nitric oxide production, as a gauge of both the duration and magnitude of inflammatory potential, were monitored for 8 weeks in the presence of scaffolds (70). Cell culture media were collected at day 2, week 1, 2, 4, 5, and 8, respectively, and mixed with Griess agent (in nitrite-free water) in equal volume for 15 min. The colorimetric absorbances at 540 nm were then recorded with a microplate reader (EL 800, Bio-Tek, Winooski, VT, USA).

4.1.9. High throughput screening of inflammatory cytokines by antibody array

Inflammatory cytokine productions under the influence of scaffold were detected using RayBio® Mouse Cytokine Antibody Array 1.1 kits (RayBiotech, Norcross, GA, USA) (cytokine map in Table 2). Briefly, cell lysates were harvested and quantified at day 3, 7 and 21, respectively, after seeding.

The array membranes were blocked for 30 min in blocking buffer and incubated with cell lysates (250 ng) at room temperature for 1 h. Blots were rinsed with wash buffers, incubated with a biotin-conjugated IgG cocktail for 1 h and probed with IR800 Dye-streptavidin (Li-Cor Biosciences, Lincoln, NE, USA) for 1 h. After rinsing 3 times in TBST (Tris-buffered saline Tween-20) and once in PBS, the

membranes were scanned and analyzed using an Odyssey IR imager (Li-Cor Biosciences, Lincoln, NE, USA). The relative protein levels were normalized by subtracting the background staining and compared to the positive controls with the relevant analysis software (RayBiotech, Norcross, GA, USA). Signal ratio indicating unaltered cytokine expression was set between 2 and 0.5; signal ratio > 2 or < 0.5 was stipulated as regulated expression.

4.1.10. Evaluation of the scaffold with mice subdermal implant model

Scaffolds were pre-sterilized by incubating in ethanol prior to implantation. Male mice (25–30g) (n=4) were placed under the general anesthesia of isoflurane (2–4%) and a small dorsal incision was made, through which subdermal pockets were created. Sterilized scaffolds were inserted into the pockets and the incisions were closed with suture. Commercially available Vicryl® PLGA suture segments (Ethicon, Sommerville, NJ) were implanted as controls. All animals received humane care in compliance with protocols approved by the SUNY-Stony Brook university IACUC (protocol # 2006-1286). Animals were euthanized with CO_2 at stipulated time points (3, 7, and 21 days, post-surgery) and the tissues surrounding the implanted scaffolds were excised, sectioned, stained with H&E and anti-F4/80 antibody, respectively, and examined under a light microscope.

4.1.11. Statistics

Two-tailed Student's t-test was used to discern the statistical difference between groups. The significant level was set as $p<0.05$.

4.2. Results

4.2.1. Cell attachment, morphology and distribution

Fig. 1 A-C (top view of the scaffold) depicted crystal violet stained cell-laden Dextran/PLGA scaffolds for direct visualization of the attachment and morphology of macrophages and fibroblasts. Evidently, both cell types attached to the scaffold 1 week after seeding. Contrary to the highly stressed morphology of fibroblasts in the same scaffold we reported previously (16), macrophages in the scaffold did not show any morphological change as compared with their scaffold-free counterparts. Co-culture of fibroblast and macrophage did not influence the morphologies of either cell type. Macrophages were further labeled with the macrophage marker anti-F4/80 to facilitate the observation of the distribution of both the macrophage and fibroblast populations (Fig.1 D-F, J) residing in the scaffold. Figure 1 demonstrated that both cell types were scattered evenly throughout the fibrous scaffold. The distribution of each cell types was neither altered by the presence of scaffold nor by co-culturing.

4.2.2. Dynamics of two cell populations

The dynamics of the macrophage and fibroblast populations in the presence of the scaffold were monitored quantitatively by flow cytometry with FITC-anti-F4/80 antibody. Originally, fibroblasts and macrophages were seeded at a ratio of 1:1, but one week after cell seeding, this ratio changed to ~2:3 (Fig. 2A) in the presence of scaffold and stayed as ~1:1 in the absence of scaffold (Fig. 2B). At week 3, the ratio of fibroblasts to macrophages further elevated to ~3:7 (Fig. 2C) and ~2:3 (Fig. 2D) in the presence and absence of scaffold, respectively. The results suggested that macrophages became dominant in the whole co-culture populations in

the presence of Dextran/PLGA scaffold. Even in the absence of scaffold, macrophages were dominant in the co-culture samples over the entire culture span.

4.2.3. Long-term biocompatibility of the scaffold & its degradation byproducts

The results of Live/Dead staining (Fig. 1 G-I) depicted that the majority (>99%) of cells residing in the scaffold were alive, and thus confirmed the viability of cells when in direct contact with the scaffold. Co-culturing has no effect on the viability of individual cell types.

The results of live/dead staining were in a good agreement with those of MTS assays. Evidently, the viabilities and proliferation rates of both fibroblasts and macrophages were not affected by the presence of scaffold and its degraded byproducts over the 8 weeks culture span, as compared with the controls (Fig. 3). In fact, the numbers of co-cultured cells as well as that of fibroblasts alone was not significantly different from the corresponding controls. In contrast, the number of macrophages residing in the scaffolds was apparently higher than their scaffold-free counterpart. In concert with the flow cytometry data (Fig. 2), these results implied that the scaffold and its degraded by-products have stimulatory effect on macrophage proliferation but not on fibroblasts.

4.2.4. Oxidative burst

The results summarized in Fig. 4 indicated that using the scaffold-free control as a baseline, 1 day after cell seeding, 5.4±0.2% macrophages in the co-culture and 4.1±0.0% macrophages (cultured alone) were activated by the scaffolds; by day 7, the

corresponding levels of activations were 4.8±0.1% for the former and 1.6±0.3% for the latter. These findings were in good agreement with the morphological observations depicted in Fig. 1, that the scaffold did not promote visually distinguishable enlargement of macrophages indicative of their activation.

4.2.5. Nitric oxide production

The potential of the Dextran/PLGA scaffold to induce inflammation *in vivo* were evaluated through induction of NO production for 8 weeks. Evidently, exposure to the scaffold did not induce significantly increased levels of NO production; while macrophages stimulated with LPS produced very high levels of NO (see Fig. 5). The presence of fibroblasts did not appear to interfere with NO production by macrophages. The results were also in good agreement with the results reported in Fig. 1 (i.e., absence of FBGCs), suggesting that the scaffolds were both low in acute and chronic inflammatory potentials.

4.2.6. High throughput screening of inflammatory cytokines by antibody arrays

The results in Fig. 6 A-F and Table 2 indicated that none of the forty cytokines were regulated in macrophages, fibroblasts and co-culture samples after incubating with the scaffolds for 3 days. However, one week after exposure to the scaffold, macrophages alone expressed higher levels of MIP-1 gamma (CCL9) (2.09) compared with their counterpart with no exposure to the scaffold (Fig. 6 I and J). IL 10 (2.77) and SDF-1 (CXCL12) (2.14) were up-regulated in fibroblasts (Fig. 6 K and L). Co-culture samples secreted higher MIP-1 gamma (2.24) and RANTES (CCL5)

(2.06) under the influence of scaffold (Fig. 6 G and H). Interestingly, three weeks after cell seeding, RANTES were markedly upregulated in both fibroblast sample (5.34) (Fig. 6 Q and R) and co-culture sample (5.36) (Fig. 6 M and N), while MIP-1 gamma were upregulated in macrophage samples (2.41) (Fig. 6 O and P) and co-culture samples (5.34) (Fig. 6 M and N).

4.2.7. *In vivo* evaluation with a mouse subdermal implantation model

The biocompatibility and immunocompatibility of the scaffolds were evaluated in mice subdermal implant models (Fig. 7). The gross appearance (not shown) of the implanted site suggested that the scaffolds and their degradation byproducts were very benign to the hosts. Lacking redness or edema adjoining the implants indicated that they did not induce extensive acute inflammatory responses; and there was no sign of tissue necrosis (Fig. 7 A), which strongly correlated with the *in vitro* findings.

Infiltration of neutrophils and monocytes/macrophages was noticeable three days after implantation (data not shown). One week post-implantation, the scaffolds were evidently encapsulated by very thin fibrous tissues (Fig. 7 A and B), inside which fibroblasts and macrophages were easily identified by their morphologies (Fig. 7 B), and by staining with anti-F4/80 (Fig. 7 D). Thin collagenous capsule and lack of foreign body giant cells suggested that the inflammation was both mild and transient. In contrast, the tissue in direct contact with the implanted poly-lactide-co-glycolide (Vicryl™) sutures, as controls, showed intense inflammation with conspicuous cell infiltration and enclosure by thick fibrous capsules (Fig. 7C). Three week

post-implant, more macrophages were found inside the implanted scaffold and much of the scaffold was replaced by loose connective tissue (with fibroblast as the predominant cell type), and could not be easily distinguished from the intact loose connective tissues (data not shown). This suggested a full recovery of the implant site with absence of macrophages implied subsiding of inflammation.

4.3. Discussion

Biocompatibility is both fundamental and crucial for designing implantable biomaterials (97). Issues concerning the safety and durability of biodegradable materials utilized in medicine, particularly for long-term applications, have yet to be adequately addressed. For example, the degradation byproducts of biocompatible polymers may induce adverse effects; this was epitomized by a number of reports (39, 75, 84, 98) showing long-term degradation of polyurethanes resulting in generating various diamines that are putative carcinogens. Therefore, the time span of cell-material interaction (and hence, their viability) has important implications in evaluating the toxicity potential of biomaterial and an insufficient time span may not show any undesirable effect of the degradation byproducts on cells (79). In many reports concerning biocompatibility assessments, cells were usually cultured with the concerned biomaterials for relatively brief durations, however, the actual time required for complete material degradation were substantially longer in general. In this study, cells were cultured and thus, in direct contact with the Dextran/PLGA scaffold, for up to eight weeks in order to assess its long-term biocompatibility.

The history of safety and biocompatibility of PLGA and dextran have been

well-documented. It is known that PLGA degrade into lactic acid and glycolic acid, and eventually into carbon dioxide and water (18); dextran could be metabolized into carbon dioxide as well (73). However, in order to prepare the Dextran/PLGA scaffold, a minor modification of dextran was needed to enable solid state photo-crosslinking, thereby stabilizing the composite scaffold and rendered it insoluble in water. The results of MTS assay and live/dead staining assay suggested that the photo-crosslinked Dextran/PLGA electrospun scaffolds and its degraded byproducts were non-toxic to fibroblasts and macrophages, therefore, suggesting good biocompatibility. Ideally, biomaterials should not exert any influence on the attachment, morphology as well as spatial distribution of residence cells as these characteristics are closely related to cell functions. Our results (Fig. 1) indicated that the scaffold did not influence the attachment, morphology and distribution of macrophages as well as fibroblasts, these results are supportive of its favorable biocompatibility.

Macrophages can be activated by numerous stimuli such as LPS, IFN-γ, and particles/materials (19). Upon activation, macrophages profoundly alter their morphology and metabolism to modulate inflammatory responses and defense against invasions (20). Activated macrophages are characterized by increased respiratory burst, measured as enhanced release of superoxide anion (O^{2-}) or hydrogen peroxide (99). The results of oxidative burst assay suggested that the scaffolds activated only a small subset of macrophages. Different degrees of maturation would lead to their functional heterogeneity which is comparable to the resident macrophages in tissues

after mild stimulations (42). In addition, fibroblasts appeared to prolong macrophage activation in the presence of scaffold at day 7. This was consistent with the finding that at later stage of culture, in the fibroblast/macrophage co-culture sample, scaffold stimulated higher lysozyme production, indicative of macrophage activation (88). It was previously reported that fibroblasts released low amounts of reactive oxygen species in response to potent phagocyte stimuli (43); however, in our study, increased H_2O_2 level was not detectable in fibroblast samples either in the presence or absence of scaffold, suggesting that the stimulus induced by scaffold was very mild. Furthermore, the production of reactive oxygen species, if in surplus, is associated with severe inflammation and has deleterious effect on cells and, thus, tissues (92, 100). The low level of oxidative burst induced by the Dextran/PLGA scaffold implies its potential of inducing minimal undesirable reaction to cells/tissues upon implantation. Moreover, in specific aim 3, we showed that macrophages alone degraded the scaffold faster than fibroblasts, whereas the scaffold exhibited the fastest degradation under the coordination of the two cell types (88). Since the extend of macrophages activation reflected the scaffold degradation rate (88), as an oxidative stress (46), H_2O_2 production induced by the scaffold may also be involved in breaking down biomaterials.

The roles of NO in inflammatory response are well-documented and NO excretion by macrophages rises markedly under inflammatory stimuli, particularly LPS and INF-γ (61). Prolonged presence of NO results in chronic inflammation (85) and NO in excess is damaging to tissues (101). In addition, contrary to normal

fibroblasts, wound fibroblasts are known to secrete NO to regulate their synthetic functions (102). The results of our study have shown that the scaffold did not evoke significantly higher NO production, which suggested low potentials to evoke both acute and chronic inflammation. It was reported that the majority of biomaterials elicited enhanced NO productions (103-105), whereas, some biocompatible materials such as chitinous materials (91) could activate macrophages but invoked undetectable NO production which enable these materials to be utilized as drug carriers especially those targeting macrophages and anti-inflammation. The results reported here implied that Dextran/PLGA scaffold has the potential to be used not only as soft tissue substitutes but also as specialized drug carriers.

Both fibroblasts and macrophages are capable of expressing multiple regulatory molecules including cytokines, growth factors, chemokines, and cell surface antigens, etc., which enables them to modulate their microenvironment and also to respond to environmental cues in a complex manner (18, 106). Cytokines signal both the action and pace of inflammation and consequently, the net effect of inflammatory response is determined by the balance between pro-inflammatory and anti-inflammatory cytokines (106). Most previous studies related to biomaterials were focused mainly on production of pro-inflammatory cytokines induced by biomaterials (94, 107, 108). Quantitative profiling of cytokines released by fibroblasts/macrophages could be a predictor of potential adverse immunological effects of biomaterials.

Over three weeks of culturing, there were no noticeable differences in the

productions of principle pro-inflammatory cytokines such as IL-1 alpha, IL-1 beta, IL-6, TNF alpha and IFN-gamma etc. (106). Existence of multinucleated giant cells typically reflects chronic inflammation (95). Recently, IL-4 (54, 95), IL-13 (95), IFN-gamma (95) and MCP-1(109) had also been implicated as potential inducers of macrophage fusion and foreign body giant cells formation. In our study, there was no change in the production of these cytokines and this could explain the absence of FBGC throughout the entire culture span (Fig. 1). Besides, the low levels of macrophage activation induced by the scaffolds (Fig. 4) could be attributed to the missing of cytokine stimuli such as IFN-gamma and IL-4/IL-13 for classical and alterative macrophage activations, respectively (110). The results obtained from cytokine profiling strongly suggested that the Dextran/PLGA scaffold did not induce severe acute and chronic inflammatory responses, which were in good agreement with the results of NO production evoked by scaffolds (Fig. 5).

The up-regulated cytokines evoked by the scaffolds were mainly chemokines that are involved in both acute and chronic inflammation. Their general role is to mediate the recruitment and homing of cells, but they also act as co-stimulators of cell growth (111). Macrophages are known to express receptors for SDF-1, MIP-1 gamma and RANTES (112, 113). Our findings could explain the observation that macrophages were the dominant cell type in the co-culture samples as indicated by flow cytometry results (Fig. 2), as well as the higher proliferation rate of macrophages detected by the MTS assay (Fig. 3). In general, the number of mobilized and recruited macrophages influence both the intensity and duration of host response as well as the

stability of biomaterials (18). However, based on the findings in this investigation, the increased amount of macrophages did not appear to be inflammatory. It is known that during acute and chronic inflammation, the macrophage population is consisted of different subsets that can be characterized as resting/residence macrophages, acute inflammatory macrophages, and proliferative /reparative /anti-inflammatory macrophages (114). In addition, the dynamics of these sub-populations depended upon the type of biomaterial present (115, 116). Therefore, the results of this investigation suggested that macrophages incubated with the scaffold could be involved in performing other functions. In fact, the results from specific aim 3 has shown that the Dextran/PLGA scaffold almost degraded completely after 8 weeks of *in vitro* incubation and macrophages contribute most in its degradation (88). It was reported that good biodegradability of biomaterials is generally associated with low potential of inducing chronic inflammation (82). Our results further support the correlation between the biocompatibility and biodegradability of the scaffold, which suggesting that the increased amount of macrophages may mainly be responsible for scaffold degradation.

Dextran/PLGA scaffolds influenced cytokine productions by fibroblasts, macrophages as well as the co-cultures. However, the cytokine production profiles in the co-culture samples did not simply reflect the combination of cytokine releases from samples cultured with either fibroblasts or macrophages, per se; this suggested a synergistic interaction of the two cell types in dealing with the Dextran/PLGA scaffolds.

Fibroblasts were actively involved in modulating the inflammatory responses to the scaffold by releasing high level of the major anti-inflammatory cytokine IL-10, which could inhibit the synthesis of pro-inflammatory cytokines like IFN-γ, TNF-α, IL-2, IL-3 and GM-CSF, etc. (106); moreover, they also produced the chemokines such as, RANTES and SDF-1, to maintain the recruitments of lymphocytes, including macrophages, to the inflammation sites (68). Interestingly, RANTES and SDF-1 are known to play important roles in resisting HIV-1 infection (117, 118). These results suggested that the Dextran/PLGA scaffold is not bioinert but rather, bioactive, which has potential for broader applications such as delivery anti-infection drugs and enhancing their efficacies.

In this study, the *in vivo* findings showed that macrophages and fibroblasts were two predominant cell types in the capsule encasing implanted scaffold, which further validated the usage of macrophages and fibroblasts as a co-culture model in this investigation. The results from our *in vitro* assays indicated that the scaffold induce H_2O_2 but not NO production, which was consistent with the report of an *in vivo* study using a rodent air pouch model to evaluate various polymeric biomaterials (87). The results from histopathological analyses of the implanted scaffold indicated very benign tissue responses, which was in good agreement with the *in vitro* results. Taken together, the fibroblast/macrophage co-culture model could simulate the *in vivo* environment which enabling mechanistic study of the interactions between scaffold with macrophages and fibroblasts, separately or cooperatively. More importantly, the co-culture model could be utilized as a facile *in vitro* screening tool to evaluate the

biocompatibility of implantable materials such as tissue substitutes and delivery vehicles for drugs, genes, proteins, and cells.

4.4. Conclusion

The Dextran/PLGA scaffold did not affect the morphology, attachment, proliferation and viability of both fibroblasts and macrophages, cultured separately or together. The scaffold activated only a small subset of macrophages but did not induce either severe acute and chronic inflammatory response. Additionally, fibroblasts played a role in prolonging macrophage activation in the presence of scaffold. Using antibody arrays, IL-10, SDF-1, MIP-1 gamma and RANTE, were found to be up-regulated when cells were incubated with the scaffold. The results of *in vivo* subdermal implantation of the Dextran/PLGA scaffold further confirmed its good biocompatibility and immunocompatibility. The fibroblast/macrophage co-culture model is adequate to simulate the *in vivo* environment and could be further developed into a more optimal *in vitro* model for initial evaluation of biomaterials as well as their interactions with host tissues.

Table 1: Scheme of inflammatory cytokine antibody array

Pos	Pos	Pos	Pos	Blank	BLC	CD30L	Eotaxin	Eotaxin-2	Fas Ligand	Fractalkine	GCSF
Neg	Neg	Neg	Neg	Blank	BLC	CD30L	Eotaxin	Eotaxin-2	Fas Ligand	Fractalkine	GCSF
GM-CSF	IFNγ	IL-1α	IL-1β	IL-2	IL-3	IL-4	IL-6	IL-9	IL-10	IL-12p40p70	IL-12p70
GM-CSF	IFNγ	IL-1α	IL-1β	IL-2	IL-3	IL-4	IL-6	IL-9	IL-10	IL-12p40p70	IL-12p70
IL-13	IL-17	I-TAC	KC	Leptin	LIX	Lymphotatin	MCP-1	MCSF	MIG	MIP-1α	MIP-1γ
IL-13	IL-17	I-TAC	KC	Leptin	LIX	Lymphotatin	MCP-1	MCSF	MIG	MIP-1α	MIP-1γ
RANTES	SDF-1	TCA-3	TECk	TIMP-1	TIMP-2	TNFα	sTNFR1	sTNFRII	Blank	Blank	Pos
RANTES	SDF-1	TCA-3	TECk	TIMP-1	TIMP-2	TNFα	sTNFR1	sTNFRII	Blank	Blank	Pos

Figure 1 The morphology, attachment, distribution, and viability of macrophages and fibroblasts in the scaffolds, cultured either together or alone after 1 week, respectively. (A-C) Crystal violet staining; (D-F) anti-F4/80 antibody staining; (G-I) Live/Dead staining; green: living cells; red: dead cells; (A, D, G) Fibroblast/macrophage co-culture; (B, E, H) Macrophages; (C, F, I) Fibroblasts. J: Cross-section of cell-laden scaffold. Arrow: Macrophages; Star: Fibroblasts. Scale bar: (A-F) 50 μm; (G-I) 100 μm; (J) 200 μm

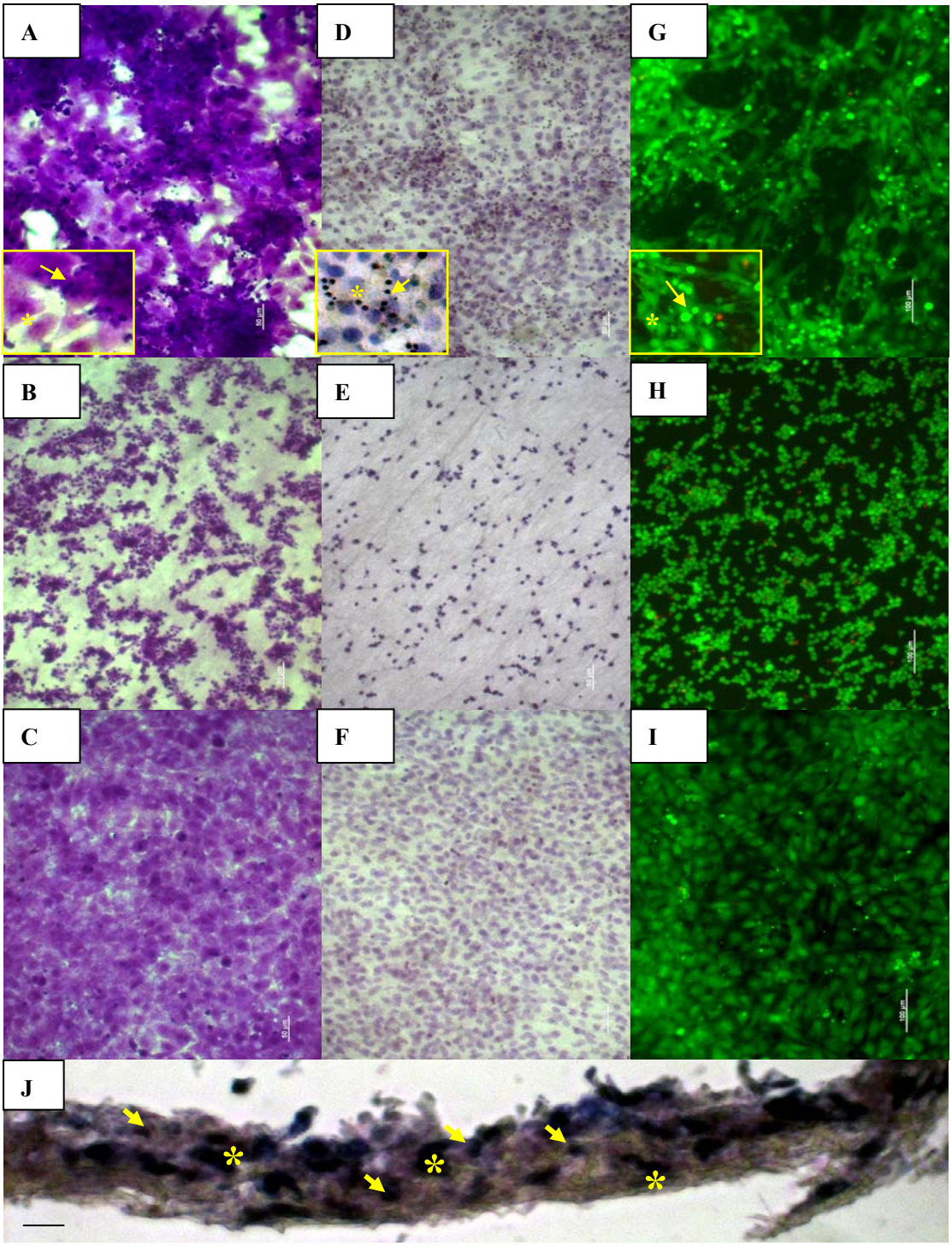

Figure 2 Flow cytometry analyses of the dynamics of macrophage population in the fibroblast/macrophage co-culture exposed to Dextran/PLGA scaffold at week 1 and 3, respectively. (A-B): 1 week and (C-D) 3 weeks after cell seeding; (A, C) in the presence of scaffold; (B, D): in the absence of scaffold. R1: Fibroblasts; R2: Macrophages; R3: Total population.

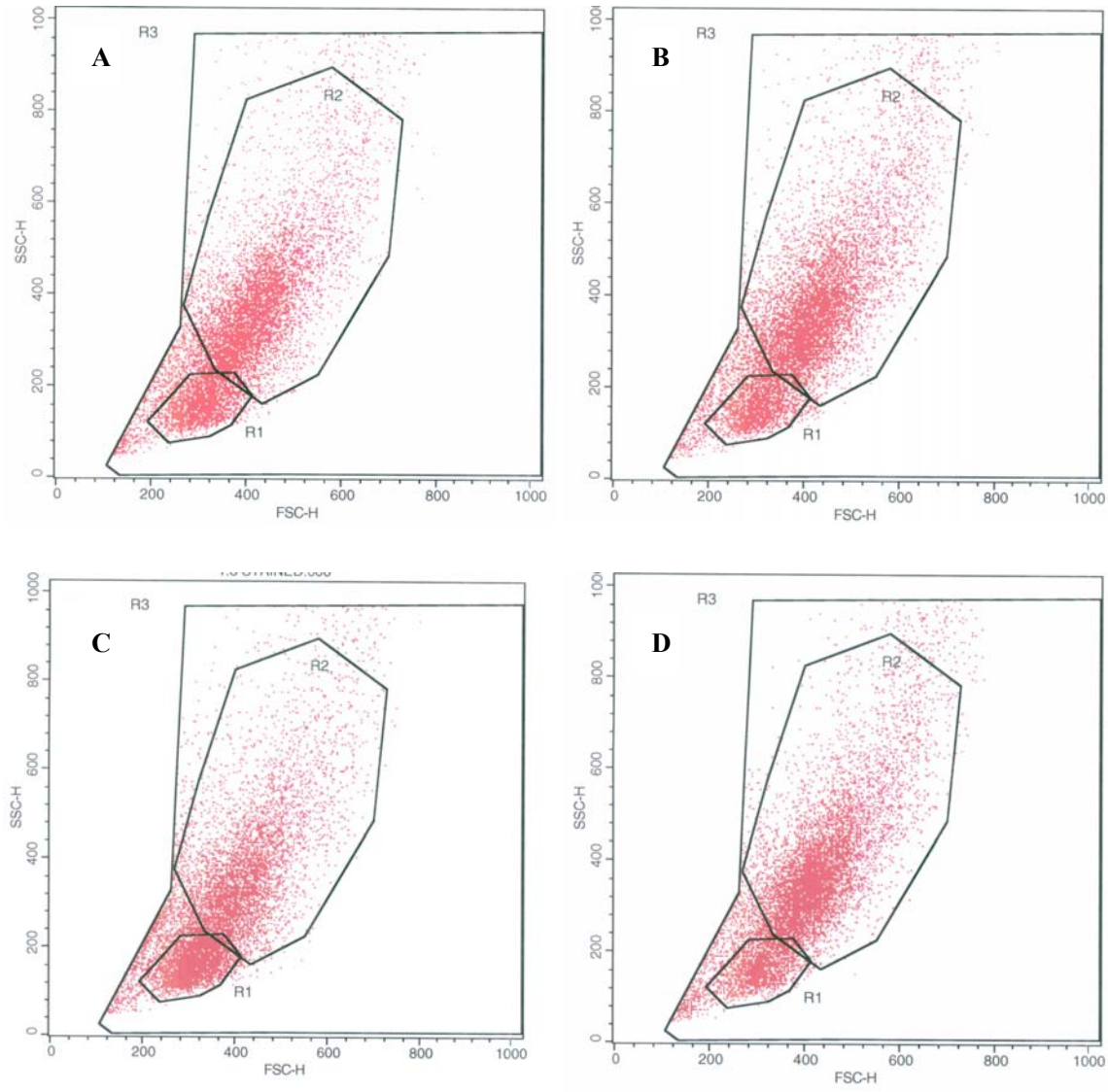

Figure 3 MTS assay for evaluating the biocompatibility of Dextran/PLGA scaffold

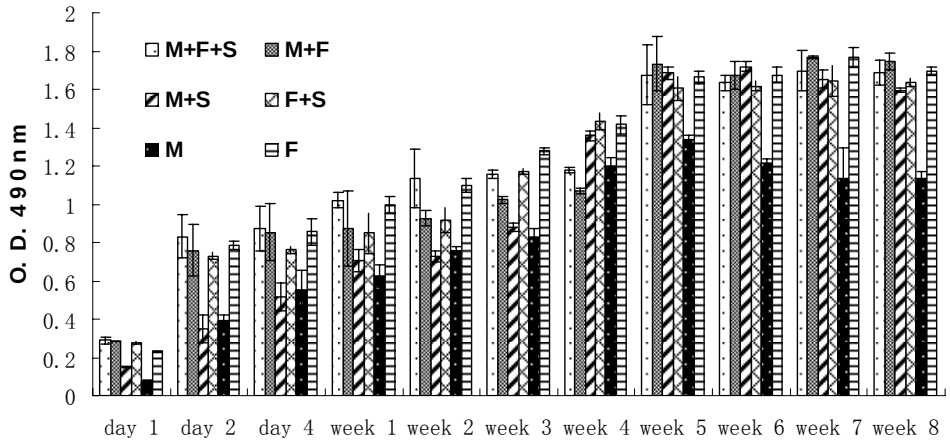

Figure 4　Oxidative burst induced by scaffold at day 1 and 7.

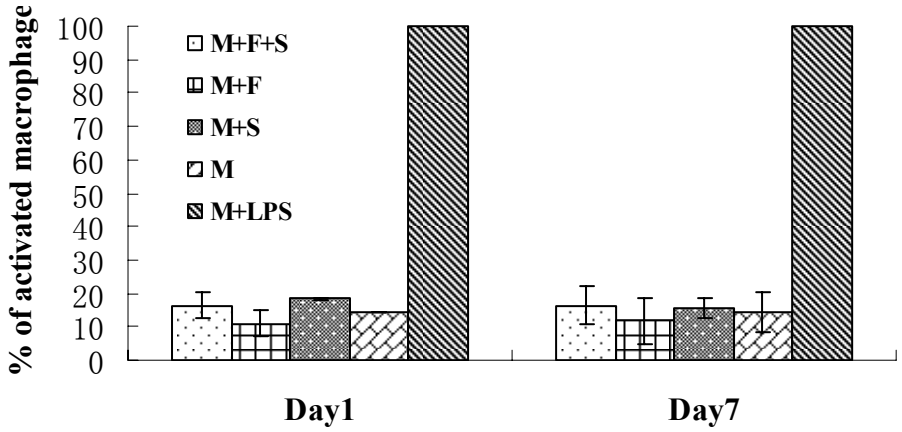

Figure 5 Nitric oxide production triggered by Dextran/PLGA scaffold

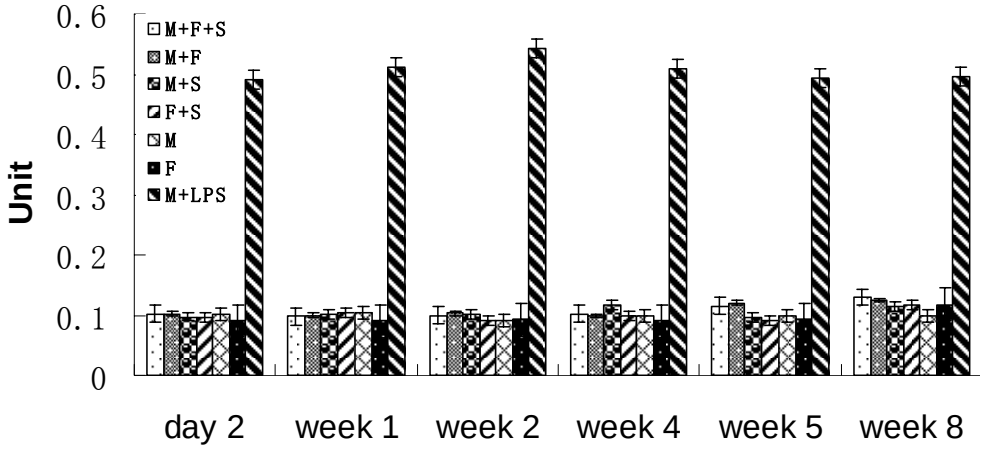

Figure 6 The effects of Dextran/PLGA scaffold on inflammatory cytokines. (A-F) day 3; (G-L) week 1; (M-R) week 3. (A, G, M) Macrophage + Fibroblast + Scaffold; (B, H, N) Macrophage + Fibroblast; (C, I, O) Macrophage + Scaffold; (D, J, P) Macrophage; (E, K, Q) Fibroblast + Scaffold; (F, L, R) Fibroblast.

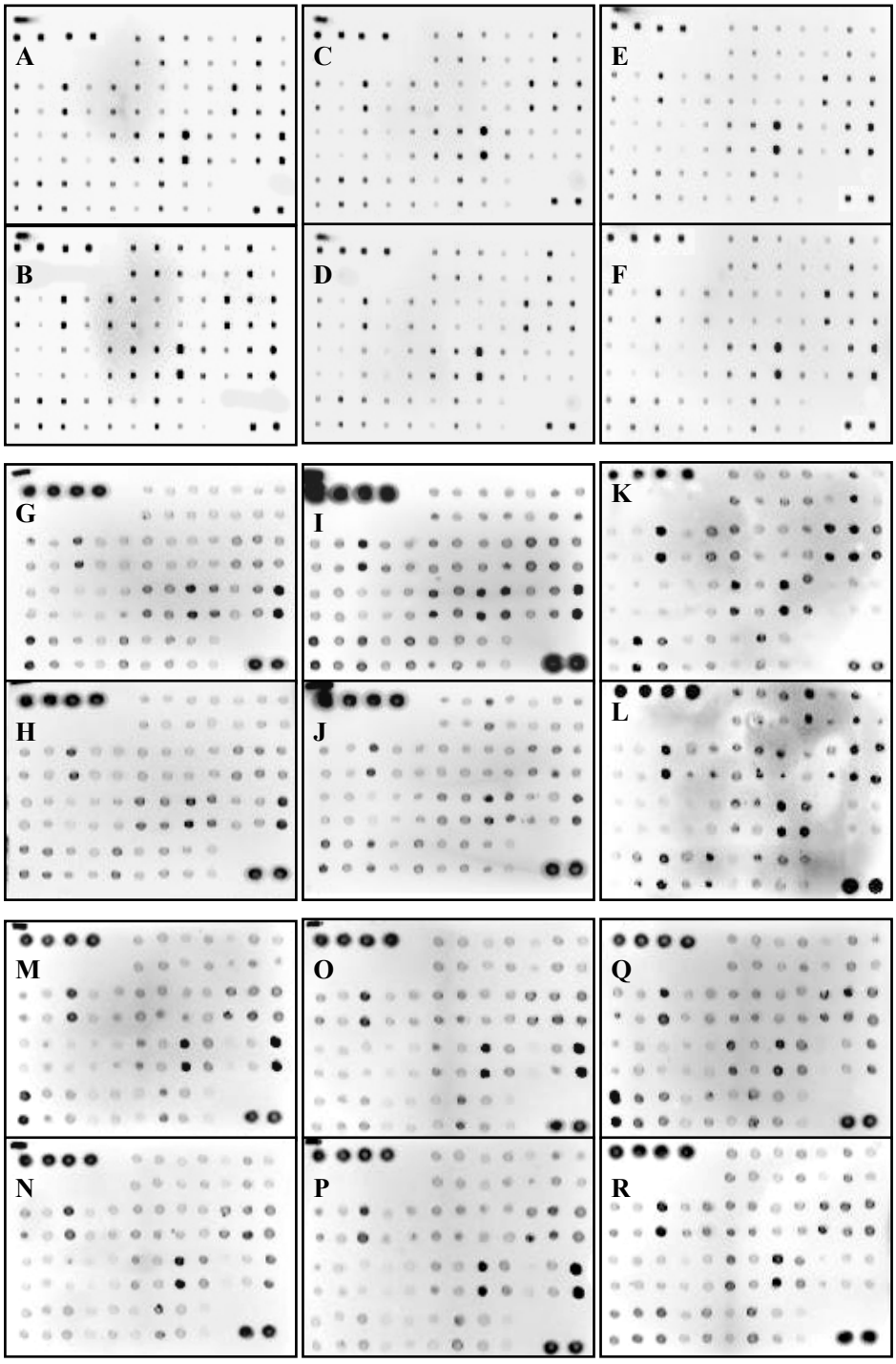

Table 2 Summary of cytokine expression ratios as compared with baselines in the antibody arrays. Bold: expression ratio over 2

Cytokines	Day 3			Week 1			Week 3		
	F +M+S	M +S	F +S	F +M+S	M +S	F +S	F +M+S	M +S	F +S
BLC	0.83	0.72	0.82	1.06	1.04	0.88	1.21	1.14	0.88
CD30L	0.77	1.07	0.66	1.26	0.77	1.01	1.47	1.02	1.46
Eotaxin	0.74	0.82	0.66	0.93	0.58	0.40	1.29	0.97	1.31
Eotaxin-2	0.92	1.28	0.74	0.99	0.66	0.62	1.21	0.99	1.07
FAS ligand	0.92	0.96	0.99	1.18	1.25	1.26	1.25	1.00	1.04
Fractalkine	0.75	0.79	0.74	1.06	1.35	1.34	1.23	1.04	1.27
G-CSF	0.92	0.72	0.99	1.11	0.84	0.79	0.98	0.62	0.38
GM-CSF	0.84	1.20	1.11	1.25	0.94	1.27	0.78	1.18	1.14
IFN-gamma	0.92	0.96	0.99	1.02	0.79	0.89	1.15	0.95	1.30
IL1-alpha	0.85	1.01	0.88	0.98	1.01	1.03	1.18	1.00	1.04
IL1-beta	0.74	0.96	0.66	1.26	1.17	0.85	1.18	1.14	0.94
IL2	0.92	0.96	0.66	1.19	0.67	0.82	1.07	1.25	0.81
IL3	0.92	0.96	1.18	1.15	1.23	0.79	1.22	1.13	0.93
IL4	0.92	0.96	0.99	0.92	1.30	1.07	1.22	1.23	1.03
IL6	0.92	0.96	1.48	1.16	1.06	1.15	1.14	1.16	1.36
IL9	0.92	0.96	0.99	1.02	1.02	1.00	1.14	1.16	1.04
IL10	0.82	0.75	0.85	1.04	1.73	**2.77**	1.23	0.98	1.11
IL12-p40/p70	0.92	0.96	0.99	1.09	1.76	1.20	1.14	0.97	1.34
IL12-p70	0.92	0.89	1.15	1.11	1.77	1.75	1.15	0.97	1.21
IL13	0.92	0.96	0.99	0.92	1.30	1.07	1.22	1.23	1.03

		92	.96	.99	89	.38	.01	98	.98	.08
	IL17	1.	0	0	1.	0	1	1.	0	1
		38	.96	.99	06	.94	.08	27	.96	.35
	I-TA	1.	0	0	0.	0	0	0.	1	0
C		05	.96	.99	92	.94	.87	92	.49	.88
	KC	0.	0	0	0.	1	0	0.	1	1
		92	.96	.99	90	.41	.88	86	.12	.23
	Lepti	0.	0	0	1.	0	1	1.	0	1
n		81	.96	.99	11	.82	.09	25	.79	.04
	LIX	0.	0	0	1.	1	1	1.	1	1
		81	.82	.90	02	.35	.19	12	.10	.26
	Lymp	1.	1	0	1.	0	1	0.	0	1
hotactin		06	.13	.90	04	.93	.07	87	.84	.11
	MCP-	0.	0	1	1.	0	0	1.	1	0
1		84	.92	.14	17	.79	.85	20	.35	.99
	M-CS	0.	0	0	1.	0	0	1.	0	1
F		92	.96	.99	26	.99	.85	15	.89	.41
	MIG	0.	0	0	1.	0	0	1.	1	1
		92	.72	.66	24	.54	.96	07	.12	.23
	MIP-1	0.	1	1	1.	1	1	1.	1	1
-alpha		99	.05	.05	96	.35	.04	29	.18	.41
	MIP-1	1.	0	0	**2.**	**2**	0	**3.**	**2**	1
-gamma		17	.96	.94	**24**	**.09**	.93	**83**	**.41**	.71
	RAN	0.	0	1	**2.**	0	1	**5.**	0	**5**
TES		92	.96	.13	**06**	.78	.26	**36**	.96	**.34**
	SDF-1	1.	0	0	0.	1	**2**	1.	1	1
		00	.96	.74	98	.03	**.14**	47	.07	.34
	TCA-	1.	0	1	1.	0	0	1.	0	1
3		00	.96	.23	02	.96	.69	16	.89	.09
	TEC	0.	0	0	1.	1	0	1.	0	1
K		66	.96	.99	11	.43	.99	19	.89	.08
	TIMP	0.	0	0	1.	1	0	1.	1	1
-1		92	.96	.99	02	.03	.67	00	.23	.01
	TIMP	0.	0	0	1.	1	1	1.	1	1
-2		69	.96	.99	26	.16	.41	07	.04	.23
	TNF-	0.	1	0	1.	0	0	0.	0	1
alpha		92	.32	.99	17	.66	.92	93	.98	.38
	sTNF	0.	1	1	1.	0	1	1.	0	1
RI		92	.20	.23	25	.79	.30	18	.89	.29
	sTNF	0.	0	0	1.	0	1	1.	1	1
RII		92	.96	.99	11	.84	.23	22	.02	.23

Figure 7 *In vivo* evaluations in mice 1 week post-implantation. (A, B) H&E staining of the implanted Dextran/PLGA scaffolds; (C) H&E staining of the implanted Vicryl® PLGA suture; D: Anti-F4/80 staining of the implanted Dextran/PLGA scaffolds; star: implants; red arrow: collagenous capsule; yellow arrow: fibroblasts; blue arrow: macrophage; scale bar: 50 µm.

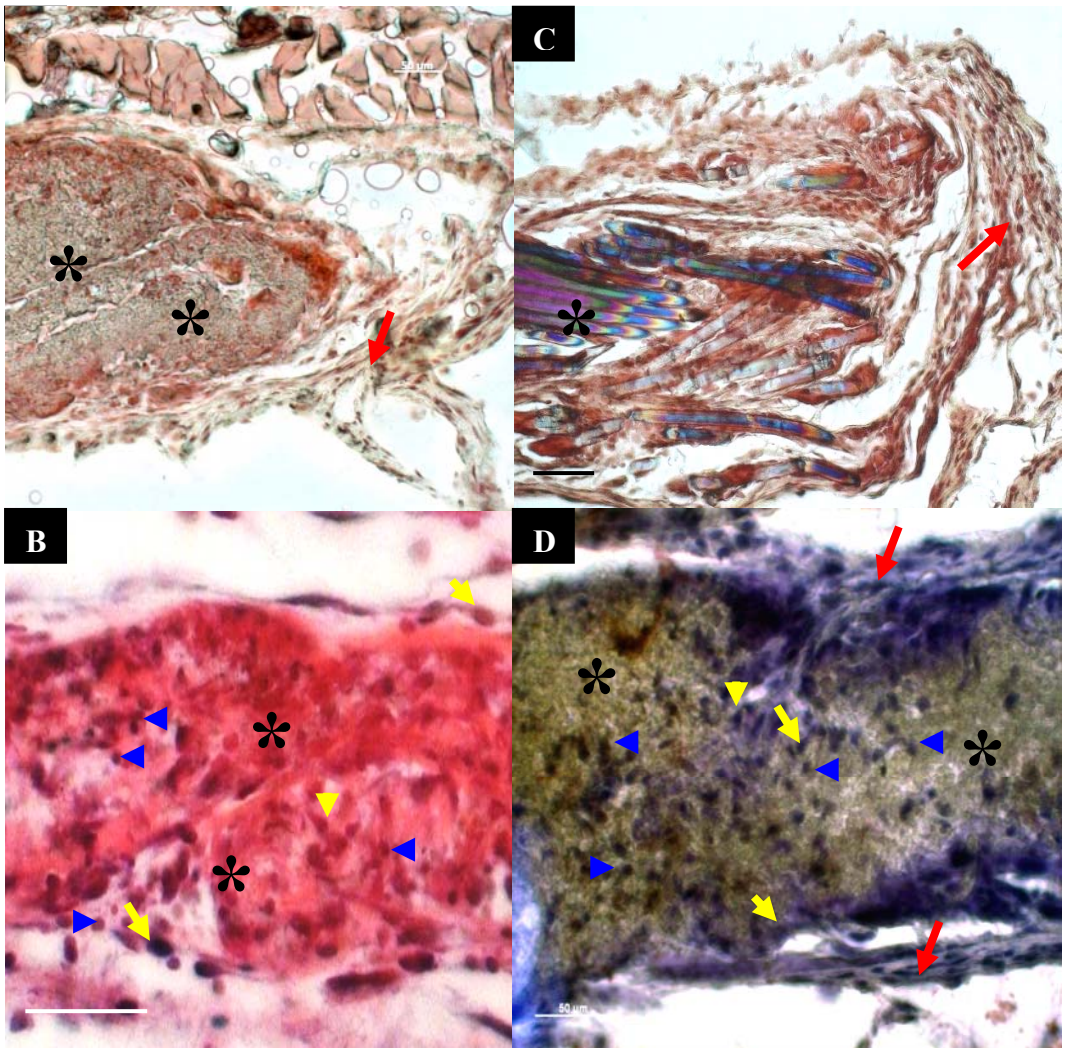

Chapter 5 Specific Aim 3

Specific aim 3: Evaluation of the biodegradability of electrospun Dextran/PLGA scaffold using an *in vitro* fibroblast/macrophage co-culture model.

5.1. Materials and Methods

5.1.1. Fibroblast/macrophage co-culture model

Co-culture model was established following the method described in specific aim 2.

Scaffolds ($\sim$0.8 cm^2) were rinsed in ethanol and deposited in 48-well plates. Equal numbers of fibroblasts and macrophages were seeded (2000 cells, each) on the scaffolds. The controls included co-cultured cells (2000 cells, each) without scaffolds; macrophages and fibroblasts, individually (2000 cells, each) with and without scaffolds. All samples (n = 8) and controls (n = 8) were incubated in DMEM with inactivated fetal bovine serum and the media were changed every 2 days. Samples were collected at day 3, 7, and 21, respectively, for enzyme activity assays and receptor studies. Two days before sample collection, phenol red-free media were used for all fluorescent signal assays and serum-free media were used for all enzyme and receptor studies, respectively. For quantitative results, data were normalized with cell

numbers or with total protein concentrations determined by BCA assay (Pierce, Rockford, IL, USA). Images were acquired with an inverted light microscope (Axiovert 200M, Zeiss, Munich, Germany) and analyzed by Axiovision 4 imaging software (Zeiss, Jena, Germany).

5.1.2. Scaffold morphological change and dry weight lost

Cell-laden scaffolds were retrieved at weeks 4 and 8, respectively, rinsed twice in PBS, and incubated with trypsin solution at 37 ºC under agitation for 10 min. After further vigorous agitation on a vortexer, the detached cells were removed. Subsequently, the scaffolds were incubated in proteinase K solution (0.5 mg/mL) (Promega, Madison, WI, USA) for 15 min to remove all cell-secreted proteins and the proteins in cell culture media adsorbed to the scaffold fibers. Pristine scaffolds subjected to the same treatments were used as controls. Scaffolds were rinsed in water extensively and air dried. The dry weight lost of the degraded scaffolds were monitored and their morphological changes (both the surface and the interior) were examined under a scanning electron microscope (LEO/Zeiss 1550, Zeiss, Munich, Germany) following a method described by us previously (16). For comparison, scaffolds incubated in PBS and cell culture medium under the same incubation conditions, respectively, were used as controls.

5.1.3. pH value variation

Cell culture media were collected from each sample group (n=20) at day 3 and day 21 after seeding, respectively, and their pH values were measured by a micro pH electrode (Lazar, Los Angeles, CA). The pH value of pure cell culture media

incubated under the same conditions as other samples was set as the baseline (arbitrarily set as 0). All data were validated with the pH decline of the corresponding scaffold-free controls.

5.1.4. Enzyme activity assays

Non-specific esterase activity: The experiment was performed following manufacturer's protocol for α-Naphthyl Acetate Non-Specific Esterase assay (Sigma, St. Louis, MO, USA). Briefly, 1 ml of sodium nitrite was mixed with 1 ml of fast blue BB base solution included in the kit, and the admixture was blended with 40 ml of pre-warmed water (37°C). Thereafter, 5 ml of TRIZMAL buffer and 1 ml of naphthyl acetate solution were added. Formaldehyde pre-fixed samples were incubated in the reagent mixture for 30 min at 37°C in dark. The stained specimens were evaluated semi-quantitatively under a microscope. The color intensity of stained samples was scored by another observer and numerical rating of 1 to 5 was assigned according to the following criteria: 1 = negative, 2 = sporadic detection, 3 = sparse but consistent, 4 = uniformly present and 5 = intense and widespread.

Lysozyme activity: Cell culture media were collected and the lysozyme activities were determined with EnzChek® Lysozyme Assay Kit (Molecular Probes; Eugene, OR, USA). Media were diluted in 50 µL of assay buffer and were mixed with 50 µL of fluorescein-conjugated *Micrococcus lysodeikticus* for 30 min at 37ºC. The fluorescence intensities were measured at 494/518 nm and the lysozyme activities of experimental samples were determined from the standard curve.

α-glucosidase activity: 10 µL of cell culture supernatant was mixed with 100

μL of 6 mM 4-methylumbelliferyl- alpha -D-glucoside (Sigma, St. Louis, MO, USA) (in 0.1 M citric acid, 0.2 M Na_2HPO_4, pH6.0) and incubated at 37ºC for 1 hour. The reaction was terminated with 2 mL of glycine buffer (0.2 M, pH 10.5) and the fluorescent intensity was recorded by a fluorescence microplate reader (Cytofluor 4000; PerSpective Biosystems, Framingham, MA, USA) at 365/445 nm (83).

β-glucosidase activity: After the cells were rinsed with 80 μL of PBS, 80 μL of acetate buffer (0.2 M, pH 4) were added to each well. Then, 100 μL of 6 mM 4-methylumbelliferyl-beta-D-glucoside (Sigma, St. Louis, MO, USA) were incubated with each sample as substrate at 37ºC for 1 hour. The assay was terminated by adding 2 mL of glycine buffer (0.2 M, pH 10.5) and the fluorescent signal was measured by cytofluor at 365/445 nm (119).

Collagenases/gelatinases activity: Detection of total collagenases/gelatinases activities with an EnzChek® Gelatinase/Collagenase Assay Kit (Molecular Probes; Eugene, OR, USA) was performed according to manufacturer's instructions. In brief, cell culture supernatants prepared in the substrate buffer at different dilutions (final volume: 100 μL), were incubated with 20 μL of fluorescent-labeled gelatin substrate in 80 μL of buffer for 24 hours at room temperature in dark. The fluorescent intensity was quantified at 495/515 nm. The enzyme activities in the samples were determined by comparing them with the activities of collagenase standards.

Hyaluronidases activity: 0.5 mL of potassium hyaluronate (4 mg/mL in PBS, pH 5.3) was added to 0.3 mL of cell culture supernatant and incubated for 30 min at

room temperature. The reactions were stopped by adding 5 mL of acid albumin (pH 3.75) at 37 ºC for 10min. Reduction in liquid turbidity at 600 nm was measured with a microplate reader (EL 800, Bio-Tek, Winooski, VT, USA) and the enzyme activity was calculated by referencing a standard plot of hyaluronidase (Sigma, St. Louis, MO, USA) (120).

5.1.5. Real-time PCR

Cells were collected and re-suspended in cell lysis buffer (Stratagen, La Jolla, CA, USA). Real-time PCR was performed with LightCycler (Roche, Mannheim, Germany) using the Brilliant® 2 step QRT-PCR Kit (Stratagen, La Jolla, CA, USA). PCR primers were summarized in Table 1. Analysis of PCR results followed the same method described in specific aim 1.

5.1.6. *In vivo* evaluation with mice subdermal implant model

Male mice (25–30 g) (n=4) were anesthetized with isoflurane (2–4%) and a small dorsal incision was created. After being pre-sterilized by ethanol, scaffolds were placed into the pockets and the incisions were sutured. All animals received humane care in compliance with a protocol approved by the SUNY-Stony Brook University IACUC (protocol number 2006-1286). Animals were euthanized by CO_2 at 3, 7, and 21 days post-surgery and the explanted scaffolds were sectioned, stained with H&E, and examined under a microscope. Likewise, explanted scaffolds were processed and their morphological changes were evaluated by SEM.

5.1.7. Statistics

All experimental results were presented as mean ± standard deviation.

Whenever appropriate, Student's t-test was used to discern the statistical difference between groups. The significant level was set as $p<0.05$.

5.2 Results and discussion

5.2.1. Scaffold morphological change and dry weight lost

Morphological changes of the degraded scaffolds were monitored by SEM and the results were depicted in Figure 1. Comparing with the smooth fibers of the pristine scaffold (Fig.1 J), the scaffolds incubated with cells for 4 weeks exhibited a morphology of abundance of pores in concert with an apparent increase in fiber surface roughness signifying obvious loss of material mass (Fig. 1A: fibroblasts, 1C: macrophages, 1E: co-culture). Moreover, the fibers in scaffold interior (Fig. 1 I: fibroblasts) showed virtually identical porous appearance suggesting a uniform pattern of degradation. The interior of scaffolds with macrophages and co-cultures, respectively, showed similar morphology (data not shown) as those incubated with fibroblasts. Compare to dextran, PLGA is known to be more resistant to degradation; thus, it could be inferred that the pores observed on the fibers were caused by preferential degradation of dextran leaving the remnant fibers composed mostly of PLGA. Moreover, scaffold degradation inevitably led to some extent of loss of crosslinking contributing to scaffold structural stabilization, which could explain the observed slight shrinkage of the scaffolds and smaller pore sizes (Fig.1 I). In contrast, after being incubated in PBS for 4 weeks, scaffolds showed very moderate change in fiber surface morphology as indicated by the small defects appearing (Fig. 1H) (scaffolds in cell culture medium data not shown, but actually identical to Fig. 1H), suggesting that the degradation rates of the scaffolds incubated in PBS was clearly slower than those of the cell-mediated processes although PLGA is known to undergo

auto-hydrolysis in aqueous environment (18). Initial breakdown of scaffold fibers resulted in the creation of surface defects leading to entrance of water, salts and enzymes into the bulk, thereby, hastening the degradation process (18). Evidently, 8 weeks after cell seeding, the sizes of pores on the fibers, indicative of degradation, increased considerably due to further erosion of the fibers' bulk (Fig. 1B, D, F), suggesting the exponential nature of scaffold degradation.

Figure 1 demonstrated that both fibroblasts and macrophages were capable of degrading the Dextran/PLGA scaffolds. Due to the phagocytotic nature of macrophages and the broader arrays of enzymes and oxidants they produced, it was not surprising that scaffold degradation mediated by macrophages was significantly faster than that mediated by fibroblasts. This was exemplified by the general disparity in both the sizes and distribution of pores on the scaffold fibers in concert with the fiber diameters (comparing Fig. 1A and 1C with Fig. 1B and 1D). Fibroblasts are known to secrete many hydrolases and capable of functioning as non-professional phagocytes (45), however, to our knowledge, it has not been reported in the literature that fibroblast, per se, is capable of digesting biomaterials, particularly, fibrous electrospun scaffolds. Results in specific aim 1 demonstrated by us that fibroblasts could deposit ECM inside the Dextran/PLGA scaffold (16). The turnover of ECM could evoke increased production of enzymes that may lead to accelerating scaffold degradation. Furthermore, we had also shown that dermal fibroblasts attached to the Dextran/PLGA scaffolds induced contraction by exerting continuous stress on the scaffold fibers (16), which could hasten scaffold degradation. Interestingly, the pattern

of fibroblast mediated scaffold degradation was similar to that produced by the macrophages (Fig. 1 A-D), suggesting that the two types of cells broke down the scaffold through similar enzyme-mediated mechanisms.

Evidently, fibroblasts and macrophages act synergistically in accelerating the breakdown of scaffold. As shown in Fig. 1F, 8 weeks after cell seeding, the scaffold had generally lost its fibrous network structure with an obvious decrease in pore sizes and the diameters of remnant fiber strands were apparently smaller. In addition, the scaffolds incubated in the co-culture samples lost approximately 75% of their original dry mass after 8 weeks with dramatic increase in brittleness, which further confirmed Dextran/PLGA scaffold degradation. The dry weight loss of scaffold after 8 weeks of incubation in PBS was about 40%, which strongly corroborated with the degradation rate deduced by analyzing the SEM scaffold morphology. The higher rates of scaffold degradation under the influence of cells further underscored the mechanisms of cell-mediated degradations such as enzymes, mechanical stress, etc.

5.2.2. pH value drop in the cell culture media

Many biodegradable polymers are designed to break down into biologically benign and progressively smaller oligomers. It is known that PLGA degrades into lactic acid and glycolic acid, and eventually into carbon dioxide and water (18). Dextran could also be metabolized into carbon dioxide (73). However, with pK_a value 3.86 and 3.83, respectively, both lactic acid and glycolic acid are not mild acids, which can alter the local pH once released from the degraded polymer. This could induce adverse tissue responses including production of free radicals and thus

accelerated aging, chronic inflammation, tissue necrosis and other complications (18). Additionally, local pH altered by acidic degradation byproducts, in turn, could further accelerate the polymer degradation (18). Therefore, it is important to determine the extent of pH drop induced by the degradation of the Dextran/PLGA scaffold.

After validated with scaffold-free samples (Fig. 2), in the presence of scaffold, 3 days after cell seeding, the relative pH drop in co-culture sample was 0.061±0.004, whereas the relative pH drop of the samples cultured with macrophages and with fibroblasts alone sample were 0.035±0.003 and 0.009±0.002, respectively. Three weeks after cell seeding, in the presence of scaffold, the pH drop in co-culture sample was 0.129±0.003, while in macrophages and in fibroblasts alone sample were 0.286±0.001 and 0.112±0.002, respectively. These results suggested that macrophages played a dominant role in scaffold degradation, with fibroblasts also playing a contributory role. In general, the significant drops in pH at week 3 appeared to be a good reflection of the exponential increase of scaffold degradation. At a later stage of scaffold degradation, pH drop detected in the co-culture samples was lower than that of its counterpart cultured with macrophages alone, which suggested that fibroblasts and macrophages interacted to buffer the environment they reside in locally, thereby contributing to the maintenance of pH stability in spite of the presence of scaffold degradation byproducts. Furthermore, although the degraded products of scaffold are not mild acids, cell-mediated degradation of the scaffold caused very modest pH decline which would less likely induce unfavorable effects on cells. In specific aim 2, we were able to show that Dextran/PLGA scaffold was very biocompatible and did

not influence the viabilities of macrophages and fibroblasts (89). The mild pH value drops induced by scaffold degradation contributed to its good biocompatibility. The results also suggested that the pH drop was not the leading mechanism of scaffold degradation.

5.2.3. Assessment of enzyme activities

Enzymatic degradation is efficient and selective provided that the enzymes are appropriate for the substrates. Turnovers of natural materials, such as hyaluronan and collagens, by substrate-specific enzymes have been well characterized (55). On the contrary, since most polymers are not specific substrates for natural enzymes, the mechanism aspect of enzyme-mediated polymer degradation are likely to be complex. Limited attention has been devoted to investigation into discerning the catalytic activities of enzymes on polymer degradation (121, 122) and many other related issues have yet to be explored. It was previously reported that the activities of various capsule-borne enzymes were elevated in a rat subdermal model two weeks after material implantation (123-125), however, abnormal expressions of many oxidative and hydrolytic enzymes are associated with diseases (93, 126-130). Therefore, a better understanding on enzyme-mediated degradation of biomaterials has important implications in appropriate biomedical applications such as implantable, drug delivery systems and so forth. The results from specific aim 2 showed that the production of H_2O_2 was elevated when macrophages were exposed to the scaffold (89), suggesting the involvement of reactive oxygen species in the process of scaffold degradation. In the current investigation, we set out to identify some of the major hydrolytic enzymes

produced by fibroblasts and macrophages which may be relevant to the degradation of the Dextran/PLGA scaffolds. We set out to identify some of the hydrolytic enzymes including non-specific esterase (NSE), lysozyme, collagenases, hyaluronidase, α-glucosidase and β-glucosidase, in scaffold degradation.

Despite being widely utilized as a marker for macrophages, the exact physiological function of NSE has not been fully elucidated (66). It was previously reported that cholesterol esterase and carboxyl esterase activities increased during long term culture of macrophages with ester bond abundant polycarbonate urethane (121, 122). Likewise, the structure of PLGA is also very abundant in ester bonds. Thus, it could be postulated that macrophages are capable of mediating degradation of Dextran/PLGA scaffolds through a comparable mechanism. Therefore, NSE was selected as a hydrolytic enzyme and its effects on the Dextran/PLGA scaffold were investigated. These results were depicted in Figure 3 and the results of semi-quantitative analyses of NSE activities in the corresponding samples were scored and summarized in Fig. 3H. The results showed that activities of NSE were elevated in the co-culture samples as well as the samples incubated with macrophage, per se, in the presence of scaffold (Fig. 3A and C). In fact, the latter exhibited the highest NSE activity (Fig. 3C and H). Interface of the macrophage-laden scaffold and the culture dish revealed high macrophage activity (Fig. 3G) in the scaffold, which showed a distinct contrast to the weak activity of macrophages residing on the culture dish. No NSE activity was detected from fibroblasts due to the lack of expression. However, fibroblasts played a role in modulating macrophage NSE activities.

Macrophages produce and secrete lysozyme consistently into body fluids, such as tear and saliva (131). Lysozyme destroys bacteria by degrading its polysaccharide cell wall (86, 132). As a bacterial derived polysaccharide, dextran is naturally susceptible to lysozyme degradation (69). In addition, a number of reports also suggested that lysozyme could degrade other natural and synthetic polymers, including chitosan (133), poly-(HEMA) (134), polyesters (62), etc. In our investigation, production of lysozyme prompted Dextran/PLGA scaffold by macrophages was examined. The results (Fig. 4) indicated that at day 3 after cell seeding, there was an increase in lysozyme activity in both the co-culture sample and macrophage sample incubated with the scaffolds. Sample lysozyme activities increased noticeably at day 7 and further elevations were detected by day 21. At day 3 and 7, macrophage samples showed higher lysozyme activities than their co-culture counterparts, whereas higher lysozyme activity was detected in co-culture samples than those incubated with the macrophage alone at day 21. The results suggested that fibroblasts played a role in regulating lysozyme activity although fibroblasts themselves do not express lysozyme. It is known that the lysozyme production is up-regulated when macrophages are activated (131) as indicated by the polyliposaccaride (LPS) stimulated macrophage as positive controls (Fig. 4). The results here were in good agreement with the finding in specific aim 2 indicating that more macrophages were activated in the co-culture samples than in the samples cultured with macrophages only, at a later stage of culture (89).

α-glucosidase and β-glucosidase are lysosomal enzymes with important roles

in metabolism of carbohydrates (135). Dextran could be metabolized into glucose, and is a potential substrate for these two enzymes. Hyaluronidases and collagenases degrade hyaluronan and collagens, respectively. However, they are also capable of degrading other substrates in non-specific manners (53, 77). More importantly, these four enzymes are produced by both fibroblasts and macrophages (135, 136). However, due to the sensitivities of the substrate-specific assays, hyaluronidases, α-glucosidase and β-glucosidase were not detectable in all samples (data not shown). Therefore, real-time PCR, a more sensitive method, was used to detect the differential expressions of α-glucosidase, β-glucosidase, hyaluronidase-1 and gelatinase (MMP9) at the mRNA level in the presence of Dextran/PLGA scaffold, and the results were summarized in Figure 5A. With the exception of β-glucosidase, all other enzymes were up-regulated throughout the entire culture span, which strongly suggested their involvement in the process of scaffold degradation. In addition, the expressions of α-glucosidase, hyaluronidase-1 and gelatinase were elevated in fibroblasts and macrophages, separately or co-cultured. These results further confirmed that both fibroblasts and macrophages were able to degrade the Dextran/PLGA scaffold. Furthermore, the expression levels of these enzymes in the co-culture samples were not simply the arithmetical sum of those observed in the samples cultured with either fibroblasts or macrophages, implicating the active interactions between these two cell types. Interestingly, the total activities of all collagenases, measured by using fluorescent-labeled gelatin, did not show any significant increase (data not shown). The results from specific aim 1 indicated that MMP-1 was not regulated in the

presence of scaffold, which could be inferred as not all types of collagenases were pertinent to the Dextran/PLGA scaffold degradation.

Taken together, lysozyme, NSE, α-glucosidase, hyaluronidase-1 as well as gelatinase were up-regulated during the process of scaffold degradation even though the materials used in scaffold fabrication were not their specific substrates. It is highly probable that there are other cell secreted hydrolases which could degrade the scaffold non-specifically.

5.2.4. Receptors involved in scaffold degradation

Most cell surface receptors are multifunctional and have important roles in regulating a range of physiological processes, including differentiation, growth, survival, adhesion, migration, phagocytosis, activation, and cytotoxicities (110). Although the interactions between these receptors with their natural ligands have been well characterized, their interactions with synthetic biomaterials poses a challenge from an evolutionary prospective (110). Both macrophages and fibroblasts actively interact with various biomaterial implants (55, 137), however, their mechanisms of recognizing and internalizing synthetic biomaterials are incompletely understood. A better understanding of this process has important implications on designing future biomaterials for relevant medical applications, such as biodegradable drug delivery systems targeting specific receptors (63).

In general, many cell surface receptors have their diverse natural ligands (110). However, there is only a dearth of information available in the literature concerning receptors and polymer degradations. Moreover, no systematic study has

yet been performed to elucidate these complex interactions. Till now, most related studies have been focused on inhalable natural particles (138, 139) and metal bone substitutes (76, 140). In our investigation, we attempted to screen for some of the receptors that were previously reported to uptake various biomaterials and would be involved in scaffold degradation. Accordingly, the expressions of putative receptors: TLR4, MARCO, CD204, CD44 and uPARAP/Endo180 were detected with real-time PCR. TLR4 is mainly a receptor for LPS but is also implicated in biomaterial activation of macrophages (17). MARCO is recognized as the major receptor for unopsonized particles and it is known to involve in mediating silica uptake (82, 141). CD204 is a variant of the class A scavenger receptor capable of up taking titanium dioxide, silica, diesel particles and latex beads (82, 141). CD44 is a major receptor that binds mainly to degraded hyaluronan but also collagen as well as fibronectin (64, 65). uPARAP/Endo180 is an essential receptor for collagen uptake and degradation (72).

Real-time PCR results (Fig. 5B) showed that none of the receptors of interest were regulated 3 days after cell seeding. However, the expressions of CD204 and TLR4 were obviously higher at week 1 and 3 after cell seeding. Moreover, there was no alteration in the expression of MARCO, CD44, uPARAP/Endo180 throughout the entire culture span. These results suggested that the regulated receptors were mainly macrophage receptors, which further supported the dominant role of macrophages in scaffold degradation. In contrast, none of the tested fibroblasts receptors were regulated, which suggested that scaffold degradation/clearance by fibroblast could be

mediated by other mechanisms. When comparing the results, the expression of CD204 and TLR4 in macrophage samples could not be fully accounted for those in co-culture samples, which suggested the interaction of the two cell types in scaffold degradation. Up-regulation of TLR4 was consistent with the observation that the Dextran/PLGA scaffold could activate macrophages in either the presence or absence of fibroblasts (89). In addition, macrophage activations are generally associated with phagocytosis of biomaterials (60, 78, 142, 143). Increased expression of TLR4 during the process of scaffold degradation suggested that TLR4 may play a role in removing the debris of degraded scaffold through receptor-mediated phagocytosis. As we have alluded to previously, CD204 plays a role in the uptake of many materials (44); however, to our knowledge, its role in interacting with either PLGA or dextran has not yet been reported. Its elevated expression suggested that CD204 may be involved in recognition/internalization degraded scaffold. Since TLR4 and CD204 are multi-functional receptors that could influence macrophages profoundly in many aspects, the roles and mechanisms of these two receptors in scaffold degradation have to be further investigated. The lack of regulations of CD44 and uPARAP/Endo 180 expressions suggested that the turnover of ECM deposited by cells was not altered, and thus the increased expression of gelatinase and hyaluronidase-1 were responsible for the scaffold degradation rather than the altered ECM turnover.

It is highly possible that other receptors are involved in the process of scaffold degradation and the elimination of degraded scaffold could also be mediated by non-receptor mediated phagocytosis.

5.2.5. *In vivo* degradation

The biodegradability of the scaffold was evaluated in mice subdermal implant models. Three days after implantation, the sizes of scaffolds decreased to approximately half of their pre-implant sizes (Fig. 6A). One week later, the sizes of the scaffolds further decreased to approximately one-fourth of their pre-implant sizes and the scaffolds were encapsulated by very thin fibrous tissues (Fig. 6B). After 3 weeks, three out of four implants were completely resorbed with the adjoining tissues fully restored. The remnant of the scaffold further decreased to approximately one-tenth of its original size (Fig. 6C). The morphologies of these retrieved scaffolds (Fig. 7A and B) showed noticeable degradation 1 week post-implantation. The *in vivo* degradation of the scaffold was considerably faster than that of their *in vitro* counterpart. The extent of *in vivo* erosion in 1 week (Fig. 7) was comparable to that of observed after one month of exposure in the co-culture model (Fig. 1E), this further underscored the extended time span needed for any credible *in vitro* model system intended to emulate *in vivo* degradations. Nonetheless, the pattern of erosion for the implanted scaffold fibers bore remarkable resemblance to their counterparts subjected to cell-mediated erosion. These result signified that the fibroblast/macrophage co-culture model could be utilized as an *in vitro* tool to evaluate and study the mechanisms of biodegradation of materials under the influence of biological systems. The information obtained could guide the design of biomaterials and their selection for different applications.

5.3. Conclusion

The Dextran/PLGA scaffold could be degraded by fibroblasts and macrophages, cultured separately or together. The activities of lysozyme, gelatinase, hyaluronidase-1, NSE, and α-glucosidase as well as the expressions of cell surface receptors CD204 and TLR4 were up-regulated, suggesting their involvements in the cell-mediated scaffold degradation. The results of *in vivo* subdermal implantation of the Dextran/PLGA scaffold further confirmed its good biodegradability.

Table 1 Real-time PCR primer sequences

Gene	Access number	Forward primer sequence	Reverse primer sequence
Alpha-glucosidase	NM_008064	5'CTCCTACCCAGGTCCTTTCC3'	5'ACAGCTCTCCCATCAGCAGT3'
Beta-glucosidase	NM_172692	5'ACCCTGGAATGTACCAGCAC3'	5'GCTCCAAGGACAGAACTTGC3'
Hyaluronidase-1	BC021636	5'CATGCACTGGCTTAGATCA3'	5'GGATGCCGTCTATGTCGTCT3'
Gelatinase	D12712	5'AATTGGGCACCTACCCCTAC3'	5'TCCTGGAATGTGTGAGCAAG3'
TLR-4	NM_021297	5'TTCTTCTCCTGCCTGACACC3'	5'TGTCATCAGGGACTTTGCTG3'
CD204	AF203781	5'GACGCTTCCAGAATTTCAGC3'	5'CCAGTGAATTCCCATGTTCC3'
MARCO	NM_010766	5'AGGGAGACAAAGGGGACCTA3'	5'CTGGTTTTCCAGCATCACCT3'
CD 44	NM_009851.2	5' CGTCCAACACCTCCCACTAT 3'	5' TCCATCGAAGGAATTGGGTA 3'
Endo180	NM-008626	5' GTCTGGCCAGCTATGAGGAG 3'	5' CTAGGGTCTCTGCGGTTCAG 3'
GAPDH	BC083080	5 ACCAACTG TTAGCCC 3′	5′ CTTCCCGTTCAGCTCT 3′

Figure 1SEM of degraded Dextran/PLGA scaffolds. (A) 4 Weeks, and (B) 8 weeks after seeding fibroblasts; (C) 4 weeks, and (D) 8 weeks after seeding macrophages; (E) 4 weeks, and (F) 8 weeks after seeding macrophages and fibroblasts; (G) a typical cell-mediated degradation sample at a higher magnification after 4 weeks, and (H) a PBS-mediated degradation control after 4 weeks; (I) a cross-section of fibroblast-mediated scaffold sample after 4 weeks; and (J) pristine scaffold (scale bar: 8.569 µm).

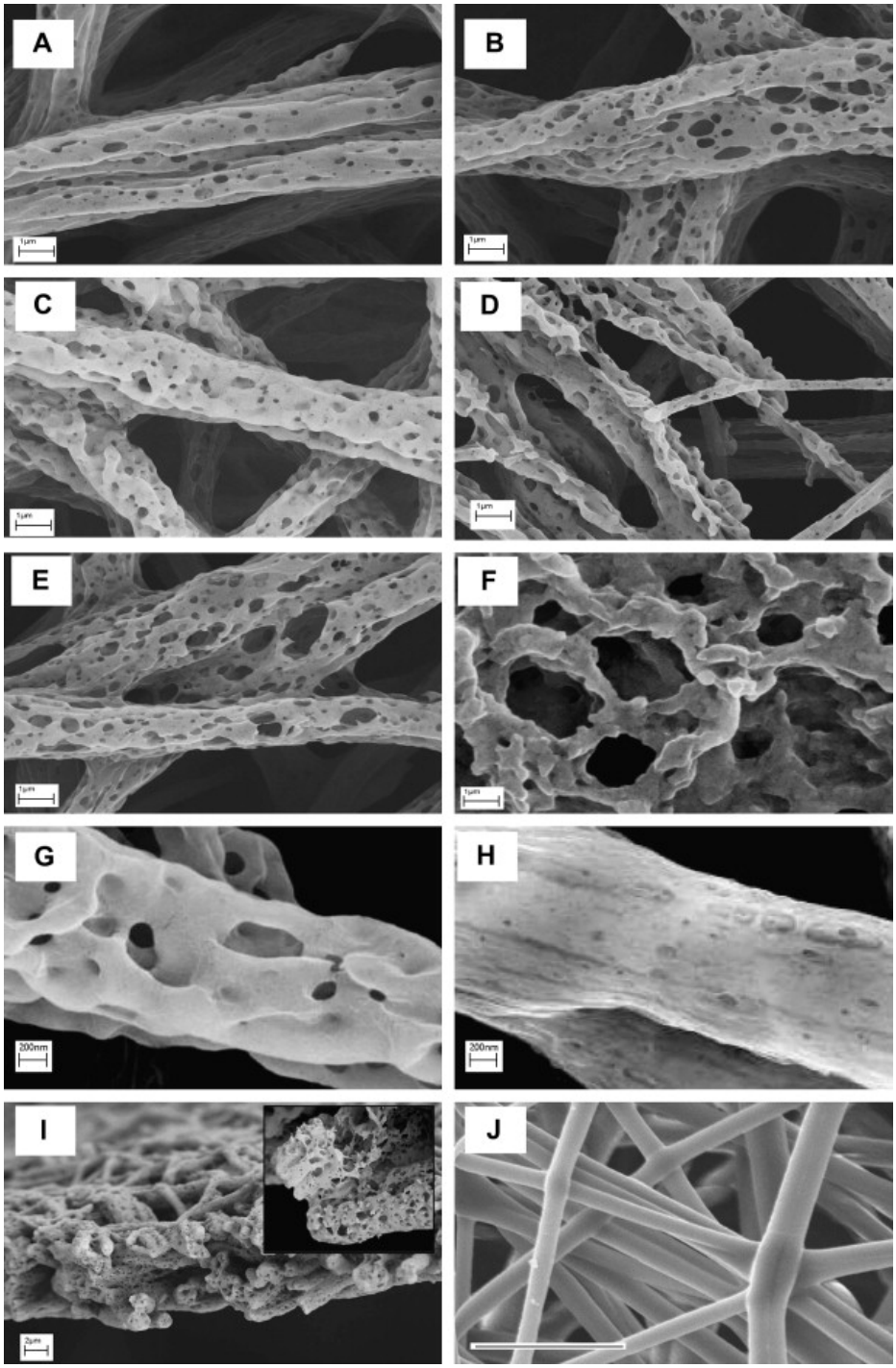

Figure 2 pH Value changes under the influence of scaffold as compared with scaffold-free controls. M: macrophages; F: fibroblasts; S: scaffold.

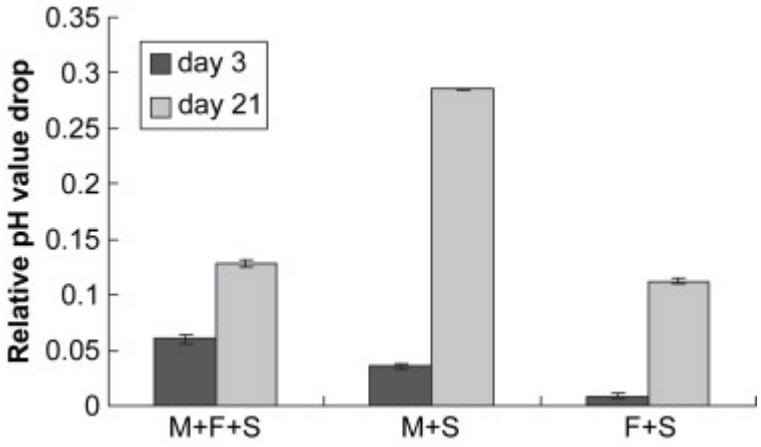

Figure 3 Activities of NSE in the presence of Dextran/PLGA scaffold at week 1. (A, C, E) Cells in the scaffolds; (B, D, F) cells on the culture dish; (A, B) macrophages/fibroblasts co-culture; (C, D) macrophages; (E, F) fibroblasts; (G) the interface of scaffold and the culture dish; S: scaffold; P: plastic culture dish; arrow: macrophages with higher NSE activities; and (H) scores for NSE activities; M: macrophages; F: fibroblasts; S: scaffold.

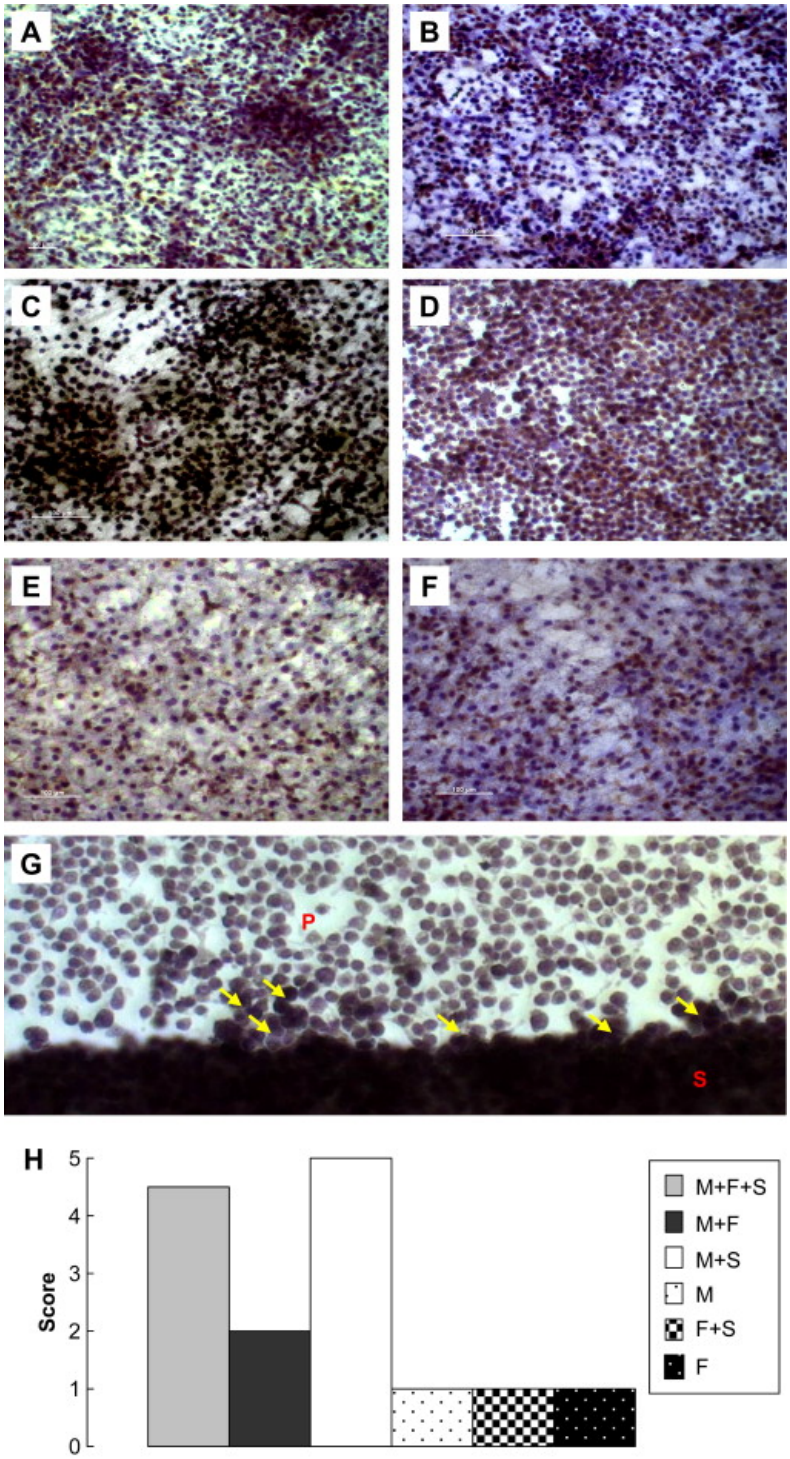

Figure 4 Lysozyme activities under the influence of Dextran/PLGA scaffold one week and four week after cell seeding. M: macrophages; F: fibroblasts; S: scaffold.

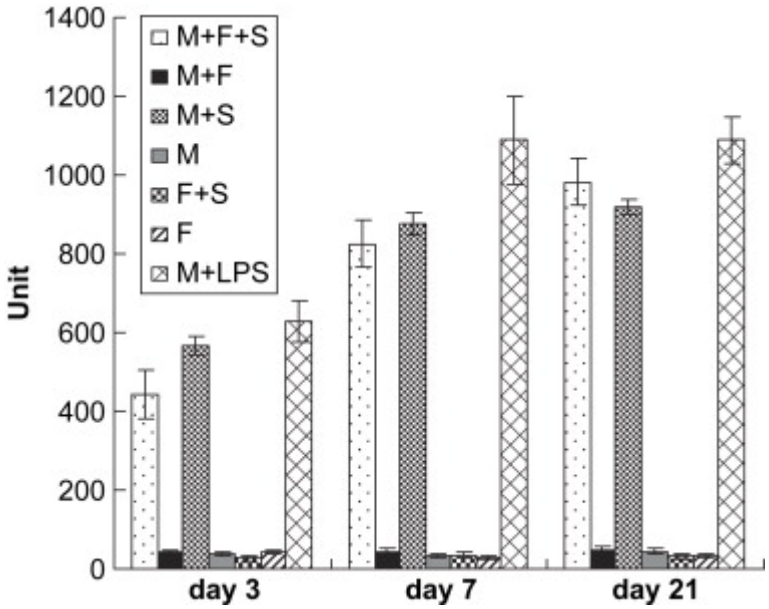

Figure 5 Relative quantitative real-time PCR analyses of gene expressions of cells in PLGA / Dextran scaffold. (A): Enzymes; (B); Receptors; M: macrophages; F: fibroblasts; S: scaffold.

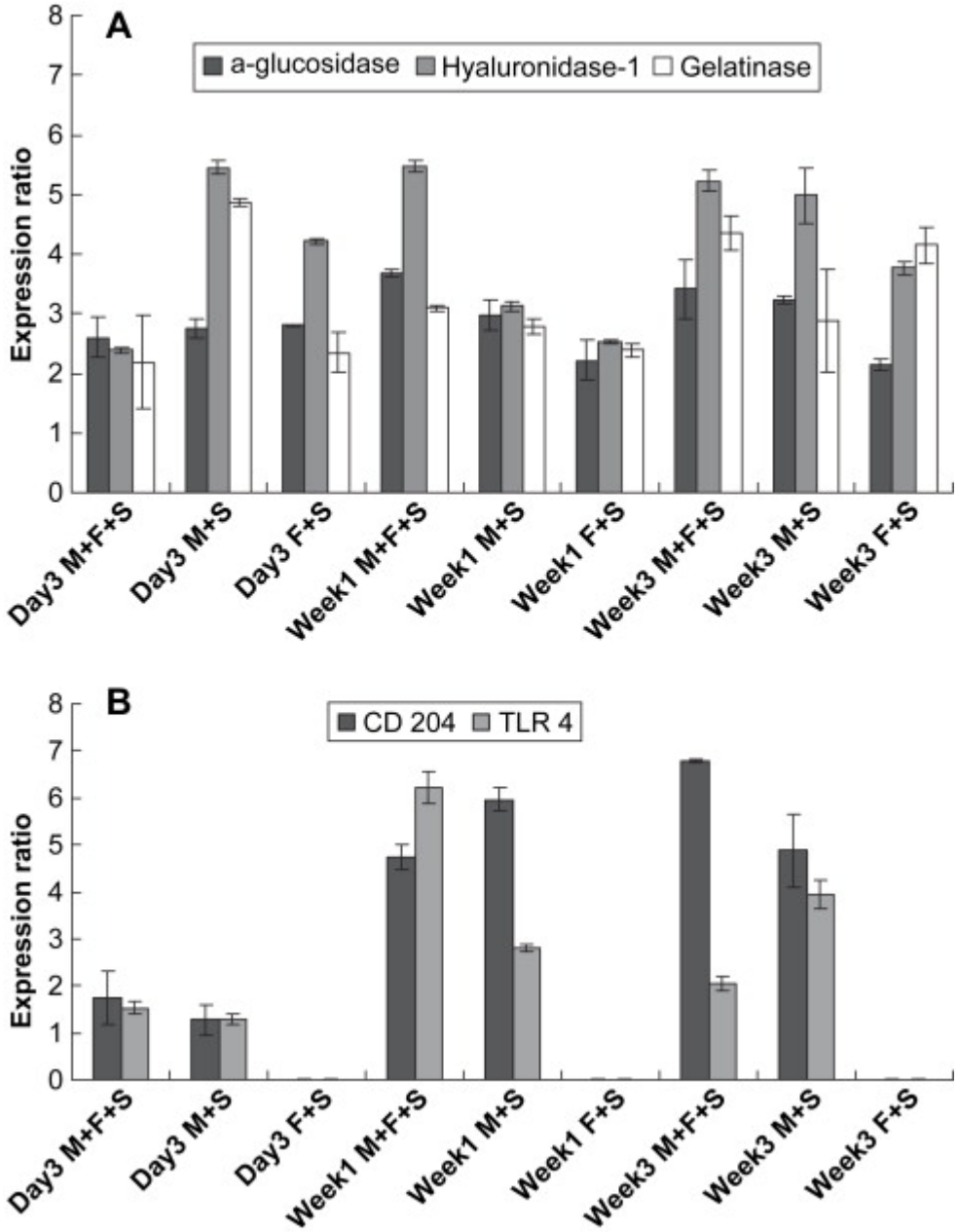

Figure 6H&E staining of the implanted Dextran/PLGA scaffolds in the mice subdermal implantation model. (A) 3 Days; (B) 1 week; and (C, D) 3 weeks after implantation. Star: the implants; arrow: macrophages; arrow head: fibroblasts; A–C: 25 X; D: 200 X.

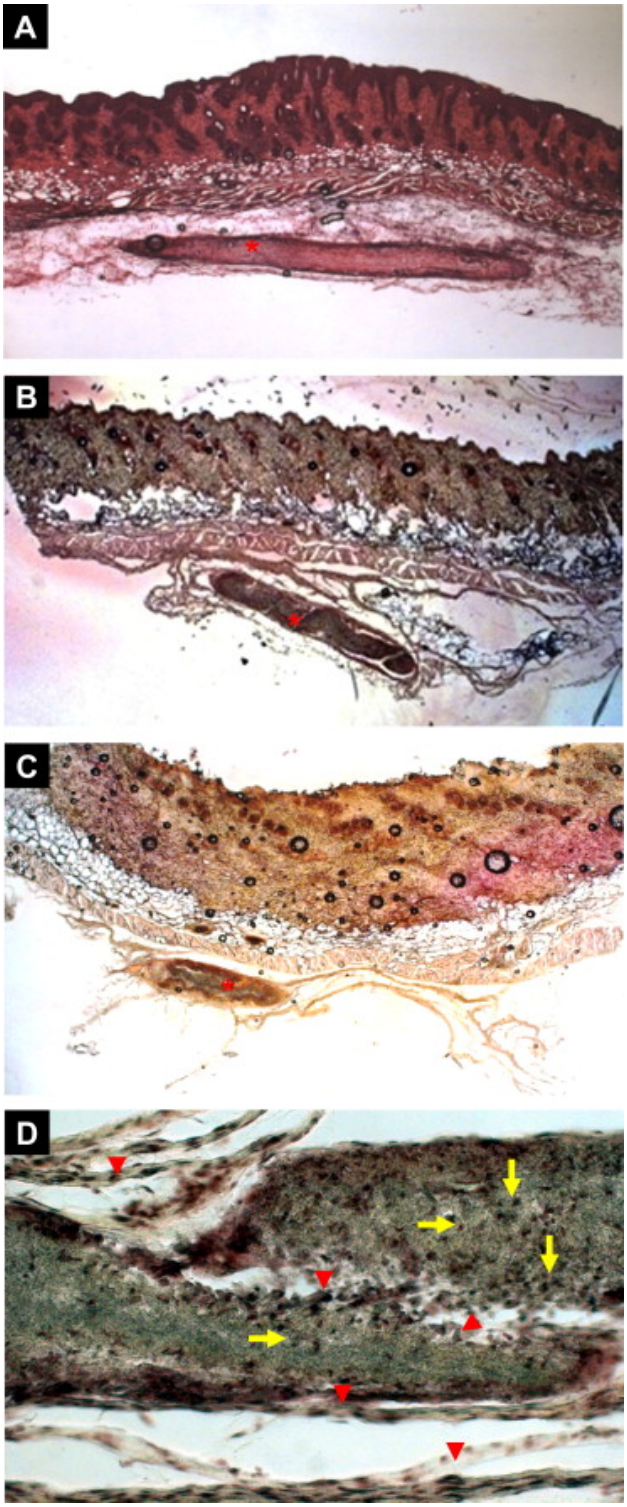

Figure 7 SEM scanning of degraded Dextran/PLGA scaffolds retrieved from *in vivo* implantation one week post-surgery.

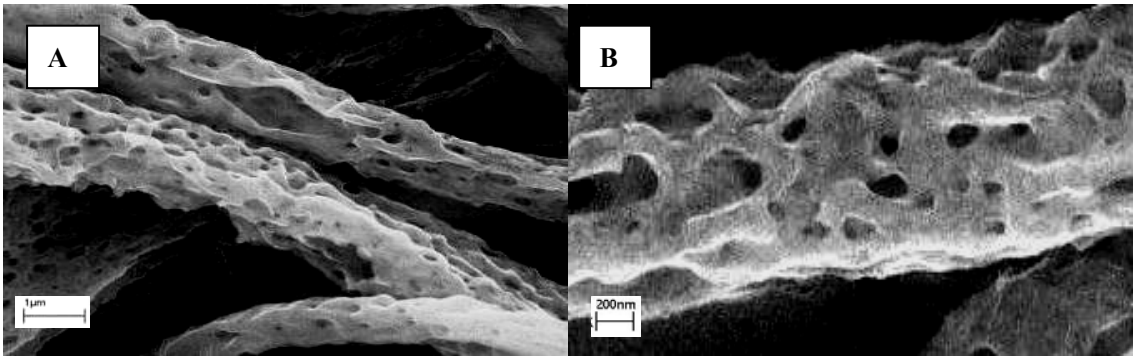

Chapter 6 Specific Aim 4

Specific aim 4: Electrospun Dextran/PLGA scaffold as a potential bioactive wound dressing in treating diabetic chronic wounds *in vivo.*

6.1. Materials and Methods

6.1.1. Animals

Male (5 week) C57BLK/J-m+/+/Lepr^{db} (*db/db*) mice (Jackson laboratories, Bar harbor, ME, USA) and their wild type littermates (C57BLK/J) were used for the studies performed in this specific aim. Homozygous mice (*db/db*) have a spontaneous genetic mutation (*Lepr^{db}*) in chromosome 4 and exhibit a series of symptoms similar to those of human adult onset diabetes including delayed wound healing; whereas their wild type littermates show no characteristics of diabetes.

6.1.2. Experimental and control groups

The Dextran/PLGA scaffolds were implanted into mice. Mice underwent the same surgical procedure but bore no implants were set as controls. Five mice in each group were used. (See Table 1)

6.1.3. *In vivo* wound healing model and implantation of samples

Anesthesia of mice was induced and subsequently maintained with isoflurane. With the hairs on their dorsal side shaved, full-thickness circular (diameter 1cm)

transcutaneous dermal wounds were created on their dorsal side. After sterilized with ethanol, scaffolds trimmed to approximately the sizes of the wound beds, were deposited in the wound beds. A sheet of Tegaderm (3M, St.Paul, MN, USA) was first plastered over each wound bed and this was followed by wrapping with a Band-Aid (Johnson and Johnson, NJ, USA) (Figure 1) (9) . Mice were euthanized at day 3, 5, 7, 14 and 21 for analyses (n=5 for each experimental group).

6.1.4. Evaluation of wounds

6.1.4.1. Gross observation of wound closure

The wound open areas were photographed and measured using image analyzing software (Image J, NIH, USA). The percentages of closure were determined according to: $Pn = Sn/Si \times 100$

where Pn is the percent closure on day n, Si is initial wound surface area and Sn is wound surface area at day n (144).

6.1.4.2. Histology

At pre-determined time-points, the wound areas were excised, cryo-embedded and 10 μm-thick cryosections were prepared for the following evaluations. H&E stained sections were captured, digitized and assembled with CorelDraw (Fremont, CA, USA). Sections were analyzed in order to obtain the general information of wound morphology and degradation/integration of implanted scaffold. A pathologist blinded to the study design was consulted.

6.1.5. Statistics

All experimental results were presented as mean ± standard deviation.

Whenever appropriate, Student's t-test was used to discern the statistical difference between groups. The significant level was set as $p<0.05$.

6.2 Result and discussion

In specific aim 1, we showed that the Dextran/PLGA scaffold was capable of supporting dermal fibroblasts attachment, migration, growth, contraction, ECM deposition, growth factor production and so forth.

In specific aim 2, we demonstrated, (i) the Dextran/PLGA scaffold did not induce detectable increase in NO production; (ii) the primary function of the increased macrophages, induced by the presence of the scaffold, was scaffold degradation rather than inflammatory responses; (iii) the scaffold did not evoke production of the major pro-inflammatory cytokines; and (iv) fibroblasts did not play unfavorable roles in modulating macrophage functions. These results indicated that the Dextran/PLGA scaffolds were minimal inflammatory and possessed good biocompatibility /immunocompatibility.

In specific aim 3, the biodegradability of the Dextran/PLGA scaffold was demonstrated, which implied that degradation would not hamper tissue regeneration and wound closure. Additionally, increased enzymatic activities, rather than ECM turnover, were responsible for scaffold degradation, which could be another favorable characteristic for the scaffold to serve as a dressing intended for enhancing wound healing.

Collectively, the biocompatible and biodegradable Dextran/PLGA scaffold has many desirable features as described above, and thus, its potential of

facilitating diabetic chronic wounds healing has to be further explored. Therefore, the scaffold was evaluated with a cutaneous wound model and the healing process was analyzed.

As shown in Figures 2, the gross appearances of all wound beds did not exhibit ulcer and chronic inflammation throughout the entire course of the healing process, implying the excellent biocompatibility of the Dextran/PLGA scaffold which was consistent with the findings in specific aim 1 and 2. Generally, the wound beds of the diabetic groups healed more slowly than those of the wild type groups. In addition, the scaffold significantly facilitated the wound healing (Figure 3), both in wild type mice and in diabetic mice, beginning at day 5 after the surgery (Pn: 0.95 ± 0.03% in db control group; 0.80 ± 0.04% in db with scaffold group; 0.92 ± 0.02% in wild type control group; 0.56 ± 0.04% in wild type with scaffold group). Apparently, the sizes of all wounds decreased extensively 14 days after surgery (Pn: 0.54 ± 0.08% in db control group; 0.31 ± 0.03% in db with scaffold group; 0.35± 0.01% in wild type control group; 0.18 ± 0.04% in wild type with scaffold group). At day 21 post-surgery, the sizes of the wounds in diabetic mice without the scaffold implants were evidently larger (Pn: 0.46 ± 0.09%) as compared with those with scaffold implants (Pn: 0.19 ± 0.07%), whereas in wild type mice the sizes of the wounds reduced from Pn: 0.15 ± 0.07% to 0.03 ± 0.06% when scaffolds were applied. It should be noted that beginning at day 7 post-surgery, the healing rate of the wound beds of db mice implanted with scaffolds was comparable to that of the wild type with no implant. The implication here is that the healing of diabetic chronic wound healing, which is typically delayed,

could be rectified by the presence of the Dextran/PLGA scaffold.

The H&E stained specimens were examined to further assess the healing response and the corresponding biodegradation/bioresorption of the implanted scaffold. In the wild type control group, 3 days post-surgery, the scaffold was clearly integrated into the adjacent tissue with evidence that cells were dispersed inside the scaffold and some scaffold debris surrounded by the loose connective tissue in the hypodermis layer (Figure 4 day 03 B and Figure 5 A). However, the scaffold did not appear to integrate with the intact skins on the edges and remained on the top of the intact skin. Moderate inflammatory cell infiltration was observed with more considerably robust re-epithelialization when compare to the control group (Figure 4 day 03 A). In addition, the hypodermis layer was significantly thicker and denser. In the diabetic control group, re-epithelialization was obviously delayed as compared with the wild type control group (Figure 4 day 03 A-B vs. C-D). Furthermore, larger scaffold fragments were found in the subcutaneous area as well. Unlike the wild type control group, the implanted scaffold did not thicken the hypodermis layer in the wound bed.

For the wild type control group (Figure 4 day 05 A), 5 days after surgery, the re-epithelialization had covered the whole wound bed with layers of well organized loose connective tissue underneath. Moreover, granulation tissue started to develop from the wound edge. In contrast, the re-epithelialization was far more robust in wild type animals implanted with scaffold (Figure 4 day 05 B and Figure 5 B), with the scaffold being enveloped between multiple layers of collagens with inflammatory

cells. On the wound edge, formation of reticular collagen tissue was observed and merged into the intact skin. Similar to its counterpart derived from the day 3 time-point, the wound bed was covered scaffold and some scaffold residues were surrounded by the thick granulation tissue underneath the wound bed. As expected, the wound beds of the diabetic group displayed obvious delayed healing (Figure 4 day 05 C-D), with modest extension of re-epithelialization area and barely discernable granulation tissue formation. Plenty of scaffold fragments could readily be identified in the dermis of the intact skin as well as the subcutaneous layer in the scaffold implanted wound beds of the diabetic mice (Figure 4 day 05 D and Figure 5 D-E).

The progress of the healing in control animal groups 7 days post-surgery (Figure 4 day 07 A and C) was not significantly different from 5 days after surgery (Figure 4 day 05 A and C). In wild type animals with implanted scaffolds, substantially denser extracellular matrix could be seen deposited in the wound beds (Figure 4 day 07 B and Figure 5 C), while more robust re-epithelialization and granulation tissue formation were observed in the diabetic group with implants (Figure 4 day 07 D and Figure 5 F). Instead of being resorbed homogenously in the wild type animals, scaffold fragments were dispersed in the subcutaneous layers in both the wound bed and in the flanking tissues (Figure 4 day 07 D and Figure 5 D).

Two weeks after surgery, virtually all wound beds were almost healed with dramatic decrease in wound sizes (Figure 4 day 14). In addition, all specimens were fully re-epithelialized; in particular, there were scar tissue formation in the samples with scaffold implants (Figure 4 day 14 B and D). Evidently, the scaffold promoted

extensive and well-organized ECM deposition in addition to formation of a thick layer of granulation tissue with abundant new blood vessels formed in the wound beds of both diabetic and wild type mice. For comparison, without the scaffold implants, only thin layers of ECM were developed (Figure 4 day 14 A and C). Besides, the healed parts of the wound beds were replaced by newly formed skin similar to the intact skin. Most of the scaffold fragments were resorbed and degraded at this stage with the residuals embedded in subcutaneous tissues (Figure 4 day 14 B and D). In general, the scaffold degraded faster and a lot more homogenous in wild type samples than in diabetic samples.

Three weeks after surgery, the wounds of wild type mice with scaffold implanted healed almost completely (Figure 4 day 21 B), while the appearance of the wound beds of wild type control mice (Figure 4 day 21 A) were similar to the wound beds implanted with scaffold 2 weeks post-surgery (Figure 4 day 14 B). Apparently, the scaffold induced extensive ECM deposition and granulation tissue formation in diabetic wounds (Figure 4 day 21 D), whereas only thin layers of ECM were produced in the wound beds without the scaffold implants (Figure 4 day 21 C). There was no discernable scaffold residues in the wound beds of wild type control samples (Figure 4 day 21 B) and only modest amount of scaffold residues was spotted in the wound beds of diabetic mice (Figure 4 day 21 D). Moreover, the scar tissues in all wild type mice were evidently thicker than those in diabetic groups (Figure 4 day 21 A-B v.s. C-D). Lastly, the healed part of skin showed no noticeable differences from the intact skins.

The above findings suggested that the Dextran/PLGA scaffold showed excellent biocompatibility and biodegradability, which were consistent with the observations made in specific aims 1-3. The pace of scaffold degradation synchronized with that of wound healing, therefore, not hindering the wound repairs during in the process. Interestingly, the patterns of scaffold degradation in wild type mice and in diabetic mice were different. In wild type animals, the scaffold degraded faster and more uniformly, while the scaffolds were fragmented into measurable pieces in diabetic animals, further suggesting the functional differences between wild type and diabetic dermal cells.

In specific aims 2-3, subcutaneous implantation of scaffolds induced collagen capsule formation, which could partially explain the enhanced ECM production by the implanted scaffold (Figure 4). Abnormal ECM production is a major contributory factor of diabetic chronic wounds, it could thus be inferred that the implanted scaffold exhibited some therapeutic efficacy. However, the exact mechanism in concert with the improved quality of healing by the scaffold warrant further exploration.

As previously mentioned, the ideal wound dressing should meet a number of requirements. Based on the findings in animal study, the Dextran/PLGA scaffold demonstrated excellent tissue compatibility, biodegradability, rapid adherence to wound surface, adequate compliance to permit motion of underlying tissue, long shelf-life, minimal storage requirements, translucent properties to allow direct observation of healing, and so on (48). In addition, we have reported that the diameters of the Dextran/PLGA scaffold fibers are very close to that of collagen fibers

with their mechanical properties emulate those of dermal tissue (16). Furthermore, the big pore sizes of the scaffold enable higher gas/liquid permeation and also protect wound bed from dehydration. All these characteristics render the electrospun Dextran/PLGA scaffold a very appealing wound dressing.

Many biomaterials in the literatures have been proposed as wound dressing to treat diabetic chronic wounds (145). Most of them were designed as delivery vehicles of bioactive agents such as drugs, cells and growth factors in treating diabetic wounds (9-14). The findings in this research demonstrated that the electrospun Dextran/PLGA scaffold alone could effectively facilitate the diabetic chronic wound healing without the need to incorporate bioactive agents.

Table 1 Controls and experimental groups.

Controls	Experimental groups
wt	wt with scaffold implants
db/db	db/db with scaffold implants

Figure 1 Mice full-thickness dorsal skin wound model.

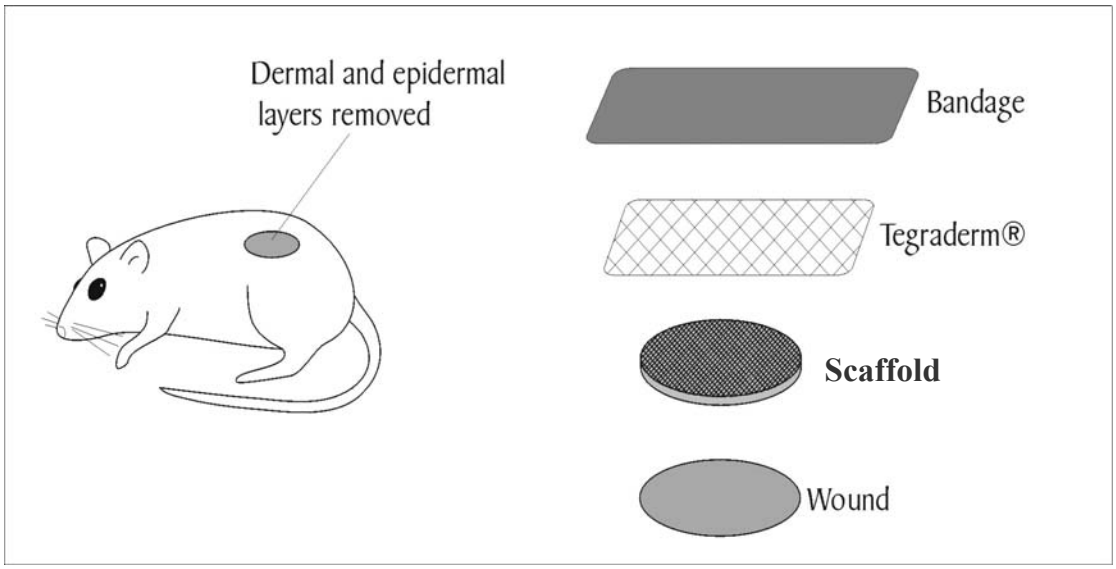

Figure 2 Gross observation of wound closure. Scare bar: 3mm.

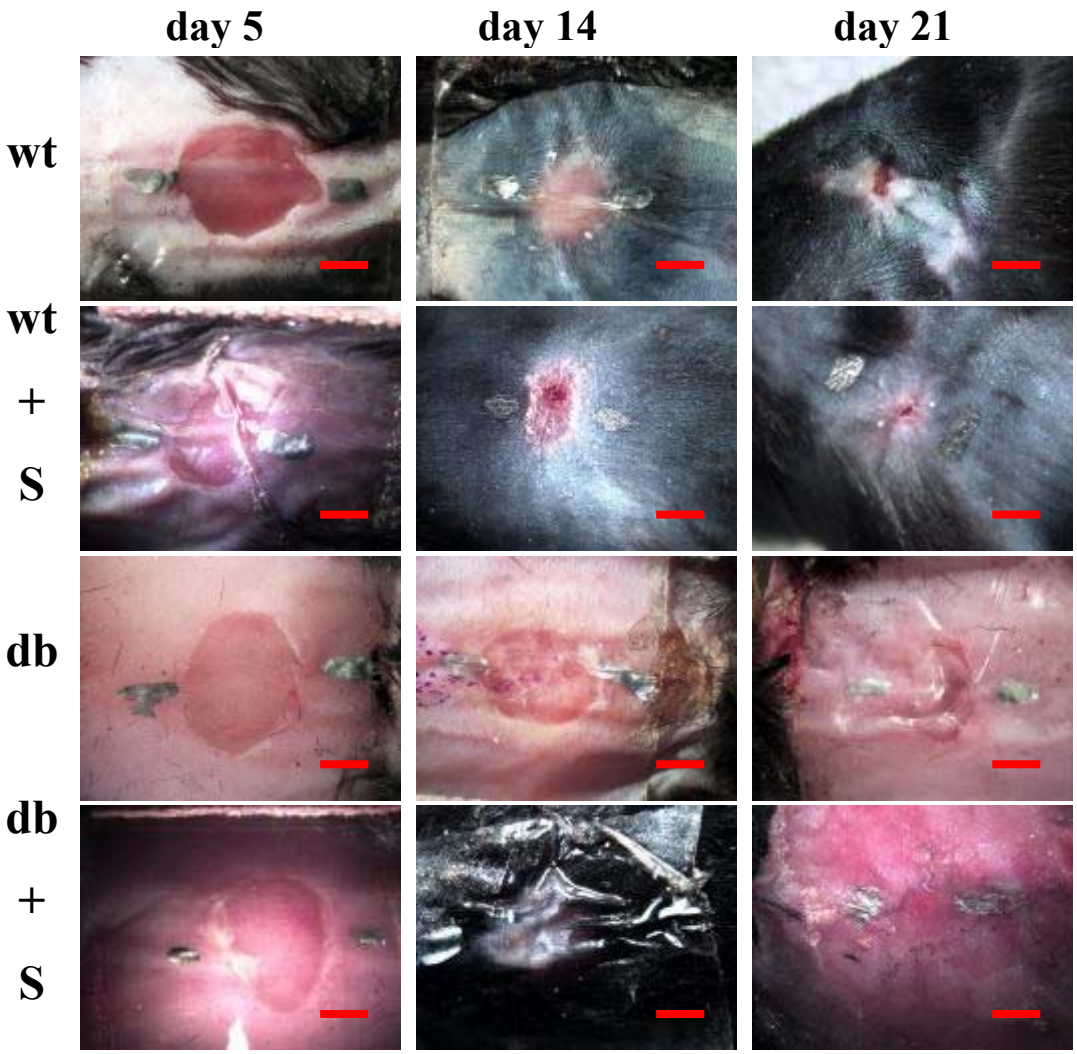

Figure 3 The percentage of closure (Pn).

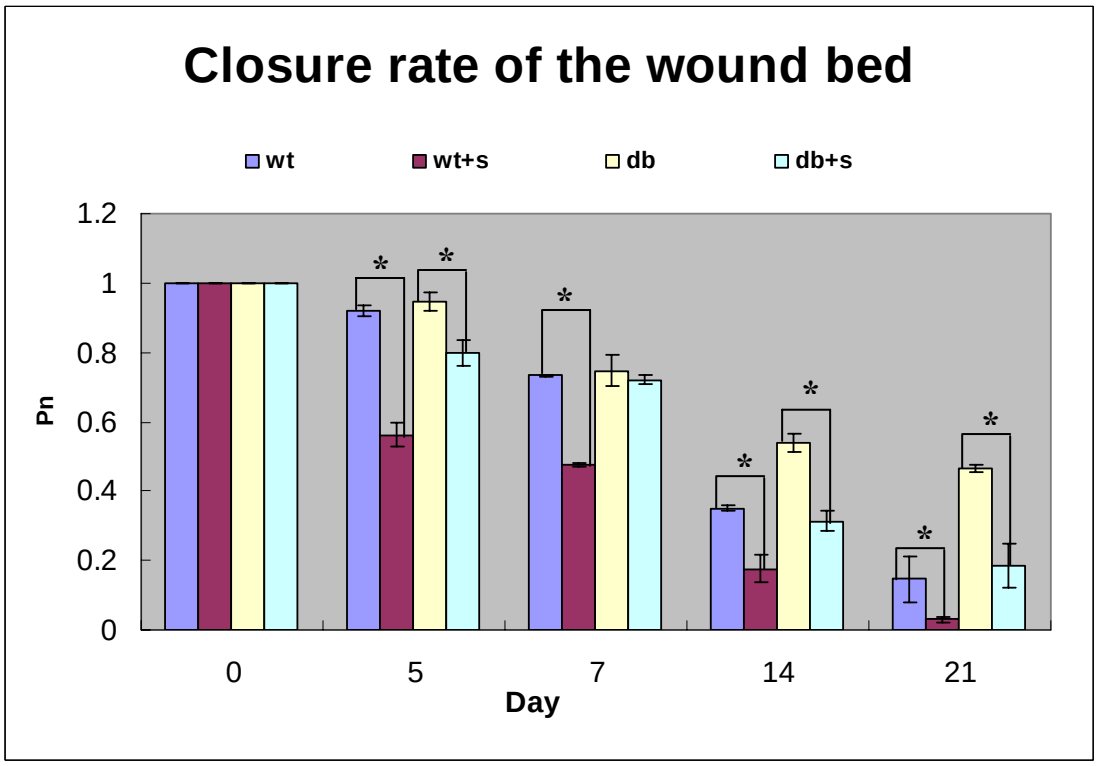

Figure 4 H&E staining of the wound samples. A: wt control; B: wt with scaffold implant; C: db control; D: db with scaffold implant; red arrow: re-epithelialization; green arrowhead: granulation tissue; green arrow: scar tissue; yellow arrowhead: scaffold fragment; F: fatty tissue; E: newly formed ECM; M: muscle; I: intact skin. Scale bar: 500μm.

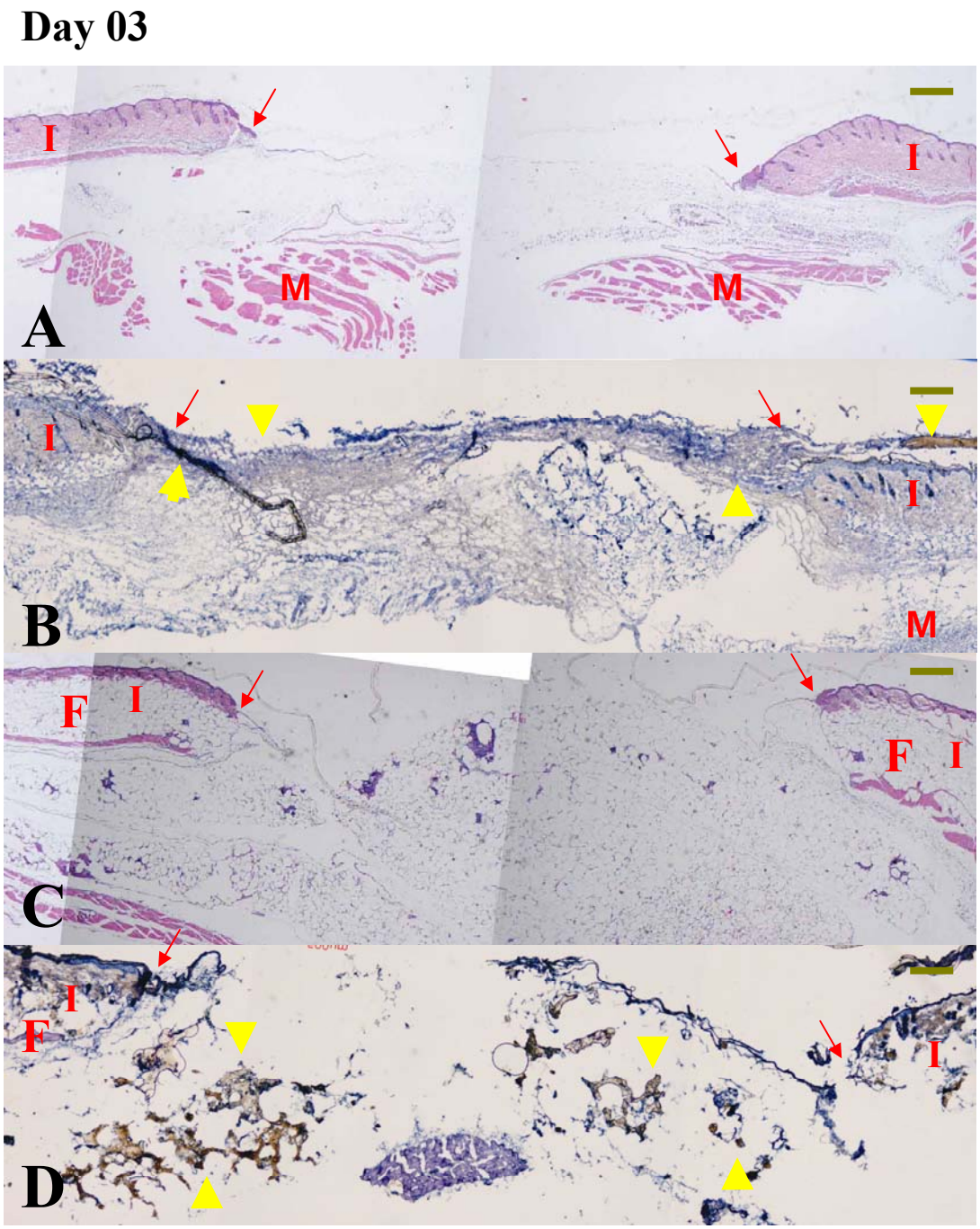

Day 05

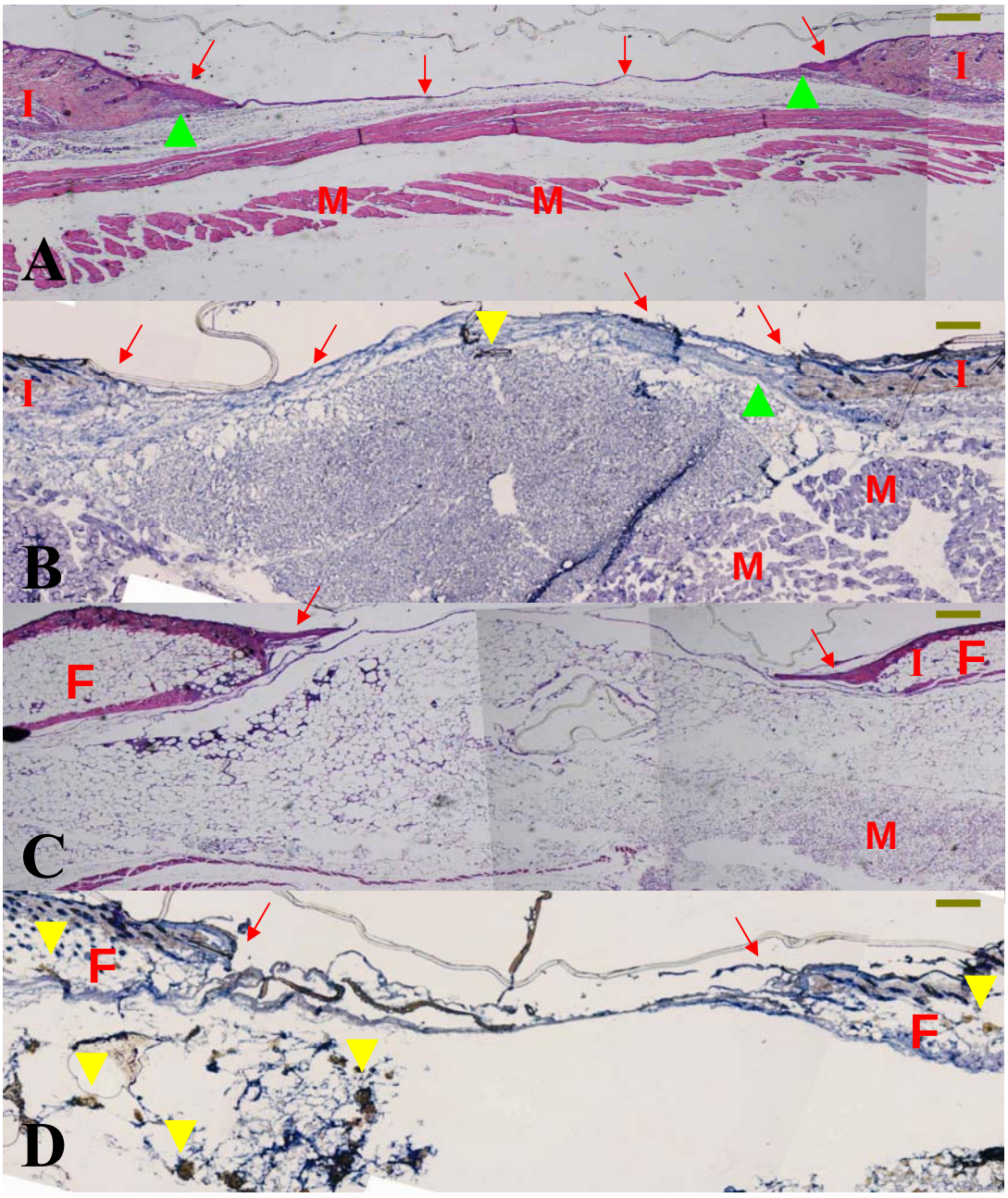

Day 07

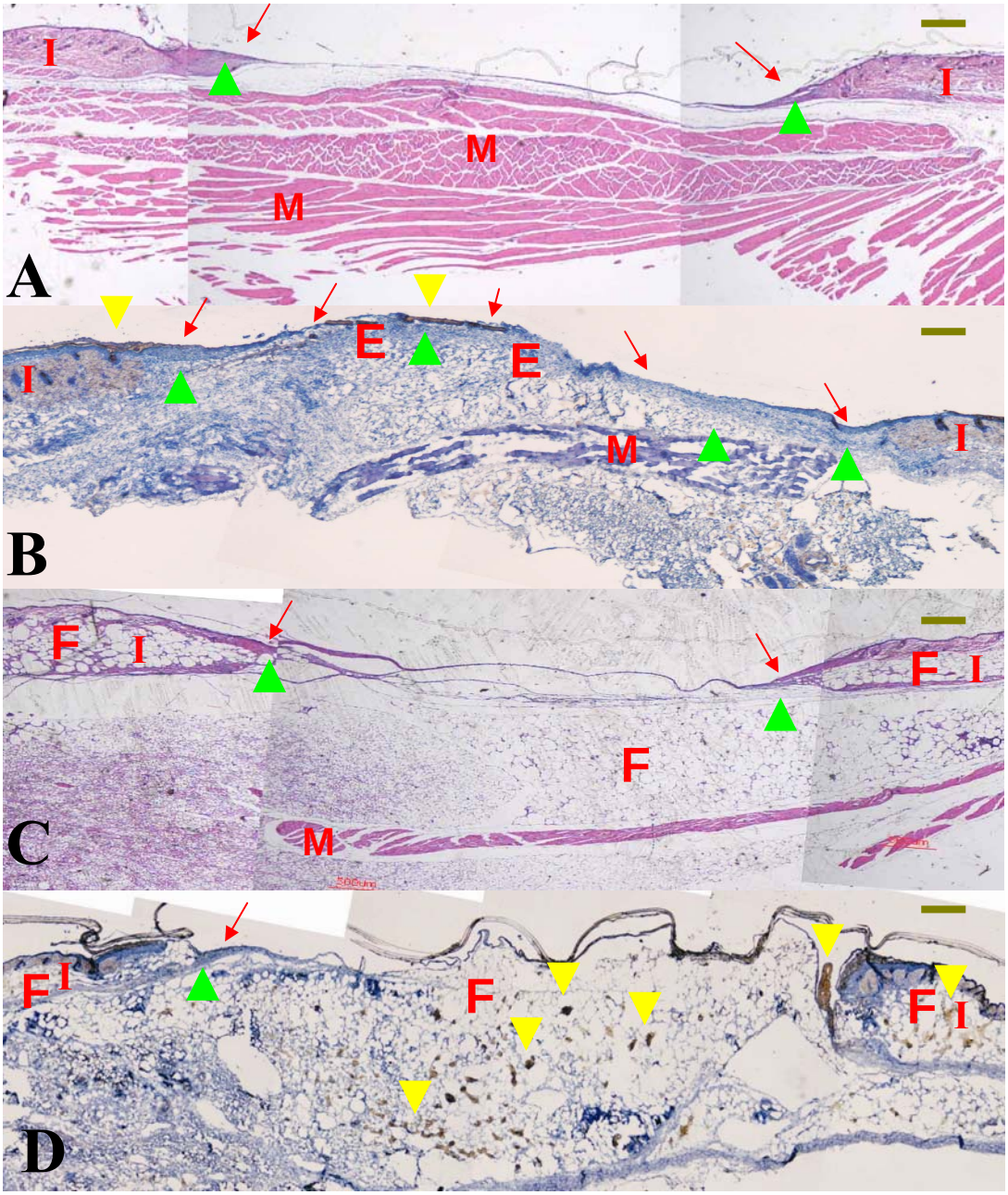

Day 14

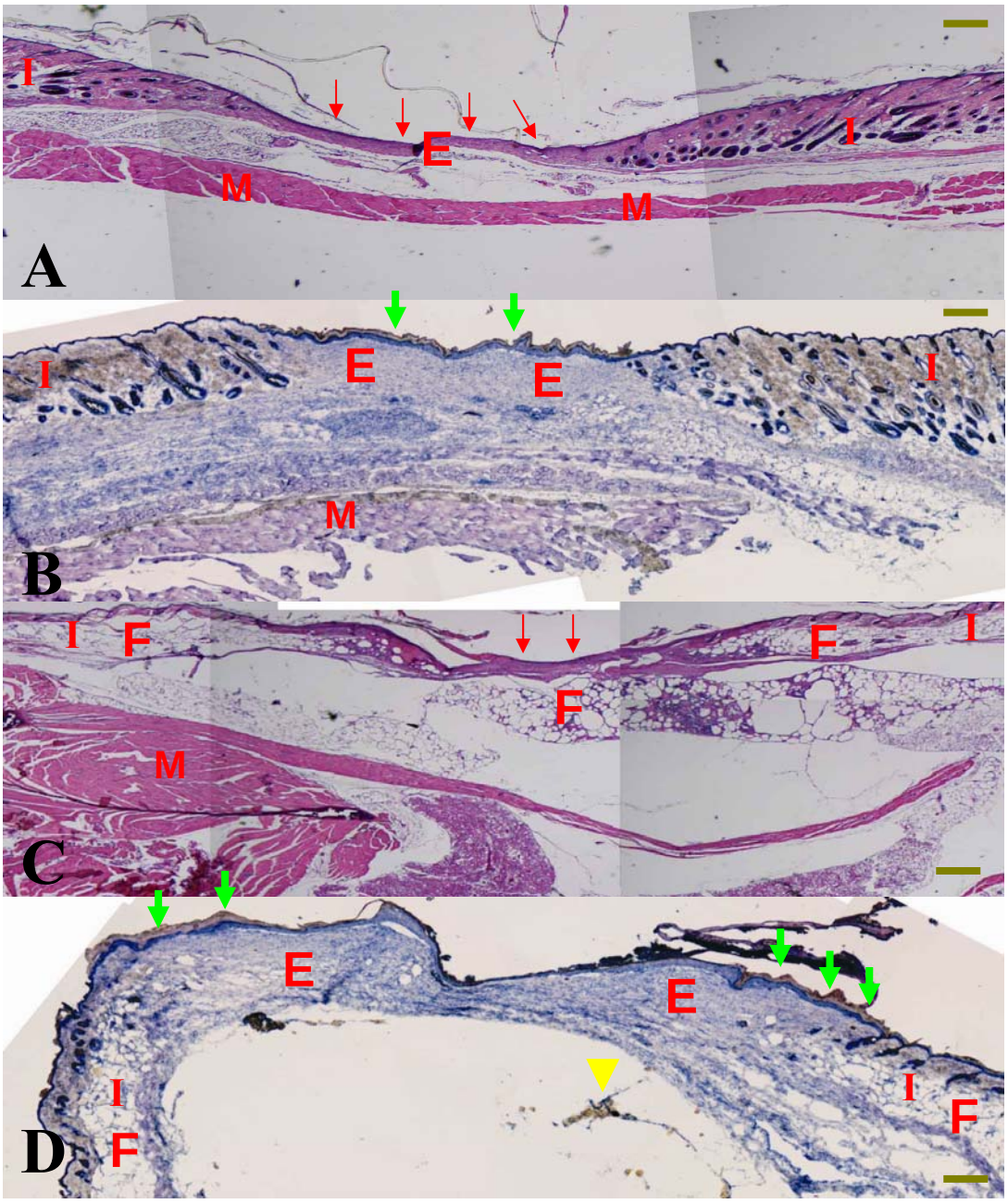

Day 21

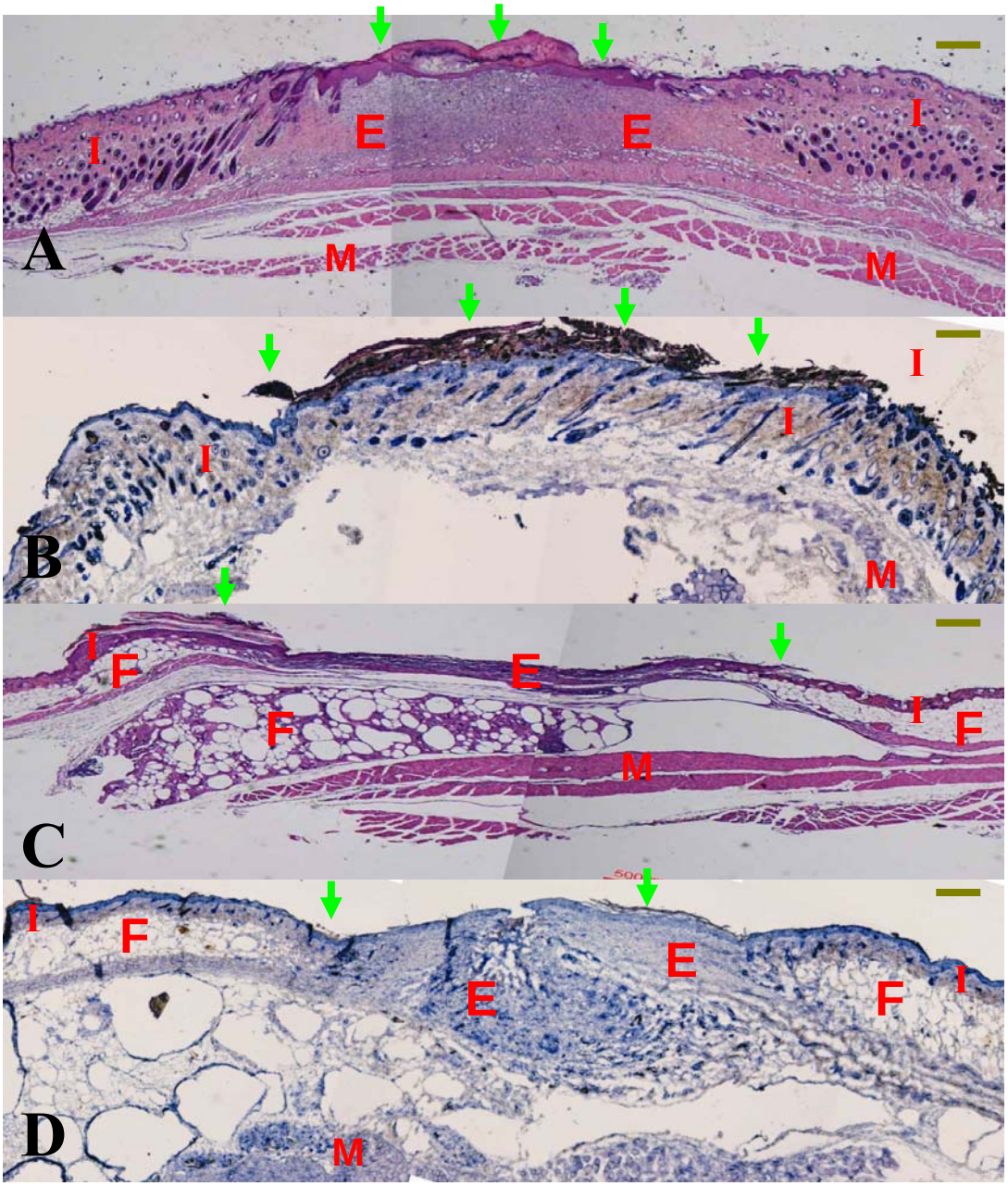

Figure 5 Scaffold degradation *in vivo* in wild type mice and in db mice. (A-C) wild type groups with scaffold implants; (D-F) db mice with scaffold implants. A: day 3; B, D, E: day 5; C, F: day 7 after surgery. D: intact skin; E: tissue under wound bed; Red arrow: scaffold residues; yellow arrow: inflammatory cells; E: ECM; F: Fatty tissue.

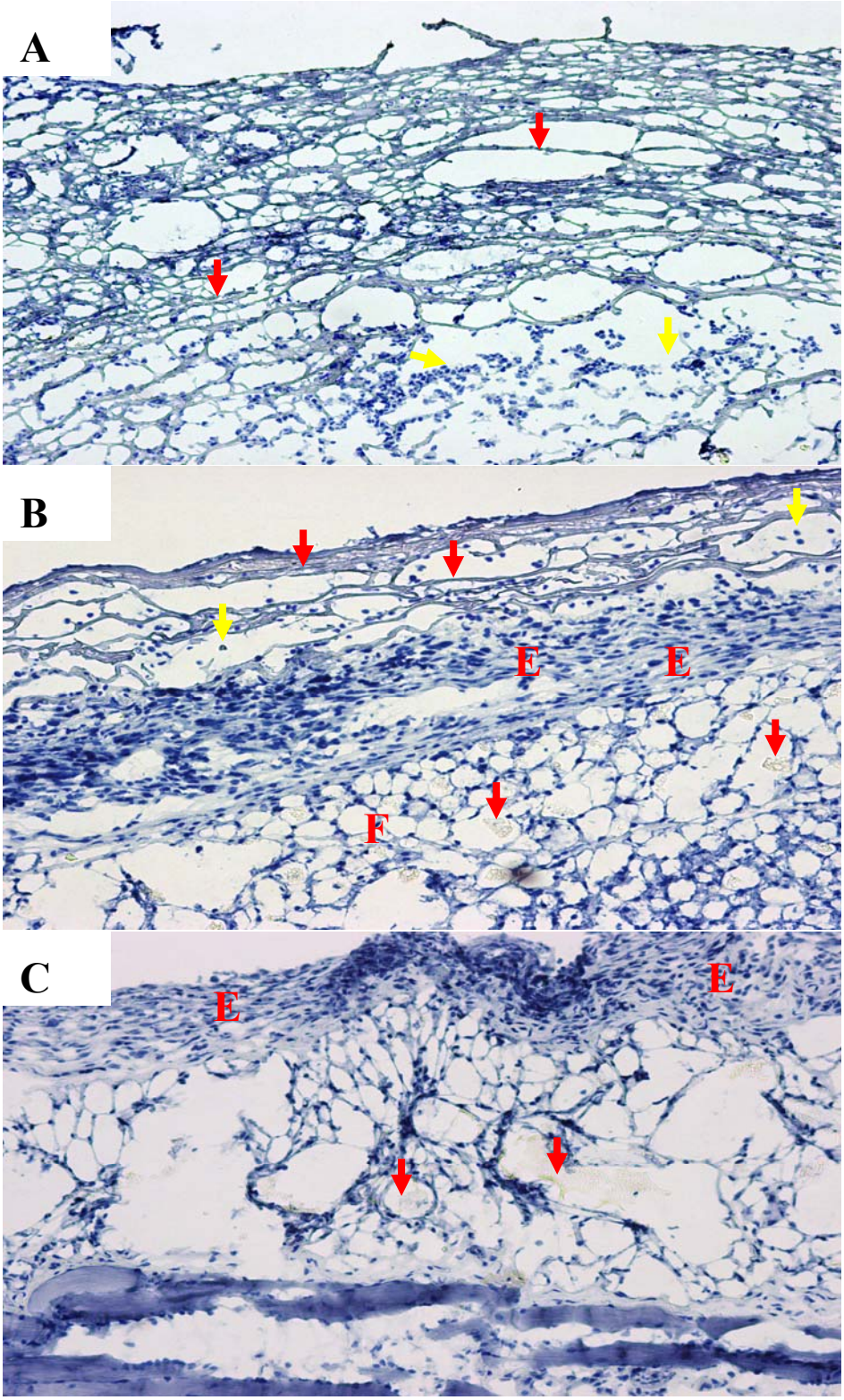

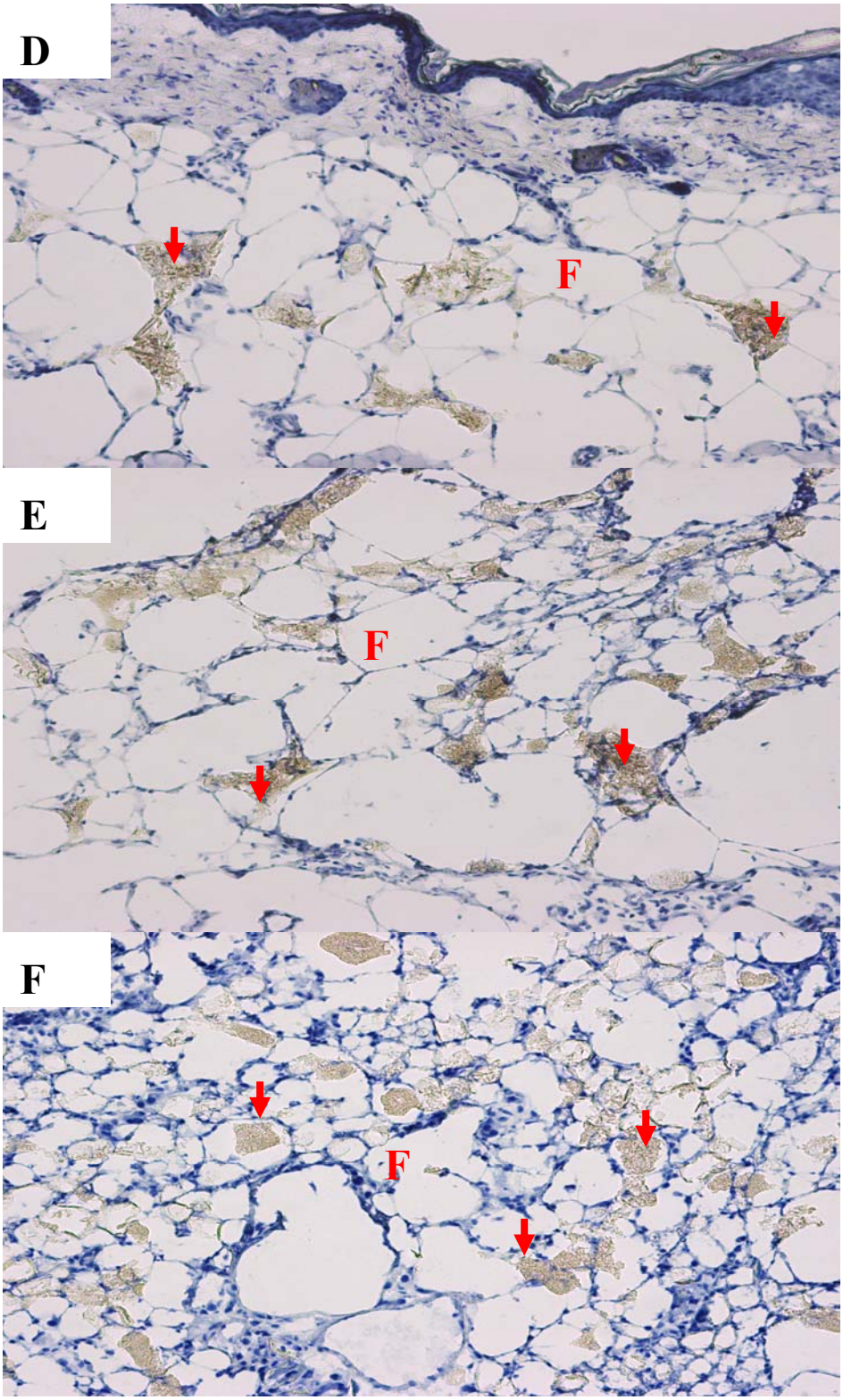
D
F
E
F
F
F

Chapter 7 Conclusion

In this investigation, we have successfully demonstrated that cells could grow inside the highly porous Dextran/PLGA scaffold with high viability and they are organized into dense multi-layered structures that resembled dermal structure. More importantly, the scaffold could support the most fundamental cell functions including proliferation, migration, contraction, protein production and ECM organization/turnover. It is worth noting that the scaffold, per se, could significantly enhance collagen gel contraction in an in vitro model. The collagen gel contraction is further enhanced by the scaffold in the presence of seeded cells. However, the mechanism of this phenomenon has yet to be resolved. In addition, the morphology and intracellular F-actin organization of cells is altered by the scaffold without affecting the cell-ECM communication.

The results of long term viability assay indicate that both the Dextran/PLGA scaffold and its degradation byproducts are non-toxic to both fibroblasts and macrophages. Additionally, the scaffold activates only a small subset of macrophage population and it can be inferred that the scaffold has low potential of inducing severe acute and chronic inflammatory responses. Additionally, fibroblasts play a role in modulating and prolonging macrophage activation in the presence of the scaffold. IL-10, SDF-1, MIP-1 gamma and RANTE are found to be up-regulated by cells

incubated with the scaffold. None of the major pro-inflammatory cytokines and the major cytokines capable of activating macrophages are expressed differently in the presence of scaffold. The exact functions of the up-regulated cytokines,,especially their roles in the coordinative interaction of fibroblasts and macrophages with the scaffold, have to be further investigated.

Interestingly, the Dextran/PLGA scaffold could be degraded by both fibroblasts and macrophages, cultured either separately or together. To our knowledge, it is the first report showing fibroblasts are capable of degrading synthetic polymer. The scaffold's morphological change, dry weight lost as well as the pH value modification all indicate its favorable biocompatibility. The results of *in vivo* subdermal implantation of the Dextran/PLGA scaffold further confirms its good biodegradability. Furthermore, the activities of lysozyme, gelatinase, hyaluronidase-1, NSE, and α-glucosidase as well as the expressions of cell surface receptors CD204 and TLR4 are up-regulated, suggesting their involvements in the cell-mediated scaffold degradation. It is possible that other enzymes and receptors participate in the scaffold degradation and this issue needs to be further addressed.

We further demonstrate that the Dextran/PLGA scaffold could significantly enhance dermal wound healing in both diabetic mice and control wild type mice. The scaffold not only serves as a temporary substitute of the damaged ECM but also doubles the role in promoting the production of endogenous ECM. However, the exact mechanism of facilitated healing by the scaffold has to be further investigated; inflammatory responses, re-epithelialization, neo-angiogenesis, as well

as ECM turnover have to be studied in greater details. We also notice that the scaffold degrades in different patterns in diabetic mice and wild type mice. Elucidating the mechanism of this differential behavior has very important implications in optimal application of the scaffold as a therapeutic modality.

In summary, the interactions of two major dermal cell types with the PLGA/Dextran scaffold have been explored. Furthermore, a macrophage/fibroblast co-culture model was established to facilitate the investigation of the interaction of implantable materials by both cell types, cooperatively. Elucidating material-tissue interaction in greater detail could result in future improvement of biomaterial design and their optimal applications. Exploring the tissue-material interactions will be the next research focus and the investigations.

References

1. Dodson WW KJ, Scruggs J, Kiel J, Wolf EG. 3-Nitrotyrosine predicts healing in chronic diabetic foot wounds treated with hyperbaric oxygen. Wounds 1999;11:129-36.

2. Brem H, Tomic-Canic M. Cellular and molecular basis of wound healing in diabetes. J Clin Invest. 2007 May;117(5):1219-22.

3. Medina A, Scott PG, Ghahary A, Tredget EE. Pathophysiology of chronic nonhealing wounds. The Journal of burn care & rehabilitation. 2005 Jul-Aug;26(4):306-19.

4. Lorenz HP LM. Wounds: Biology, Pathology, and Management. Chapter 7. Stanford University Medical Center; 2003.

5. Blakytny R, Jude E. The molecular biology of chronic wounds and delayed healing in diabetes. Diabet Med. 2006 Jun;23(6):594-608.

6. Mustoe TA, O'Shaughnessy K, Kloeters O. Chronic wound pathogenesis and current treatment strategies: a unifying hypothesis. Plastic and reconstructive surgery. 2006 Jun;117(7 Suppl):35S-41S.

7. Falanga V. Wound healing and its impairment in the diabetic foot. Lancet. 2005 Nov 12;366(9498):1736-43.

8. Eldor R, Raz I, Ben Yehuda A, Boulton AJ. New and experimental approaches to treatment of diabetic foot ulcers: a comprehensive review of emerging treatment strategies. Diabet Med. 2004 Nov;21(11):1161-73.

9. Liu Y, Cai S, Shu XZ, Shelby J, Prestwich GD. Release of basic fibroblast growth factor from a crosslinked glycosaminoglycan hydrogel promotes wound healing. Wound Repair Regen. 2007 Mar-Apr;15(2):245-51.

10. Ishihara M, Fujita M, Obara K, Hattori H, Nakamura S, Nambu M, et al. Controlled releases of FGF-2 and paclitaxel from chitosan hydrogels and their subsequent effects on wound repair, angiogenesis, and tumor growth. Curr Drug Deliv. 2006 Oct;3(4):351-8.

11. Arul V, Kartha R, Jayakumar R. A therapeutic approach for diabetic wound healing using biotinylated GHK incorporated collagen matrices. Life sciences. 2007 Jan 2;80(4):275-84.

12. Garcia-Esteo F, Pascual G, Gallardo A, San-Roman J, Bujan J, Bellon JM. A biodegradable copolymer for the slow release of growth hormone expedites scarring in diabetic rats. J Biomed Mater Res B Appl Biomater. 2007 May;81(2):291-304.

13. Obara K, Ishihara M, Fujita M, Kanatani Y, Hattori H, Matsui T, et al. Acceleration of wound healing in healing-impaired db/db mice with a photocrosslinkable chitosan hydrogel containing fibroblast growth factor-2. Wound Repair Regen. 2005 Jul-Aug;13(4):390-7.

14. Ono I, Tateshita T, Inoue M. Effects of a collagen matrix containing basic fibroblast growth factor on wound contraction. Journal of biomedical materials research. 1999;48(5):621-30.

15. Jiang H, Fang D, Hsiao BS, Chu B, Chen W. Optimization and characterization of dextran membranes prepared by electrospinning. Biomacromolecules. 2004 Mar-Apr;5(2):326-33.

16. Pan H, Jiang H, Chen W. Interaction of dermal fibroblasts with electrospun composite polymer scaffolds prepared from dextran and poly lactide-co-glycolide. Biomaterials. 2006 Jun;27(17):3209-20.

17. Zhidao Xia JTT. A review on macrophage responses to biomaterials. Biomed Mater. 2006;1:1–9.

18. B.D. Ratner ASH, F.J. Schoen and J.E. Lemons, editor. Biomaterials science: an introduction to materials in medicine (2nd ed), : Elsevier, Amsterdam 2004.

19. Luzardo-Alvarez A BN, Peter K, Romero J F, Reymond C, Corradin G, Gander B. Biodegradable microspheres alone do not stimulate murine macrophages in vitro, but prolong antigen presentation by macrophages in vitro and stimulate a solid immune response in mice. J Control Release. 2005 Dec 5;109(1-3):62-76.

20. Schmidt DR, Kao WJ. The interrelated role of fibronectin and interleukin-1 in biomaterial-modulated macrophage function. Biomaterials. 2007 Jan;28(3):371-82.

21. Dovi JV, He LK, DiPietro LA. Accelerated wound closure in neutrophil-depleted mice. Journal of leukocyte biology. 2003 Apr;73(4):448-55.

22. Waugh HV, Sherratt JA. Macrophage dynamics in diabetic wound dealing. Bulletin of

mathematical biology. 2006 Jan;68(1):197-207.

23. Zhao Y, Shimizu T, Nishihira J, Koyama Y, Kushibiki T, Honda A, et al. Tissue regeneration using macrophage migration inhibitory factor-impregnated gelatin microbeads in cutaneous wounds. The American journal of pathology. 2005 Dec;167(6):1519-29.

24. Marisa C, Lucci I, Di Giulio C, Bianchi G, Grilli A, Patruno A, et al. MCP-1 and MIP-2 expression and production in BB diabetic rat: effect of chronic hypoxia. Molecular and cellular biochemistry. 2005 Aug;276(1-2):105-11.

25. Wetzler C, Kampfer H, Stallmeyer B, Pfeilschifter J, Frank S. Large and sustained induction of chemokines during impaired wound healing in the genetically diabetic mouse: prolonged persistence of neutrophils and macrophages during the late phase of repair. The Journal of investigative dermatology. 2000 Aug;115(2):245-53.

26. Yamakawa T, Tanaka S, Yamakawa Y, Kiuchi Y, Isoda F, Kawamoto S, et al. Augmented production of tumor necrosis factor-alpha in obese mice. Clinical immunology and immunopathology. 1995 Apr;75(1):51-6.

27. Shabani M, Pulfer SK, Bulgrin JP, Smith DJ. Enhancement of wound repair with a topically applied nitric oxide-releasing polymer. Wound Repair Regen. 1996 Jul;4(3):353-62.

28. Witte MB, Kiyama T, Barbul A. Nitric oxide enhances experimental wound healing in diabetes. The British journal of surgery. 2002 Dec;89(12):1594-601.

29. Barbato JE, Zuckerbraun BS, Overhaus M, Raman KG, Tzeng E. Nitric oxide modulates vascular inflammation and intimal hyperplasia in insulin resistance and the metabolic syndrome. American journal of physiology. 2005 Jul;289(1):H228-36.

30. Jones LC, Tucci M, Frondoza C. Macrophages and fibroblasts respond differently to PMMA particles and mechanical strain. Biomedical sciences instrumentation. 2006;42:223-30.

31. Matheson LA, Labow RS, Santerre JP. Biodegradation of polycarbonate-based polyurethanes by the human monocytes-derived macrophage and U937 cell systems. Journal of biomedical materials research. 2002 Sep 15;61(4):505-13.

32. Xia Z, Huang Y, Adamopoulos IE, Walpole A, Triffitt JT, Cui Z. Macrophage-mediated biodegradation of poly(DL-lactide-co-glycolide) in vitro. Journal of biomedical materials research. 2006 Dec 1;79(3):582-90.

33. Austyn JM, Gordon S. F4/80, a monoclonal antibody directed specifically against the mouse macrophage. European journal of immunology. 1981 Oct;11(10):805-15.

34. Mano JF, Silva GA, Azevedo HS, Malafaya PB, Sousa RA, Silva SS, et al. Natural origin biodegradable systems in tissue engineering and regenerative medicine: present status and some moving trends. J R Soc Interface. 2007 Apr 3.

35. Wu L, Ding J. In vitro degradation of three-dimensional porous poly(D,L-lactide-co-glycolide) scaffolds for tissue engineering. Biomaterials. 2004 Dec;25(27):5821-30.

36. Yang J, Hao Q, Liu X, Ba C, Cao A. Novel biodegradable aliphatic poly(butylene succinate-co-cyclic carbonate)s with functional carbonate building blocks. 1. Chemical synthesis and their structural and physical characterization. Biomacromolecules. 2004 Jan-Feb;5(1):209-18.

37. Zhang S, Borazjani RN, Salamone JC, Ahearn DG, Crow SA, Jr., Pierce GE. In vitro deposition of lysozyme on etafilcon A and balafilcon A hydrogel contact lenses: effects on adhesion and survival of Pseudomonas aeruginosa and Staphylococcus aureus. Cont Lens Anterior Eye. 2005 Sep;28(3):113-9.

38. Huang Y, Onyeri S, Siewe M, Moshfeghian A, Madihally SV. In vitro characterization of chitosan-gelatin scaffolds for tissue engineering. Biomaterials. 2005 Dec;26(36):7616-27.

39. Santerre JP, Woodhouse K, Laroche G, Labow RS. Understanding the biodegradation of polyurethanes: from classical implants to tissue engineering materials. Biomaterials. 2005 Dec;26(35):7457-70.

40. Dadsetan M CE, Unger F, Ausborn M, Kissel T, Hiltner A, Anderson JM. In vivo biocompatibility and biodegradation of poly(ethylene carbonate). J Control Release. 2003 Dec 12;93(3):259-70.

41. Wilson CJ, Clegg RE, Leavesley DI, Pearcy MJ. Mediation of biomaterial-cell interactions by adsorbed proteins: a review. Tissue Eng. 2005 Jan-Feb;11(1-2):1-18.

42. Adams DO, Hamilton TA. The cell biology of macrophage activation. Annu Rev Immunol.

1984;2:283-318.

43. Meier B, Radeke HH, Selle S, Habermehl GG, Resch K, Sies H. Human fibroblasts release low amounts of reactive oxygen species in response to the potent phagocyte stimulants, serum-treated zymosan, N-formyl-methionyl-leucyl-phenylalanine, leukotriene B4 or 12-O-tetradecanoylphorbol 13-acetate. Biological chemistry Hoppe-Seyler. 1990 Oct;371(10):1021-5.

44. Arlein WJ, Shearer JD, Caldwell MD. Continuity between wound macrophage and fibroblast phenotype: analysis of wound fibroblast phagocytosis. The American journal of physiology. 1998 Oct;275(4 Pt 2):R1041-8.

45. Rabinovitch M. Professional and non-professional phagocytes: an introduction. Trends in cell biology. 1995 Mar;5(3):85-7.

46. Christenson EM, Dadsetan M, Wiggins M, Anderson JM, Hiltner A. Poly(carbonate urethane) and poly(ether urethane) biodegradation: in vivo studies. Journal of biomedical materials research. 2004 Jun 1;69(3):407-16.

47. Steed DL, Attinger C, Colaizzi T, Crossland M, Franz M, Harkless L, et al. Guidelines for the treatment of diabetic ulcers. Wound Repair Regen. 2006 Nov-Dec;14(6):680-92.

48. Ehrenreich M, Ruszczak Z. Update on tissue-engineered biological dressings. Tissue engineering. 2006 Sep;12(9):2407-24.

49. http://www.polydex.com/v2/images/img_dextran_m.gif.

50. JA. K. Histological and Histochemical Methods: Theory and Practice. . 3rd ed ed. Butterworth Heinemann, editor.: Oxford, ; 2000.

51. Chen G, Sato T, Ushida T, Hirochika R, Tateishi T. Redifferentiation of dedifferentiated bovine chondrocytes when cultured in vitro in a PLGA-collagen hybrid mesh. FEBS Letters. 2003;542(1-3):95-9.

52. Sumiyoshi K, Nakao A, Setoguchi Y, Okumura K, Tsuboi R, Ogawa H. Smads regulate collagen gel contraction by human dermal fibroblasts. 2003. p. 464-70.

53. Ala-aho R, Kahari VM. Collagenases in cancer. Biochimie. 2005 Mar-Apr;87(3-4):273-86.

54. Al-Saffer N IH, Revell P.A. Direct activation of mast cells by prosthetic biomaterial particles. Journal of materials science: materials in medicine. 1998;9:849-53.

56. Peter N. Gray MECMJG. Population density and regulation of cell division in 3T3 cells. I. Inorganic phosphate levels, uptake and release. 1976. p. 225-33.

57. Ishizaki Y CL, Mudge AW, Raff MC. Programmed cell death by default in embryonic cells, fibroblasts, and cancer cells. Mol Biol Cell. 1995;6:1443–58.

58. Miyamoto S, Teramoto H, Coso OA, Gutkind JS, Burbelo PD, Akiyama SK, et al. Integrin function: molecular hierarchies of cytoskeletal and signaling molecules. 1995. p. 791-805.

59. Bhardwaj RS HU, Klein B, Zwadlo-Klarwasser G, Klinge U, Mittermayer C, Klosterhalfen

B. . Monocyte—biomaterial interaction inducing. phenotypic dynamics of monocytes: a possible role. of monocyte subsets in biocompatibility. Journal of materials science: materials in medicine. 1997;8 737 - 42.

60. Branchaud RM, Garant LJ, Kane AB. Pathogenesis of mesothelial reactions to asbestos fibers. Monocyte recruitment and macrophage activation. Pathobiology. 1993;61(3-4):154-63.

61. Bredt DS, Snyder SH. Nitric oxide: a physiologic messenger molecule. Annu Rev Biochem. 1994;63:175-95.

62. Calvo P, Vila-Jato JL, Alonso MJ. Effect of lysozyme on the stability of polyester nanocapsules and nanoparticles: stabilization approaches. Biomaterials. 1997 Oct;18(19):1305-10.

63. Chellat F, Merhi Y, Moreau A, Yahia L. Therapeutic potential of nanoparticulate systems for macrophage targeting. Biomaterials. 2005 Dec;26(35):7260-75.

64. Chiu RK, Droll A, Cooper DL, Dougherty ST, Dirks JF, Dougherty GJ. Molecular mechanisms regulating the hyaluronan binding activity of the adhesion protein CD44. Journal of neuro-oncology. 1995 Dec;26(3):231-9.

65. Culty M, Nguyen HA, Underhill CB. The hyaluronan receptor (CD44) participates in the uptake and degradation of hyaluronan. The Journal of cell biology. 1992 Feb;116(4):1055-62.

66. Czajkowska B, Ptak M, Bobek M, Bryniarski K, Szczepanik M. Different isoenzyme patterns of nonspecific esterases and the level of IL6 production as markers of macrophage functions. Folia histochemica et cytobiologica / Polish Academy of Sciences, Polish

Histochemical

and Cytochemical Society. 1995;33(2):111-5.

67. Lerman OZ GR, Armour M, Levine JP, Gurtner GC. . Cellular dysfunction in the diabetic fibroblast: impairment in migration, vascular endothelial growth factor production, and response to hypoxia. Am J Pathol. 2003;162:303-12.

68. Daniele Brouty-Boye CP-C, Christelle Doucet, Claude Jasmin, Bruno Azzarone. Chemokines and CD40 expression in human fibroblasts. European of journal of immunology. 2000;30(3):914-9.

69. de Jong SJ, van Eerdenbrugh B, van Nostrum CF, Kettenes-van den Bosch JJ, Hennink WE. Physically crosslinked dextran hydrogels by stereocomplex formation of lactic acid oligomers: degradation and protein release behavior. J Control Release. 2001 Apr 28;71(3):261-75.

70. De Rosa G, Maiuri MC, Ungaro F, De Stefano D, Quaglia F, La Rotonda MI, et al. Enhanced intracellular uptake and inhibition of NF-kappaB activation by decoy oligonucleotide released from PLGA microspheres. The journal of gene medicine. 2005 Jun;7(6):771-81.

71. Dodson WW KJ, Scruggs J, Kiel J, Wolf EG. 3-Nitrotyrosine predicts healing in chronic diabetic foot wounds treated with hyperbaric oxygen. Wounds. 1999;11:129-36.

72. Engelholm LH LK, Netzel-Arnett S, Cukierman E, Mitola DJ, Aaronson H, Kjoller L, Larsen JK, Yamada KM, Strickland DK, Holmbeck K, Dano K, Birkedal-Hansen H, Behrendt N, Bugge TH. uPARAP/Endo180 is essential for cellular uptake of collagen and promotes fibroblast

collagen adhesion. The Journal of cell biology. 2003 Mar 31;160(7):1009-15.

73. Evonuk E. Hemodynamic and metabolic responses of infused low molecular weight dextran. The American journal of physiology. 1967 Feb;212(2):514-8.

74. Forman HJ, Torres M. Reactive oxygen species and cell signaling: respiratory burst in macrophage signaling. American journal of respiratory and critical care medicine. 2002 Dec 15;166(12 Pt 2):S4-8.

75. Friis S, McLaughlin JK, Mellemkjaer L, Kjoller KH, Blot WJ, Boice JD, Jr., et al. Breast implants and cancer risk in Denmark. International journal of cancer. 1997 Jun 11;71(6):956-8.

76. Fujikawa Y, Itonaga I, Kudo O, Hirayama T, Taira H. Macrophages that have phagocytosed particles are capable of differentiating into functional osteoclasts. Modern rheumatology / the Japan Rheumatism Association. 2005 Oct;15(5):346-51.

77. Girard N, Maingonnat C, Bertrand P, Tilly H, Vannier JP, Delpech B. Human monocytes synthesize hyaluronidase. British journal of haematology. 2002 Oct;119(1):199-203.

78. Grandjean-Laquerriere A, Tabary O, Jacquot J, Richard D, Frayssinet P, Guenounou M, et al. Involvement of toll-like receptor 4 in the inflammatory reaction induced by hydroxyapatite particles. Biomaterials. 2007 Jan;28(3):400-4.

79. Guidoin MF, Guidoin R, Frayssinet P, Legrand AP, How T. Poly-L-lactide surfaces subjected to long-term cell cultures: cell proliferation and polymer degradation. Artificial cells, blood substitutes, and immobilization biotechnology. 2005;33(4):411-22.

80. Gwinn MR, Vallyathan V. Respiratory burst: role in signal transduction in alveolar macrophages. Journal of toxicology and environmental health. 2006 Jan-Feb;9(1):27-39.

81. Hamilton JA. Nondisposable materials, chronic inflammation, and adjuvant action. Journal of leukocyte biology. 2003 Jun;73(6):702-12.

82. Hamilton RF, Jr., Thakur SA, Mayfair JK, Holian A. MARCO mediates silica uptake and toxicity in alveolar macrophages from C57BL/6 mice. J Biol Chem. 2006 Nov 10;281(45):34218-26.

83. Hasilik A, Neufeld EF. Biosynthesis of lysosomal enzymes in fibroblasts. Synthesis as precursors of higher molecular weight. J Biol Chem. 1980 May 25;255(10):4937-45.

84. Hester TR Jr FN, Gale PJ, Hammett JL, Raymond R, Turnbull D, Frankos VH, Cohen MB. Measurement of 2,4-toluenediamine in urine and serum samples from women with Meme or Replicon breast implants. Plastic and reconstructive surgery. 1997 Oct;100(5):1291-8.

85. Hofseth LJ SS, Hussain SP, Espey MG, Miranda KM, Araki Y, Jhappan C, Higashimoto Y, He P, Linke SP, Quezado MM, Zurer, I, Rotter V, Wink DA, Appella E, Harris CC. Nitric oxide-induced cellular stress and p53 activation in chronic inflammation. Proceedings of the National Academy of Sciences of the United States of America. 2003 Jan 7;100(1):143-8.

86. Holtje JV. Lysozyme substrates. Exs. 1996;75:105-10.

87. Hooper KA, Nickolas TL, Yurkow EJ, Kohn J, Laskin DL. Characterization of the

inflammatory response to biomaterials using a rodent air pouch model. Journal of biomedical materials research. 2000 Jun 5;50(3):365-74.

88. Hui Pan HJ, Weiliam Chen. In vitro Evaluation of the Degradability of Electrospun Dextran/PLGA scaffold by with a Fibroblast/Macrophage Co-culture Model In preparation.

89. Hui Pan HJ, Weiliam Chen. A Fibroblast/Macrophage Co-culture Model for Evaluation of the Biocompatibility and Immunocompatibility of an Electrospun Dextran/PLGA scaffold. Submitted.

90. Hwang SM, Chen CY, Chen SS, Chen JC. Chitinous materials inhibit nitric oxide production by activated RAW 264.7 macrophages. Biochemical and biophysical research communications. 2000 Apr 29;271(1):229-33.

91. Hwang SM CC, Chen SS, et al. . Chitinous materials inhibit nitric oxide production by activated RAW 264.7 macrophages. Biochem Biophys Res Commun, . 2000;271:229-33.

92. Iles KE, Forman HJ. Macrophage signaling and respiratory burst. Immunol Res. 2002;26(1-3):95-105.

93. Inoue S, Sayo T. [Hyaluronan turnover and disease]. Seikagaku. 2005 Sep;77(9):1152-64.

94. Iwamoto M KM, Nakashima T, Kim D, Yamaguchi K, Oda T, Iwamoto Y, Muramatsu T. Structure-activity relationship of alginate oligosaccharides in the induction of cytokine production from RAW 264.7 cells. FEBS letters. 2005;579:4423-9.

95. J.M. A. Multinucleated giant cells. Current Opinion in Hematology. 2000;7:40-7.

96. McCaffrey RL, Allen LA. Francisella tularensis LVS evades killing by human neutrophils via inhibition of the respiratory burst and phagosome escape. Journal of leukocyte biology. 2006 Dec;80(6):1224-30.

97. Rihova B. Immunocompatibility and biocompatibility of cell delivery systems. Adv Drug Deliv Rev. 2000 Aug 20;42(1-2):65-80.

98. Kulig K. Lifetime risk from polyurethane covered breast implants. Environ Health Perspect. 1998 Nov;106(11):A526-7.

99. Johnston RB, Jr., Kitagawa S, Edwards CK, 3rd, Channon JY, Suzuki H, Pabst MJ. The respiratory burst in activated macrophages: studies of its molecular basis and evidence for downregulation in chronic infection. Adv Exp Med Biol. 1988;239:63-72.

100. Aliyev E, Sakallioglu U, Eren Z, Acikgoz G. The effect of polylactide membranes on the levels of reactive oxygen species in periodontal flaps during wound healing. Biomaterials. 2004 Aug;25(19):4633-7.

101. A. Tomasi TÖaVPS, editor. Free Radicals, Nitric Oxide and Inflammation: IOS Press; 2003, 264 pp.

102. Schaffer MR, Efron PA, Thornton FJ, Klingel K, Gross SS, Barbul A. Nitric oxide, an autocrine regulator of wound fibroblast synthetic function. J Immunol. 1997 Mar 1;158(5):2375-81.

103. Saad B MS, Ciardelli G, Uhlschmid GK, Welti M. Neuenschwander P, Suter UW. Interactions of osteoblasts and macrophages with biodegradable and highly porous polyesterurethane foam and its degradation products. Journal of biomedical materials research. 1996 Nov;32(3):355-66.

104. Laczka-Osyczka A, Turyna B, Dubin A, Laczka M. Comparison of biocompatibility of gel-derived bioactive ceramics in macrophage culture conditions. Biomaterials. 1997 Sep;18(18):1243-50.

105. Thorns M, Benghuzzi H, Tucci M, Cason Z. The physiological response associated with large particles of TCP, HA, and ALCAP implants using raw 264.7 cells. Biomedical sciences instrumentation. 2001;37:287-92.

106. Ross J.A. AMJ. The macrophage. 2nd ed. Burke B LCE, editor. New York: Oxford University Press Inc.; 2002.

107. Valles G G-MP, Gonzalez-Carrasco JL, Saldana L, Aanchez-Sabate E, Munuera L, Vilaboa N. Differential inflammatory macrophage response to rutile and titanium particles. Biomaterials. 2006;27:5199-211.

108. Warme B.A. ENJ, Trindade M.C.D., Miyanishi K, Ma T, Saket R.R., Regula D, Goodman S.B., Smith R.L. Proinflammatory mediator expression in a Novel Murine Model of Titanium-Particle-Induced Intramedullary Inflammation. J Biomed Mater Res Part B. 2004;71B:360-6.

109. Kyriakides T.R. FMJ, Keeney G.E., Tsai A., Giachelli C.M., Clark-Lewis I, Rollins B.J., Bornstein P. The CC chemokine Ligand, CCL2/MCP-1 Participates in Macrophage Fusion and Foreign Body Giant Cell Formation. American Journal of Pathology. 2004;165(6):2157-66.

110. Taylor PR, Martinez-Pomares L, Stacey M, Lin HH, Brown GD, Gordon S. Macrophage receptors and immune recognition. Annu Rev Immunol. 2005;23:901-44.

111. Taub DD OJ. Chemokines, inflammation and the immune system. Ther Immunol. 1994;1(4):229-46.

112. Berahovich RD MZ, Wang Y, Premack B, Howard MC, Schall TJ. Proteolytic activation of alternative CCR1 ligands in inflammation. J Immunolo. 2005;174(11):7341-51.

113. Walsh L. The chemokine superfamily. L W, editor. Cambridge: Cambridge University Press; 2002.

114. Sorg C. Macrophages in acute and chronic inflammation. Chest. 1991 Sep;100(3 Suppl):173S-5S.

115. Bhardwaj RS HU, Klein B, Zwadlo-Klarwasser G, Klinge U, Mittermayer C, Klosterhalfen B. . Monocyte—biomaterial interaction inducing. phenotypic dynamics of monocytes: a possible role. of monocyte subsets in biocompatibility. JOURNAL OF MATERIALS SCIENCE: MATERIALS IN MEDICINE 1997;8 737 - 42.

116. Rhodes NP, Hunt JA, Williams DF. Macrophage subpopulation differentiation by

stimulation with biomaterials. Journal of biomedical materials research. 1997 Dec 15;37(4):481-8.

117. Xuabg J GS, Wunschmann S, Chang Q, Klinzman D, Stapleton JT. Inhibition of HIV-1 replication by GB virus C infection through increases in RANTES, MIP-1 alpha, MIP-beta, and SDF-1. Lancet. 2004;363(9426):2040-6.

118. Arenzana-Seisdedos F. PM. Genetics of resistance to HIV infection: Role of co-receptors and co-co-receptor ligands. Semin Immunol. 2006;18(6):387-403.

119. Sawkar AR, Cheng WC, Beutler E, Wong CH, Balch WE, Kelly JW. Chemical chaperones increase the cellular activity of N370S beta -glucosidase: a therapeutic strategy for Gaucher disease. Proceedings of the National Academy of Sciences of the United States of America. 2002 Nov 26;99(24):15428-33.

120. www.faizyme.com/assahyal.htm.

121. Labow RS, Meek E, Matheson LA, Santerre JP. Human macrophage-mediated biodegradation of polyurethanes: assessment of candidate enzyme activities. Biomaterials. 2002 Oct;23(19):3969-75.

122. Santerre JP, Labow RS, Adams GA. Enzyme-biomaterial interactions: effect of biosystems on degradation of polyurethanes. Journal of biomedical materials research. 1993 Jan;27(1):97-109.

123. Lee JS, Basalyga DM, Simionescu A, Isenburg JC, Simionescu DT, Vyavahare NR. Elastin calcification in the rat subdermal model is accompanied by up-regulation of degradative and

osteogenic cellular responses. The American journal of pathology. 2006 Feb;168(2):490-8.

124. Mercuri JJ, Lovekamp JJ, Simionescu DT, Vyavahare NR. Glycosaminoglycan-targeted fixation for improved bioprosthetic heart valve stabilization. Biomaterials. 2007 Jan;28(3):496-503.

125. Vasudev SC, Chandy T, Umasankar MM, Sharma CP. Inhibition of bioprosthesis calcification due to synergistic effect of Fe/Mg ions to polyethylene glycol grafted bovine pericardium. Journal of biomaterials applications. 2001 Oct;16(2):93-107.

126. Nawrocka E. [Lysozyme in good health and in disease]. Pediatria polska. 1978 Nov;53(11):1321-5.

127. Liso V, Lortholary P, Lejeune F, Turpin F, Hetfleis E, Daniel MT, et al. [Nonspecific esterase activity of polynuclears in Chediak's disease]. Pathologie-biologie. 1971 May;19(9):507-9.

128. Shingleton WD, Hodges DJ, Brick P, Cawston TE. Collagenase: a key enzyme in collagen turnover. Biochemistry and cell biology = Biochimie et biologie cellulaire. 1996;74(6):759-75.

129. Morrow T. Pompe disease therapy presents coverage challenge. Managed care (Langhorne, Pa. 2006 Jun;15(6):63-4.

130. Schmitz J, Poll LW, vom Dahl S. Therapy of adult Gaucher disease. Haematologica. 2007 Feb;92(2):148-52.

131. Unanue ER, Beller DI, Calderon J, Kiely JM, Stadecker MJ. Regulation of immunity and

inflammation by mediators from macrophages. The American journal of pathology. 1976 Nov;85(2):465-78.

132. Shockman GD, Daneo-Moore L, Kariyama R, Massidda O. Bacterial walls, peptidoglycan hydrolases, autolysins, and autolysis. Microbial drug resistance (Larchmont, NY. 1996 Spring;2(1):95-8.

133. Yomota C, Komuro T, Kimura T. [Studies on the degradation of chitosan films by lysozyme and release of loaded chemicals. Yakugaku Zasshi. 1990 Jun;110(6):442-8.

134. Lord MS, Stenzel MH, Simmons A, Milthorpe BK. Lysozyme interaction with poly(HEMA)-based hydrogel. Biomaterials. 2006 Mar;27(8):1341-5.

135. Sun Y, Quinn B, Witte DP, Grabowski GA. Gaucher disease mouse models: point mutations at the acid beta-glucosidase locus combined with low-level prosaposin expression lead to disease variants. Journal of lipid research. 2005 Oct;46(10):2102-13.

136. Tian G WD, Perry VH, Rudd PM, Dwek RA, Platt FM, Platt N. Inhibition of alpha-glucosidases I and II increases the cell surface expression of functional class A macrophage scavenger receptor (SR-A) by extending its half-life. J Biol Chem. 2004 Sep 17;279(38):39303-9.

137. Ziats NP, Miller KM, Anderson JM. In vitro and in vivo interactions of cells with biomaterials. Biomaterials. 1988 Jan;9(1):5-13.

138. Arredouani MS, Palecanda A, Koziel H, Huang YC, Imrich A, Sulahian TH, et al. MARCO

is the major binding receptor for unopsonized particles and bacteria on human alveolar macrophages. J Immunol. 2005 Nov 1;175(9):6058-64.

139. Palecanda A, Kobzik L. Receptors for unopsonized particles: the role of alveolar macrophage scavenger receptors. Current molecular medicine. 2001 Nov;1(5):589-95.

140. Wang W, Ferguson DJ, Quinn JM, Simpson AH, Athanasou NA. Biomaterial particle phagocytosis by bone-resorbing osteoclasts. The Journal of bone and joint surgery. 1997 Sep;79(5):849-56.

141. Palecanda A PJ, Al-Mutairi E, Imrich A, Qin G, Suzuki H, Kodama T, Tryggvason K, Koziel H, Kobzik L. Role of the scavenger receptor MARCO in alveolar macrophage binding of unopsonized environmental particles. The Journal of experimental medicine. 1999 May 3;189(9):1497-506.

142. Mori T, Murakami M, Okumura M, Kadosawa T, Uede T, Fujinaga T. Mechanism of macrophage activation by chitin derivatives. The Journal of veterinary medical science / the Japanese Society of Veterinary Science. 2005 Jan;67(1):51-6.

143. Saad B, Matter S, Ciardelli G, Uhlschmid GK, Welti M, Neuenschwander P, et al. Interactions of osteoblasts and macrophages with biodegradable and highly porous polyesterurethane foam and its degradation products. Journal of biomedical materials research. 1996 Nov;32(3):355-66.

144. Joseph HL, Roisen FJ, Anderson GL, Barker JH, Weiner LJ, Tobin GR. Inhibition of wound

contraction with locally injected lathyrogenic drugs. American journal of surgery. 1997 Sep;174(3):347-50.

145. Pietramaggiori G, Yang HJ, Scherer SS, Kaipainen A, Chan RK, Alperovich M, et al. Effects of poly-N-acetyl glucosamine (pGlcNAc) patch on wound healing in db/db mouse. J Trauma. 2008 Mar;64(3):803-8.